ornl

OAK RIDGE
NATIONAL
LABORATORY

MARTIN MARIETTA

ORNL/CON-150

Air-Source Heat Pump: Field Measurement of Cycling, Frosting, and Defrosting Losses, 1981–83

V. D. Baxter
J. C. Moyers

OPERATED BY
MARTIN MARIETTA ENERGY SYSTEMS, INC.
FOR THE UNITED STATES
DEPARTMENT OF ENERGY

Printed in the United States of America. Available from
National Technical Information Service
U.S. Department of Commerce
5285 Port Royal Road, Springfield, Virginia 22161
NTIS price codes—Printed Copy: A06 Microfiche A01

This report was prepared as an account of work sponsored by an agency of the United States Government. Neither the United States Government nor any agency thereof, nor any of their employees, makes any warranty, express or implied, or assumes any legal liability or responsibility for the accuracy, completeness, or usefulness of any information, apparatus, product, or process disclosed, or represents that its use would not infringe privately owned rights. Reference herein to any specific commercial product, process, or service by trade name, trademark, manufacturer, or otherwise, does not necessarily constitute or imply its endorsement, recommendation, or favoring by the United States Government or any agency thereof. The views and opinions of authors expressed herein do not necessarily state or reflect those of the United States Government or any agency thereof.

ORNL/CON-150

Energy Division

AIR-SOURCE HEAT PUMP: FIELD MEASUREMENT OF CYCLING, FROSTING, AND DEFROSTING LOSSES, 1981–83

V. D. Baxter
Energy Division

J. C. Moyers
Engineering Technology Division

Date Published—November 1984

Prepared for the
Office of Buildings Energy
Research and Development

Prepared by the
OAK RIDGE NATIONAL LABORATORY
Oak Ridge, Tennessee 37831
operated by
MARTIN MARIETTA ENERGY SYSTEMS, INC.
for the
U.S. DEPARTMENT OF ENERGY
under Contract No. DE-AC05-84OR21400

CONTENTS

LIST OF FIGURES v

LIST OF TABLES ix

ACKNOWLEDGMENTS xi

ABSTRACT xiii

1. INTRODUCTION 1

2. TEST SITE AND EQUIPMENT 3

   2.1 TEST FACILITIES 3

   2.2 TEST EQUIPMENT 3

   2.3 DATA ACQUISITION 8

3. HEATING SEASON PERFORMANCE 13

   3.1 STEADY-STATE PERFORMANCE BASE 13
   3.2 TEST RESULTS 15
      3.2.1 Effect of Cycling Rate Reduction 17
      3.2.2 Defrost Cycle Characterization 21
   3.3 DYNAMIC LOSS ANALYSIS 24
      3.3.1 Modal Coefficients of Performance 24
      3.3.2 Degradation of Capacity and COP at Part Load 26
      3.3.3 Analysis of Cycling Loss During Heating 30
      3.3.4 Analysis of Defrost Time as a Function of Frosting Potential 37
   3.4 EFFECT OF DESUPERHEATER OPERATION ON CYCLING, FROSTING, AND DEFROSTING LOSSES 43

4. COOLING SEASON PERFORMANCE 51

   4.1 MANUFACTURER'S RATINGS AND ON-SITE STEADY-STATE TESTS 51
   4.2 DERIVED STEADY-STATE PERFORMANCE 57
      4.2.1 Determination of Steady-State Capacity Curve 57
      4.2.2 Determination of Steady-State COP Curve 59
      4.2.3 Discussion of Derived Steady-State Performance 59
   4.3 OVERALL SUMMER CYCLING TEST RESULTS 64
      4.3.1 Effect of Cycling Rate 68
      4.3.2 Effect of Desuperheater Operation 72

5. ANNUAL PERFORMANCE SUMMARY 75

6. CONCLUSIONS AND RECOMMENDATIONS 77

6.1 HEATING SEASON CONCLUSIONS 77
6.2 COOLING SEASON CONCLUSIONS 77
6.3 ANNUAL PERFORMANCE 78
6.4 RECOMMENDATIONS 78

REFERENCES 79

Appendix A. TEST DATA AND SAMPLE CALCULATIONS 81

Appendix B. AIR-SIDE HEAT FLOW INSTRUMENTATION 93

LIST OF FIGURES

2.1 Tennessee Energy Conservation in Housing (TECH) complex 3
2.2 Heat pump indoor unit 4
2.3 Heat pump outdoor unit 5
2.4 Heat pump system schematic 6
2.5 Installed desuperheater 6
2.6 Control system schematic 7
2.7 Data acquisition system 8
2.8 Typical heat pump heating cycle with defrost 9
2.9 TECH House III instrumentation 10
2.10 (a) Data acquisition interface; (b) data control logic interface 11
3.1 Steady-state heating COP vs outdoor air temperature 14
3.2 Steady-state heating capacity vs outdoor air temperature 14
3.3 Measured normal-mode capacity vs outdoor air temperature: April 1983 15
3.4 Measured normal-mode capacity vs outdoor air temperature: December 1981 16
3.5 Frosting/defrosting energy use penalty vs ambient operating temperature: 1981–82 heating season 19
3.6 Frosting/defrosting energy use penalty vs ambient operating temperature: 1982–83 heating season 19
3.7 Cycling energy use penalty vs ambient operating temperature: 1981–82 heating season 20
3.8 Cycling energy use penalty vs ambient operating temperature: 1982–83 heating season 21
3.9 Heat pump indoor unit inlet and exit air temperature vs time for a heating cycle with defrost 22
3.10 Fraction of defrost cycle space heating delivered during recovery from defrost period vs defrost time 23
3.11 Modal COP vs ambient operating temperature for 4-min transient period 25
3.12 Modal COP vs ambient operating temperature for 2-min transient period 26
3.13 Effects of dynamic losses on heating COP 27
3.14 COPRAT and CAPRAT vs heating load factor (Γ_h) based on steady-state, dry-coil capacity 28

3.15 COPRAT and CAPRAT vs heating load factor (Γ_h) based on normal-mode capacity ... 29
3.16 Cycles per hour vs ambient temperature ... 31
3.17 On-time per cycle vs ambient temperature ... 32
3.18 Off-time per cycle vs ambient temperature ... 33
3.19 Output loss per cycle vs ambient operating temperature ... 34
3.20 Output loss per cycle vs percent on-time ... 35
3.21 Output loss per cycle vs off-time per cycle ... 36
3.22 Increased input per cycle vs ambient operating temperature ... 38
3.23 Increased input per cycle vs off-time per cycle ... 39
3.24 Defrost time vs frosting potential ($-10°C < T < -5°C$) ... 40
3.25 Defrost time vs frosting potential ($-5°C < T < 0°C$) ... 40
3.26 Defrost time vs frosting potential ($0°C < T < 5°C$) ... 41
3.27 Defrost time vs frosting potential and outdoor air temperature ... 42
3.28 Heat pump modal COP vs ambient operating temperature with and without desuperheater (2-min delay time for start-up transient) ... 43
3.29 Heat pump modal COP vs ambient operating temperature with and without desuperheater (4-min delay time for start-up transient) ... 44
3.30 Normal-mode space heating capacity vs ambient operating temperature with and without desuperheater ... 45
3.31 Percent on-time vs outdoor air temperature ... 46
3.32 COPRAT and CAPRAT vs heating load factor (Γ_h) with and without desuperheater ... 47
3.33 Output loss per cycle vs off-time per cycle with and without desuperheater ... 47
3.34 Increased energy input per cycle vs off-time per cycle with and without desuperheater ... 48
3.35 Defrost time vs frosting potential with and without desuperheater ($-10°C < T < -5°C$) ... 49
3.36 Defrost time vs frosting potential with and without desuperheater ($-5°C < T < 0°C$) ... 49
3.37 Defrost time vs frosting potential with and without desuperheater ($0°C < T < 5°C$) ... 49
3.38 Overall energy consumption penalty vs ambient operating temperature with and without desuperheater ... 50
4.1 Steady-state cooling COP vs outdoor air temperature ... 53
4.2 Steady-state cooling capacity vs outdoor air temperature ... 53
4.3 Percent on-time vs outdoor air temperature ... 54
4.4 COPRAT and CAPRAT vs cooling load factor (Γ_c) based on manufacturer's steady-state rating ... 55
4.5 COPRAT and CAPRAT vs cooling load factor (Γ_c) based on 1980 on-site tests ... 56
4.6 COPRAT and CAPRAT vs cooling load factor (Γ_c) based on 1982 and 1983 on-site tests ... 56

4.7 COPRAT and CAPRAT vs cooling load factor (Γ_c), idealized 57
4.8 COPRAT and CAPRAT vs cooling load factor (Γ_c) based on derived steady-state performance (Eqs. 4.3 and 4.5) 60
4.9 Derived steady-state COP (Eq. 4.5) vs outdoor air temperature, with on-site test results 60
4.10 Derived steady-state capacity (Eq. 4.3) vs outdoor air temperature, with on-site test results 61
4.11 Derived steady-state COP and capacity (Eqs. 4.6 and 4.7) vs outdoor air temperature, with on-site test results 62
4.12 COPRAT and CAPRAT vs cooling load factor (Γ_c) based on derived steady-state performance (Eqs. 4.6 and 4.7) 63
4.13 Average ambient operating temperature vs average outdoor air temperature 65
4.14 Average COP vs average outdoor air temperature 66
4.15 Average COP vs average latent-to-total cooling ratio (25°C < T < 30°C) 67
4.16 Average COP vs average latent-to-total cooling ratio (30°C < T < 35°C) 68
4.17 Energy use penalty due to start-up transients vs ambient operating temperature 69
4.18 Energy use penalty due to start-up transients vs off-time per cycle 70
4.19 Energy use penalty due to start-up transients vs off-time per cycle (neglecting no-load hours) 71
4.20 Energy use penalty due to start-up transients vs percent on-time (neglecting no-load hours) 72
4.21 Normal-mode COP vs ambient operating temperature with and without desuperheater active 73
B.1 Averaging RTD used in air-side heat flow measurement 93
B.2 Vane anemometer used in air-side heat flow measurement 94
B.3 Schematic of heat pump indoor unit showing location of air-side heat flow instrumentation 94

LIST OF TABLES

2.1 ARI ratings for the test heat pump 5
2.2 TECH House III data variables and descriptions 12
3.1 Heating season monthly data sets 13
3.2 Energy consumption penalties due to dynamic losses during heating season 17
3.3 Effect of dynamic losses on heating seasonal performance factor (HSPF) 17
3.4 Comparison of heat pump performance degradation with different thermostats 18
3.5 Heating output and energy consumption at very cold ambient temperatures 20
3.6 Comparison of dynamic losses and cycling rates for 1981–82 and 1982–83 heating seasons 22
3.7 Average defrost cycle parameters 24
3.8 Percent on, CAPRAT, COPRAT, and heating load factor (Γ_h) vs ambient operating temperature for November 28, 1983, through December 11, 1983 29
4.1 Cooling season monthly data sets 51
4.2 Results of on-site steady-state cooling tests 52
4.3 Manufacturer's rated steady-state cooling performance data 52
4.4 Data for points 1 and 2 in Fig. 4.7 58
4.5 Measured average full-hour cooling mode power draw 59
4.6 Cooling season monthly dynamic losses, loads, and average temperatures 64
4.7 Average ambient conditions, indoor temperatures, and latent-to-total cooling ratios 67
4.8 Average monthly thermostat cycle parameters and energy use penalties due to start-up transients 68
5.1 Annual performance summary: 1982–83 75
5.2 Annual energy consumption fractions 76
5.3 Rated versus measured seasonal performance factors 76
A.1 Heating season condensed data 82
A.2 Dynamic loss characterization of heating operation 84
A.3 Cooling season condensed data 86
A.4 Cooling mode cycling parameters and losses 87

ACKNOWLEDGMENTS

The authors wish to express their gratitude to the following persons:

1. Phil Childs, who provided immeasurable help in taking the data and maintaining the test site;
2. D. R. Miller, who designed the data acquisition hardware;
3. Richard Higginbotham of Higginbotham Heating and Air Conditioning for his help in interfacing the data acquisition equipment with the heat pump control circuitry; and
4. Carolyn Srite, Kim Gaddis, and LeRoy Gilliam for many hours spent in preparing this report for publication.

ABSTRACT

An air-to-air heat pump was installed in a single-family residence near Knoxville, Tennessee, and was operated in a multiyear test to permit characterization of dynamic losses in capacity and efficiency due to cycling, frosting, and defrosting. The residence and heat pump were extensively instrumented, and a state-of-the-art data acquisition system logged data for each of the several system operating modes (start-up transient heating and cooling, normal-mode heating and cooling, and defrost with recovery) throughout the testing period.

For the test heating seasons, defrosting was responsible for 10.1%, losses due to frosting for 3.6%, on-off cycling losses for 8.4%, and off-cycle parasitics for 4.3% of the total energy consumption (exclusive of supplemental electric resistance heater energy use as required by second-stage thermostat demand). An overall heating seasonal performance factor of 1.96 was realized, and the value of the cyclic degradation factor, C_d, in heating was found to be 0.24. Both output loss per cycle and input energy increase per cycle were directly related to off-time per cycle, increasing strongly with off-times up to approximately 20 min and at a much lower rate thereafter. Defrost time per defrost cycle and the associated energy use penalty varied directly with frosting potential; the effect of ambient temperature on defrost time is not clear, and additional investigation is warranted. Use of a desuperheater for domestic water heating reduced the heat pump's space heating capacity but had no measurable effect on dynamic loss levels.

The steady-state cooling capacity and coefficient of performance (COP) of the heat pump were degraded from the manufacturer's ratings and those which were measured in initial steady-state tests, precluding definitive evaluation of dynamic losses during cooling operation. The cyclic degradation factor, C_d, in cooling was estimated to be between 0.20 and 0.25.

Air-Conditioning and Refrigeration Institute-rated heating seasonal performance factors (SPFs) for units with steady-state performance ratings similar to those of the test unit are within 4% of the measured values. Rated cooling SPFs appear to be about 34% higher than those measured in these tests. The steady-state performance degradation of the test unit accounted for about half of this difference.

1. INTRODUCTION

The performance of an air-to-air heat pump, when operating under field conditions, is degraded from that measured at steady state under laboratory conditions and reported by equipment manufacturers. During the heating season, this degradation in both capacity and coefficient of performance (COP) is due to three causes: frosting, defrosting, and cycling. During the cooling season, cycling is the prime cause of performance degradation.

Frost forms on the outside coil during heating operation when the coil surface temperature is below freezing and the ambient humidity is high. The buildup of frost restricts airflow across the coil and insulates the coil surface from the air stream. Both of these effects lower the refrigerant evaporating temperature, lowering both heating capacity and COP.

Periodically during heating operation, the heat pump switches to the defrost mode of operation to melt and drain away any frost that has accumulated on the outside coil. In this mode, the unit operates as an air conditioner, consuming power to run the compressor and indoor blower (the outside fan is idle) while pumping heat from the indoor air to the outside coil. To overcome this cooling effect and maintain indoor comfort, the auxiliary electric heaters are energized during defrosting (defrost tempering I^2R). The net result is the consumption of a significant amount of energy with little net heat addition to the indoor air.

The almost universally used method for matching the heat output or cooling rate (capacity) of a residential heat pump to the building requirements for heating or cooling is to cycle the heat pump on and off, with the product of fractional on-time and capacity approximating the building heating or cooling requirement. At the beginning of the on portion of each on-off cycle, a finite period of time elapses before the heat pump reaches a steady-state operating condition and produces its full heating or cooling capacity. As a result, for each on-off cycle, energy is consumed by the compressor and indoor and outdoor air movers while system equilibrium is being established, and the heating or cooling output rate is low.

A multiyear test was conducted to permit characterizing performance of a residential heat pump operating in a real-world setting; the objective was to quantify, insofar as possible, the magnitudes of its various operating losses. The test unit was installed in a single-family house, which was dedicated exclusively to the test, and was operated to provide total comfort conditioning for the house over two winters and two summers. The house and heat pump were extensively instrumented, and a state-of-the-art data acquisition system (DAS) logged data for each of the several system operating modes (start-up transient heating and cooling, normal-mode heating and cooling, and defrost with recovery) throughout the testing period.

The house and heat pump system were exposed to a wide spectrum of operating conditions during the test. Unlike laboratory tests, where conditions are imposed and

carefully controlled, the house and system faced the rigors of completely uncontrolled ambient conditions, including rain, snow, wind, and sunshine, that few laboratories can effectively simulate. As a result, some of the collected data as reported in the following sections contain a degree of scatter that may appall the investigator accustomed to dealing with laboratory-acquired data and that certainly presents a challenge in interpretation.

Our analysis and interpretation of the data admittedly borders on speculation in some areas. However, we feel that the data are valid and that real performance trends have been identified and, in many cases, quantified. In this context, the following sections present a description of the test facilities and the testing procedures, the data derived therefrom, and our analysis of those data.

Results reported herein are equipment-specific and cannot be generalized for all heat pumps. Certain dynamic losses are known to be related to specific design features such as type of defrost control or heat exchanger configuration. The results can be quite useful, however, for validation of computer codes used to predict annual or seasonal performance of air-source heat pumps.

2. TEST SITE AND EQUIPMENT

2.1 TEST FACILITIES

TECH House III is located on the Tennessee Energy Conservation in Housing (TECH) complex (Fig. 2.1), near Knoxville, Tennessee. TECH House III is a 167-m^2, well-insulated structure. It was unoccupied during the tests but had internal loads simulating occupancy by a family of four. The TECH complex is a joint project of the U.S. Department of Energy (DOE), the University of Tennessee, the Tennessee Valley Authority, and Oak Ridge National Laboratory (ORNL) for the purpose of testing various means of conserving energy in residences. A complete description of the complex may be found in refs. 1 and 2.

ORNL-PHOTO 1797-81R

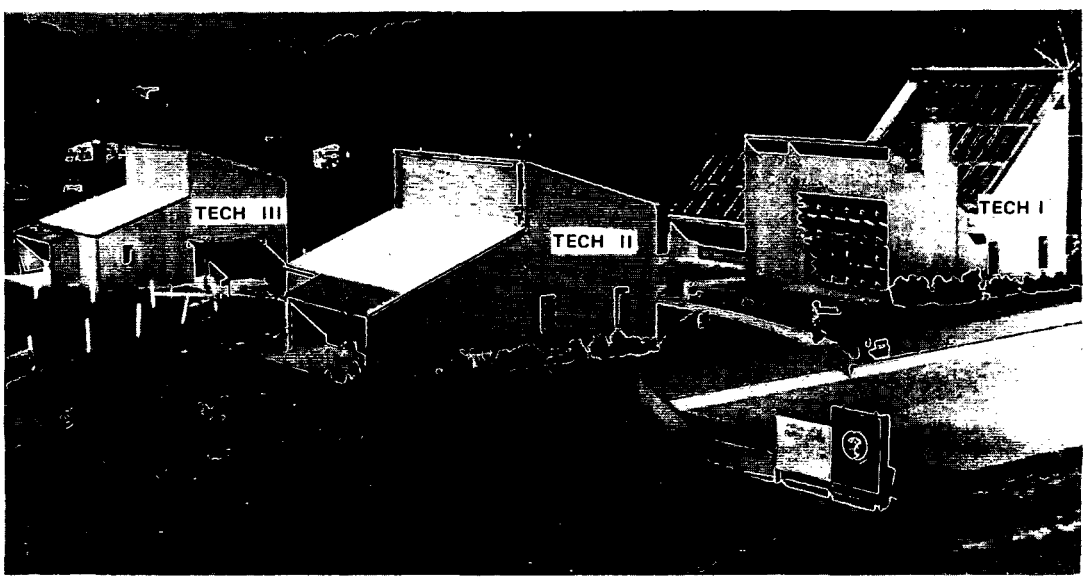

Fig. 2.1. Tennessee Energy Conservation in Housing (TECH) complex.

2.2 TEST EQUIPMENT

The heat pump system used for these tests was a state-of-the-art heat pump, installed in November 1979, which has a rated COP of 3.11 at 8.3°C. Figures 2.2 and 2.3 show the indoor and outdoor units of the heat pump. The Air-Conditioning and Refrigeration Institute (ARI) heating and cooling ratings are given in Table 2.1. Tests during 1979 and 1980 showed the heat pump to have heating and cooling seasonal performance factors of 1.99 and 2.27 respectively.[2] The unit employed a time-temperature type of defrost control.

ORNL-PHOTO 6903-80

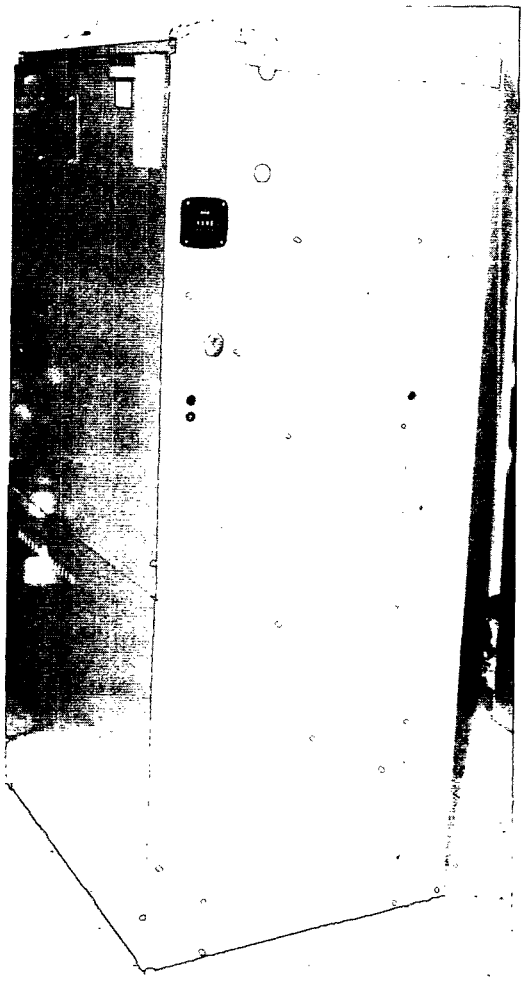

Fig. 2.2. Heat pump indoor unit.

In the fall of 1980 the system was modified by addition of a desuperheater water heater (DSWH), a small heat exchanger that uses hot refrigerant gas leaving the heat pump compressor to provide domestic hot water. Figures 2.4 and 2.5 show schematics of the modified system and a picture of the DSWH, respectively. From November 1981 through September 1982 the system was operated with the desuperheater active in alternate months. After September 1982 the desuperheater was not used. Reference 3 reports on the performance of the heat pump/DSWH system.

A schematic of the heat pump control wiring is shown in Fig. 2.6. Two significant modifications were made to the controls in November 1982. The original thermostat, a Honeywell Chronotherm, which cycled at a maximum rate of 6 cycles per hour (cph) at 50% load, was replaced with a standard General Electric (GE) model with a maximum cycling rate of 5 cph. This was done to test the effect of cycling rate on measured cycling losses. At the same time, it was noticed that the heat pump compressor sometimes failed to start immediately when the thermostat signaled a need for heat. A hard-start kit (to provide

ORNL-PHOTO 6901-80

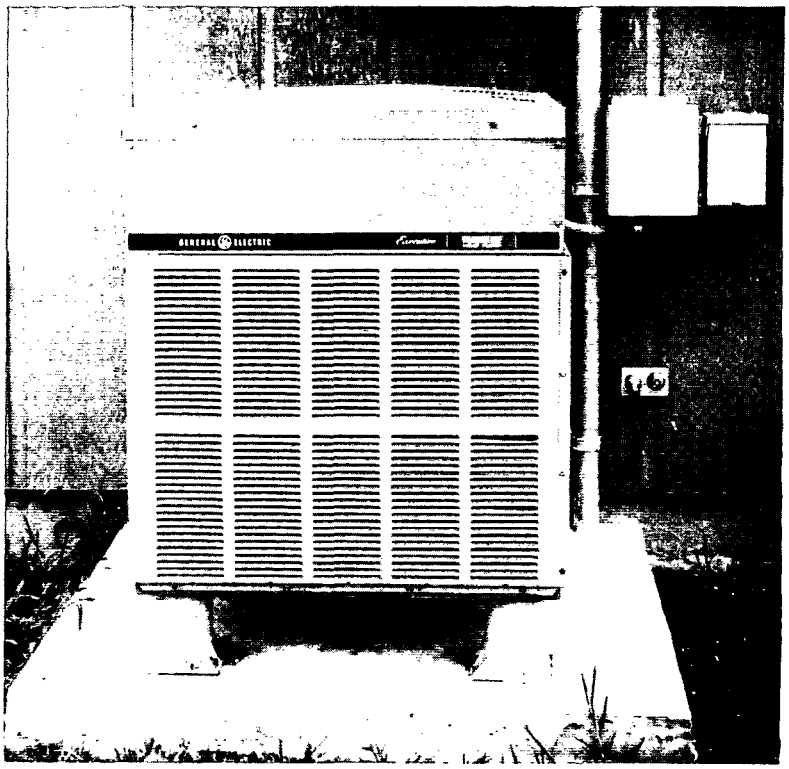

Fig. 2.3. Heat pump outdoor unit.

Table 2.1. ARI ratings for the test heat pump

	Heating ratings		Cooling rating
	High temperature	Low temperature	
Temperature, °C	8.3	−8.3	35.0
Capacity, W	9965	5276	9818
Energy input, W	3200	2550	3900
COP	3.11	2.07	2.52

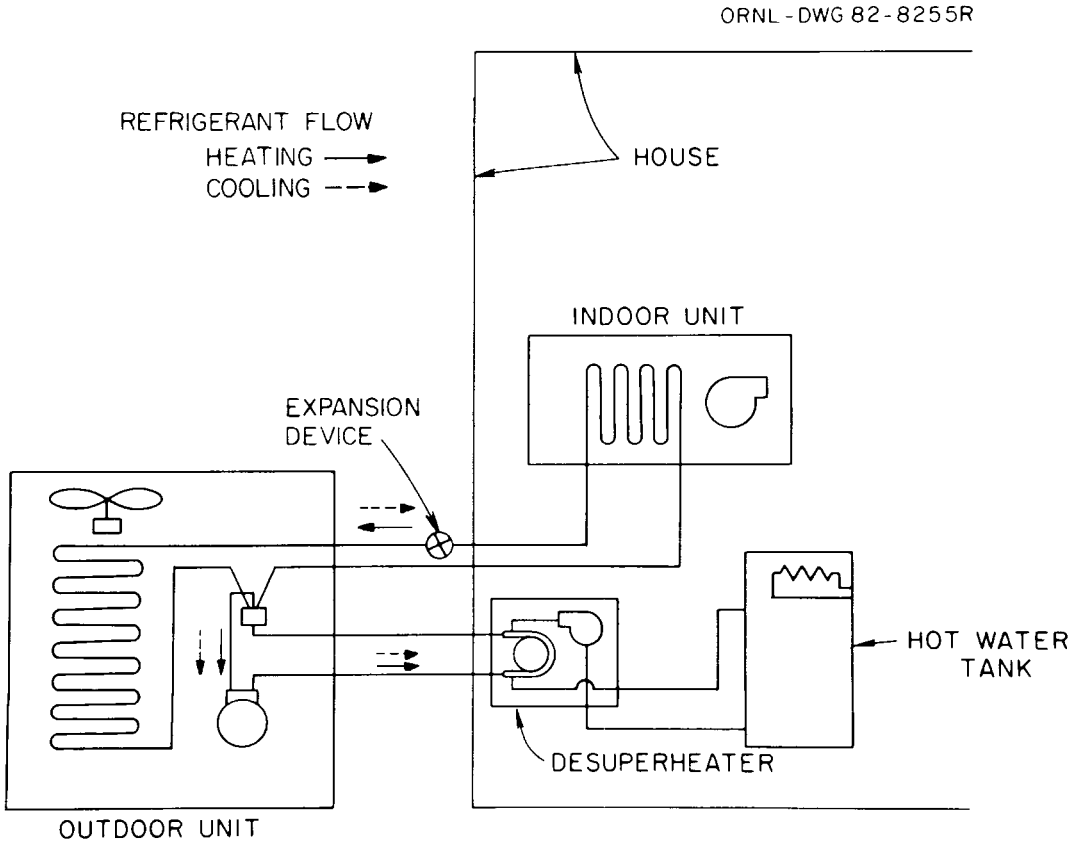

Fig. 2.4. Heat pump system schematic.

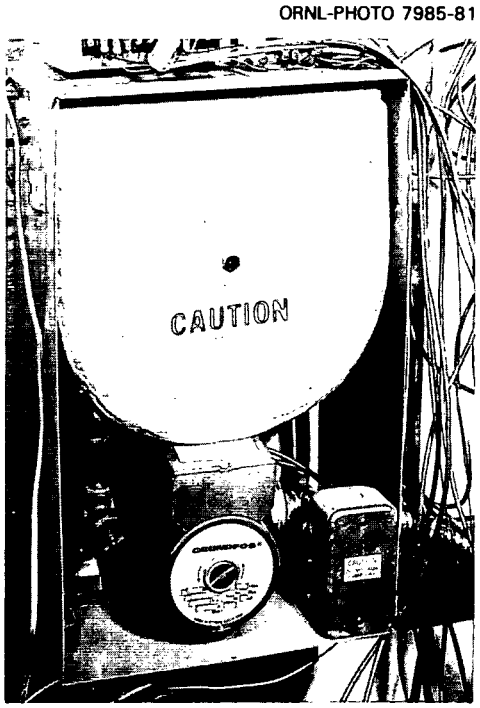

Fig. 2.5. Installed desuperheater.

ORNL-DWG 82-7958RA

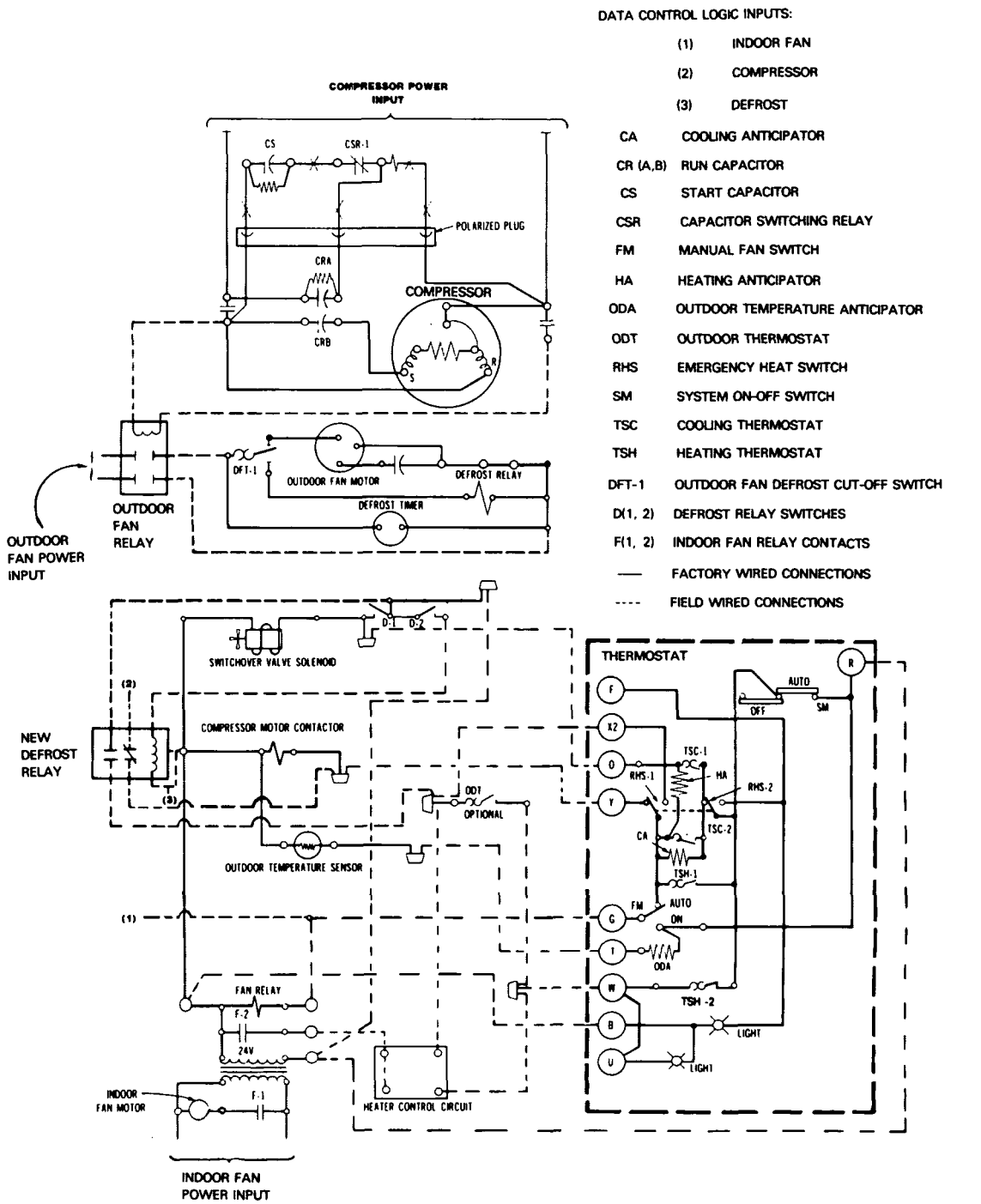

Fig. 2.6. Control system schematic.

increased torque to the compressor motor on start-up) was added to the control circuit to alleviate this problem. Addition of this kit raised the off-cycle energy use rate from 53.5 to 80.0 W.

2.3 DATA ACQUISITION

A DAS located in TECH House II monitors data in all houses of the complex (Fig. 2.7). For the tests described in this report, the DAS monitored hourly integrated totals of space heating and sensible cooling heat flows; energy consumption by compressor, indoor and outdoor fans, and backup electric resistance (I^2R) space heating elements; and condensate collection during the cooling season. In addition, an on-site weather station monitored dry-bulb and dew-point temperatures, wind speed, rainfall, barometric pressure, wind direction, and solar radiation. All data were logged hourly.

ORNL-PHOTO 1812-83

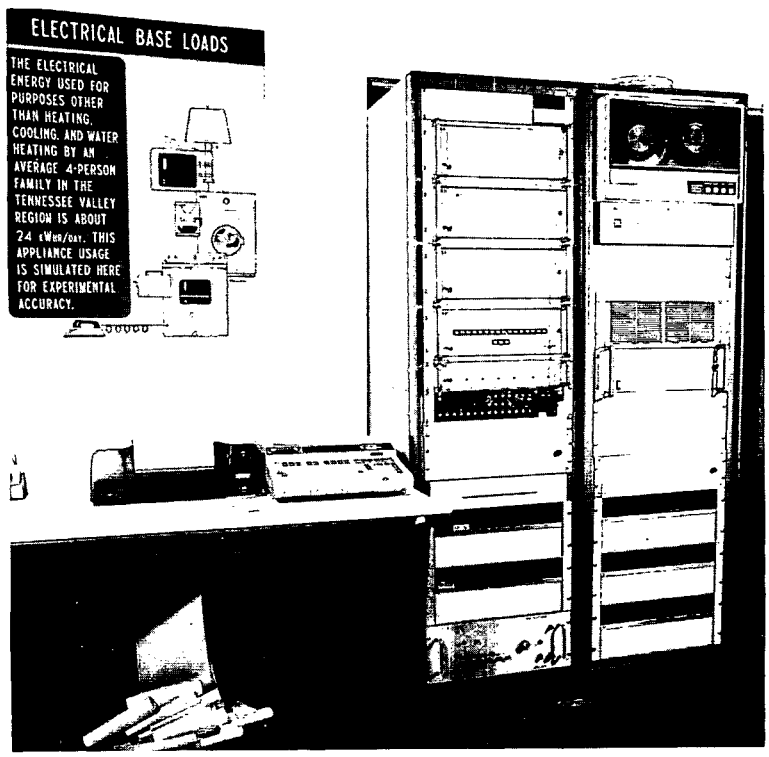

Fig. 2.7. Data acquisition system.

Space heating and sensible cooling loads delivered by the heat pump were measured by means of an air-side heat flow metering system consisting of two averaging resistance temperature devices (RTDs) and a vane anemometer located in the return air duct. Electric energy consumption is measured by conventional watt-hour meters fitted with optical disc revolution counters. Condensate collection in the cooling season is measured by a recording rain gage. A more detailed description of the instrumentation is given in refs. 4 and 5.

In order to be able to quantify the dynamic losses of the heat pump it was necessary to store energy consumption and delivery data in different sets of channels according to mode of operation (start-up transient, normal operation, defrost operation). Figure 2.8 shows heat pump capacity through a typical heating cycle with a defrost, illustrating the different data acquisition modes. Instrumentation for this experiment is shown in Fig. 2.9. The DAS interface [Fig. 2.10(a)] was set up to store data in one set of channels during the first 2 to

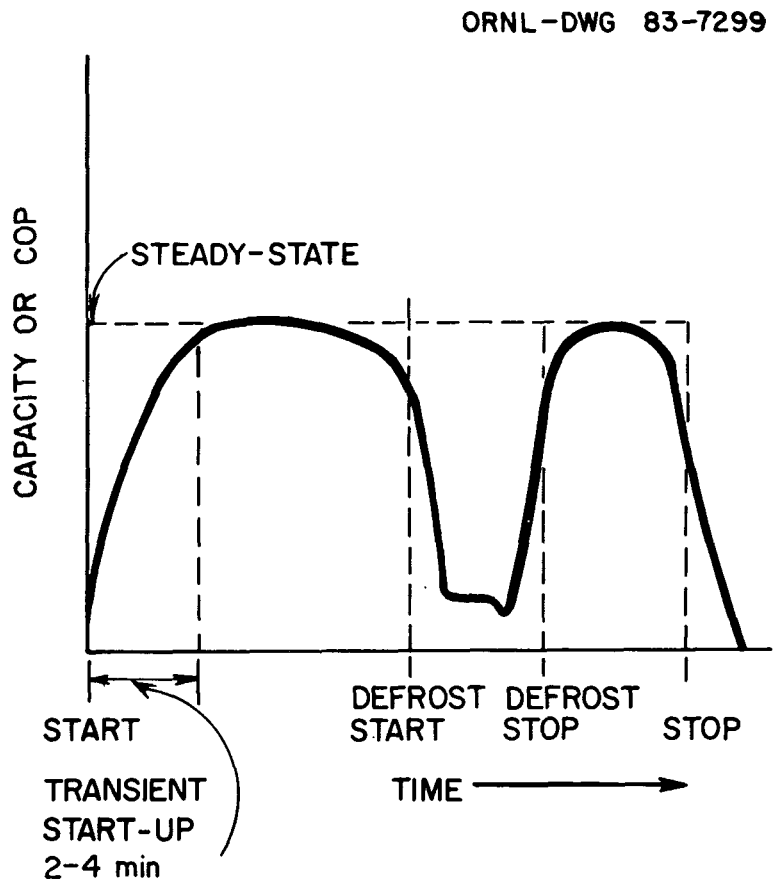

Fig. 2.8. Typical heat pump heating cycle with defrost.

5 min of each cycle (start-up transient), in a second set during defrost and return from defrost recovery periods (defrost), and a third set at all other times during the cycle (normal). A logic interface [Fig. 2.10(b)] accepts 24-V AC signals from the heat pump control system and converts them to 10-V DC logic signals which control the DAS interface. The logic signals used are

1. indoor fan—initiates a start-up transient delay time period each time the indoor fan starts,
2. compressor—indicates that the system is delivering heating or cooling and permits data to be sent to the DAS, and
3. defrost—causes the interface to send data to defrost channels during defrost cycle and for 1.25 min after defrost.

The logic interface also provides signals to monitor the number of thermostat cycles and defrost cycles each hour. This interface originally used the 24-V AC control power of the heat pump as its power source. This caused no problem during the heating season; however, it was discovered that it induced longer-than-normal cycles in the cooling season. The

ORNL-PHOTO 3976-84

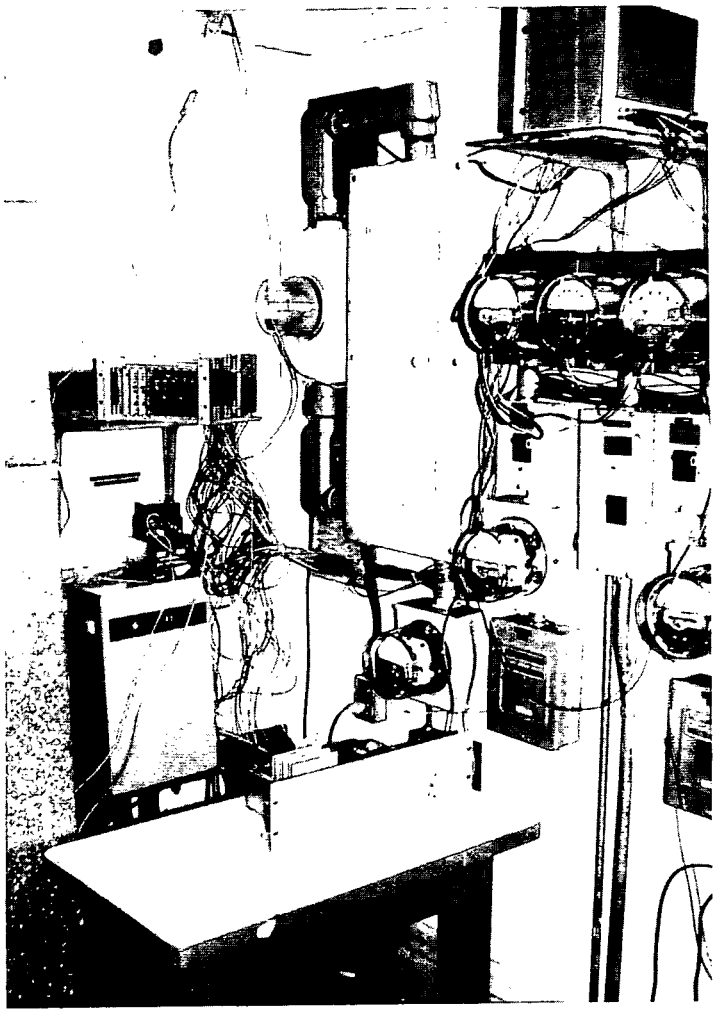

Fig. 2.9. TECH House III instrumentation.

(a)

ORNL-PHOTO 7983-81

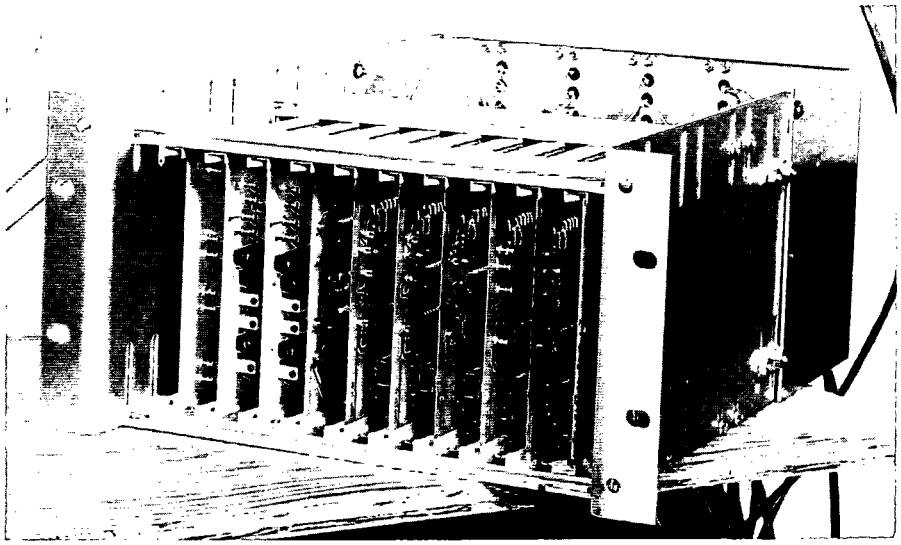

(b)

ORNL-PHOTO 3975-84

Fig. 2.10. (a) Data acquisition interface; (b) data control logic interface.

interface was replaced in early July 1982 with one that is independently powered [Fig. 2.10(b)], and the problem was resolved.

A list of the TECH site data variables used for the TECH House III experiments is given in Table 2.2.

Table 2.2. TECH House III data variables and descriptions

Variable[a]	Name	Description
		Measured data
50	IDFt	Indoor fan energy use during start-up transient, Wh
51	IDFn	Indoor fan energy use during normal mode, Wh
52	IDFd	Indoor fan energy use during defrost, Wh
53	ODFt	Outdoor fan energy use during start-up transient, Wh
54	ODFn	Outdoor fan energy use during normal mode, Wh
55	ODFd	Outdoor fan energy use during defrost, Wh
56	COMt	Compressor energy use during start-up transient, Wh
57	COMn	Compressor energy use during normal mode, Wh
58	COMd	Compressor energy use during defrost, Wh
59	I2Rt	Backup heat energy use during start-up transient, Wh
60	I2Rn	Backup heat energy use during normal mode, Wh
61	I2Rd	Backup heat energy use during defrost, Wh
63	ONCY	Thermostat cycles
64	DFCY	Defrost cycles
65	CONc	Cooling mode condensate collection, kg
76	HFLt	Sensible heat/cool delivered during start-up transient, Wh
77	HFLn	Sensible heat/cool delivered during normal mode, Wh
78	HFLd	Sensible heat/cool delivered during defrost, Wh
80	Qsen	Total sensible heat/cool delivered, Wh
130	Tdew	Outdoor dew point, °C
131	Tdry	Outdoor dry-bulb temperature, °C
		Values calculated by DAS each hour
15	ODRH	Outdoor relative humidity, %
30	CCHE	Off-cycle energy use, Wh
219(399)[b]	HTLD	Total heating delivered, Wh
220(400)	COOL	Total cooling delivered, Wh
222(402)	Qlat	Latent cooling delivered, Wh

[a]For 235-variable data sets.
[b]Numbers in parentheses are variable numbers for 420-variable data sets.

3. HEATING SEASON PERFORMANCE

The results of tests run during eight winter months over the 1981-82 and 1982-83 heating seasons and analyses of the test data are described in this section. Table 3.1 lists the eight monthly data sets and the number of hours included in each upon which the subsequent test results and analyses are based. A detailed tabulation of the compressed raw data set and test results is given in Appendix A, Tables A.1 and A.2, for 5°C-wide bins for each month (bin-month). Unless otherwise indicated, data in figures and tables are presented on a bin-month basis. The following sections will discuss steady-state performance, measured energy use penalties caused by the various loss mechanisms, the effect of reducing cycling rate on overall performance, defrost-mode performance, and the results of the data analyses. About two weeks of additional data were collected in November and December of 1983 to supplement the data available for 4-min start-up transient time.

Table 3.1. Heating season monthly data sets

Month	Days included in data set	Data hours[a]
December 1981	December 16–30	359
February 1982	February 1-28	666
April 1982	April 2–May 2	743
December 1982	December 3-31	649
January 1983	January 1-5, 11-31	622
February 1983	February 1-7, 16-28	488
March 1983	March 1-8, 15-31	597
April 1983	April 1-30	719

[a]Total hours minus those hours with missing or suspect data.

3.1 STEADY-STATE PERFORMANCE BASE

Two sources are available for determining the steady-state performance of the test heat pump—the ARI ratings and steady-state laboratory tests performed by Miller[6] at ORNL on an identical unit. Figures 3.1 and 3.2, COP and capacity plots of both the laboratory data and the ARI ratings, show slight differences between the two. Hourly field measurements of normal-mode capacity vs temperature for April 1983 and December 1981 are plotted in Figs. 3.3 and 3.4. It is apparent that the straight line developed from the laboratory data fits the site-measured capacities better than the line taken from the ARI rating points,

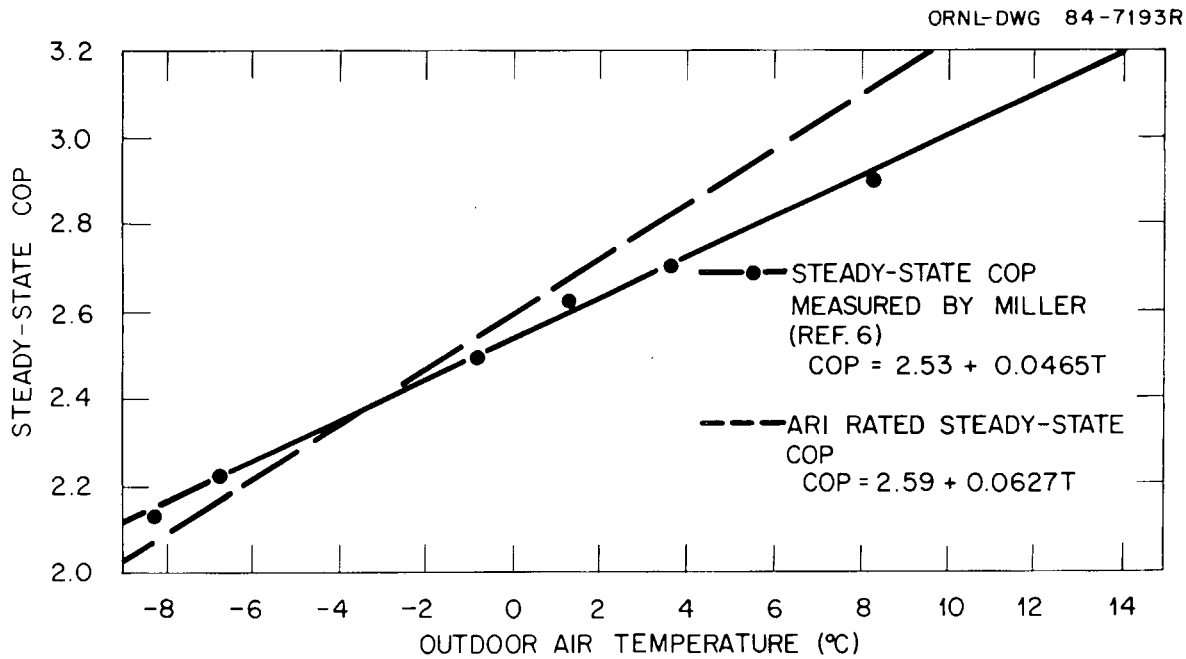

Fig. 3.1. Steady-state heating COP vs outdoor air temperature.

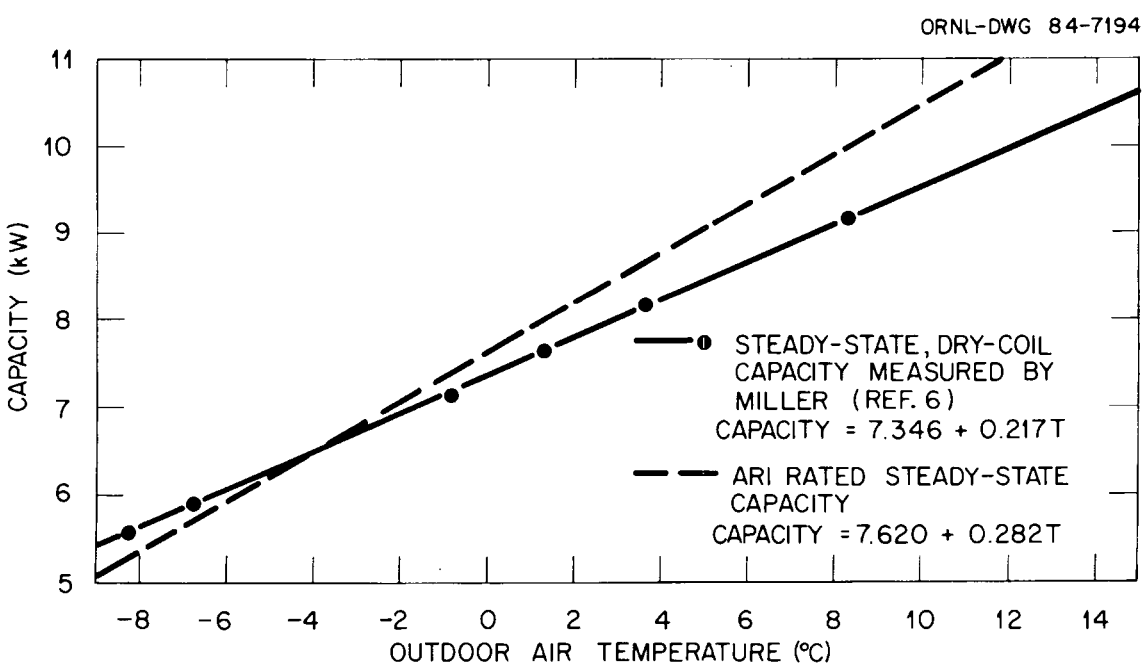

Fig. 3.2. Steady-state heating capacity vs outdoor air temperature.

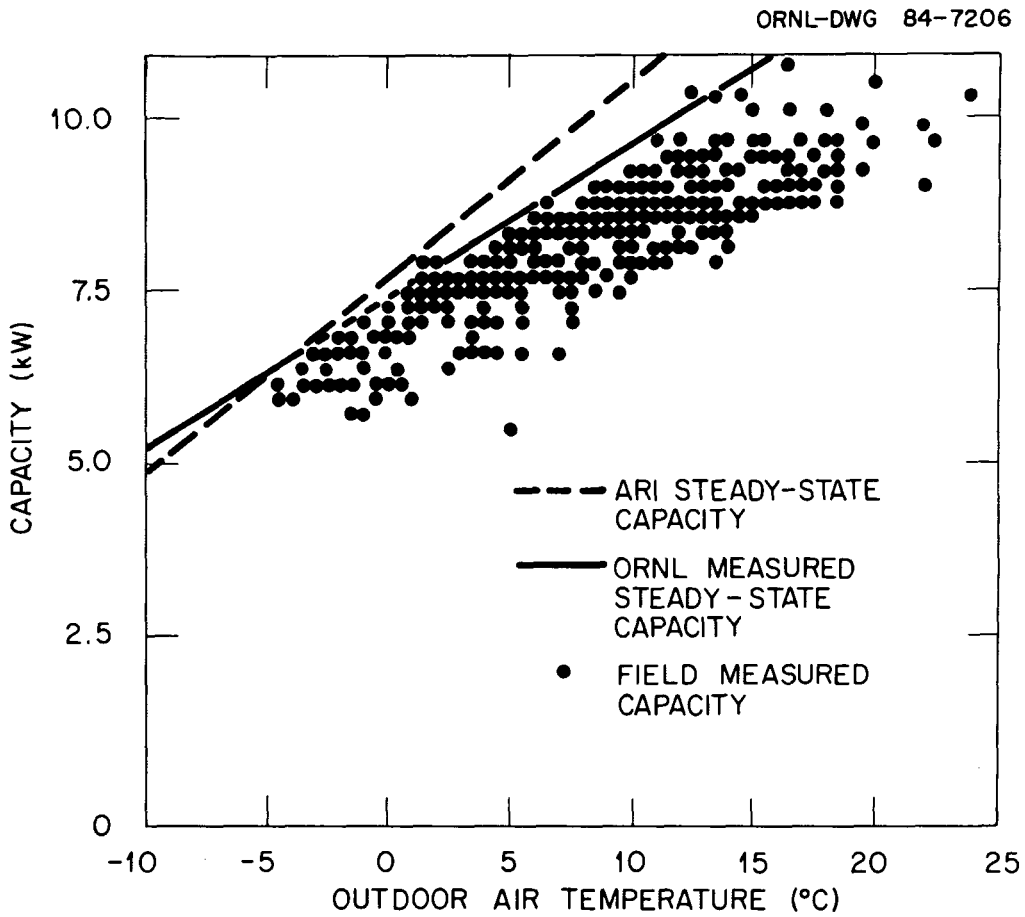

Fig. 3.3. Measured normal-mode capacity vs outdoor air temperature: April 1983.

especially at the higher and lower ends of the temperature scale. A large number of the hourly measurements do not reach steady-state performance level because of frosting and/or cycling effects.

Based on the results presented above, it was decided to use the laboratory measurements as the base steady-state performance for the heating mode.

3.2 TEST RESULTS

Table 3.2 lists energy consumption penalties due to cycling, frosting, and defrosting. The table gives, for each monthly data set, the following:

1. delivered heating load,
2. supplemental resistance heat (I^2R) required if the unit ran at steady-state efficiency with no dynamic losses,
3. I^2R required to make up for loss in capacity due to frosting,
4. off-cycle energy use,

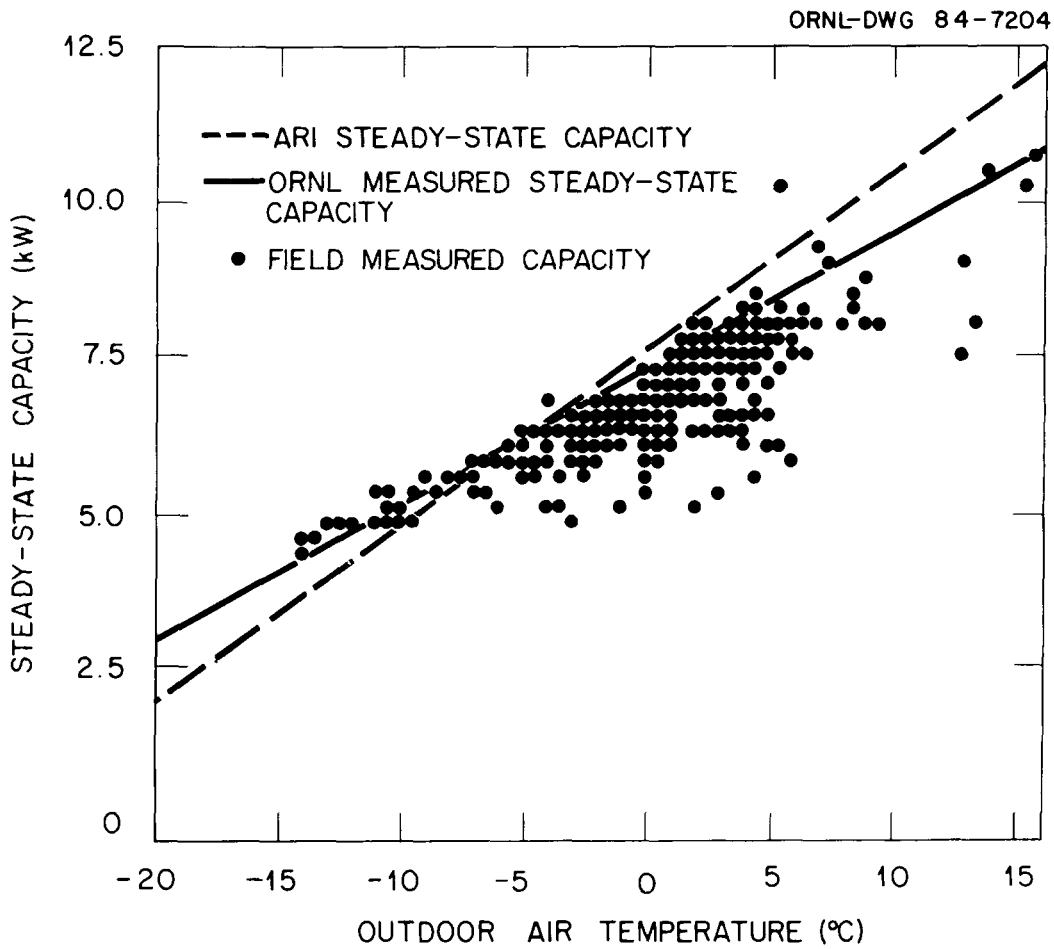

Fig. 3.4. Measured normal-mode capacity vs outdoor air temperature: December 1981.

5. start-up transient energy use penalty,
6. defrost energy use penalty (including defrost tempering I^2R),
7. non-I^2R frosting energy use penalty,
8. steady-state energy use required to meet the load (minus required supplemental I^2R), and
9. total energy use minus required supplemental I^2R.

A sample calculation of energy use penalties is given in Appendix A (Sect. A.2.3).

Examination of the data in the table reveals that, overall, defrosting accounted for 10.1% of the total energy use, frosting (including I^2R use due to capacity reduction) 3.6%, start-up transients 8.4%, and off-cycle parasitics 4.3%. "Total energy use" here and subsequently in all figures and tables is to be understood as total minus required supplemental I^2R unless otherwise specified.

Table 3.2. Energy consumption penalties due to dynamic losses during heating season

Month	Heating load (kWh)	Supplemental I^2R (kWh)		Off-cycle energy use (kWh)	Start-up transient energy use penalty (kWh)	Defrost energy use penalty (kWh)	Frosting energy use penalty (kWh)	Steady-state energy use required[a] (kWh)	Total energy use[b] (kWh)
		required	caused by frosting capacity loss						
December 1981	1,332.4	26.2	9.1	8.4	45.8	103.1	12.0	525.6	704.1
February 1982	1,828.9	4.3	4.6	22.0	81.4	93.3	27.1	689.2	917.6
April 1982	586.1	0.0	0.0	35.6	52.5	7.6	5.6	206.6	308.0
December 1982	1,419.1	0.7	2.6	34.8	48.6	97.3	30.5	536.1	749.8
January 1983	2,102.3	6.9	1.8	24.6	58.4	126.0	54.0	816.0	1,080.8
February 1983	1,331.5	0.0	0.0	23.4	48.3	76.4	25.7	504.3	678.1
March 1983	974.7	0.0	0.0	36.9	54.0	26.8	14.7	355.4	487.9
April 1983	1,039.3	0.0	0.0	46.3	67.6	21.7	11.2	369.6	516.4
Total	10,614.2	38.1	18.1	232.0	456.6	552.2	180.8	4,002.8	5,442.5
Percent[c]			0.3	4.3	8.4	10.1	3.3	73.6	100.0

[a]Energy required to meet heating load minus required supplemental I^2R.
[b]Does not include required supplemental I^2R.
[c]Percent of total energy use.

Table 3.3 shows the effect of these energy consumption penalties on heating seasonal performance factor (HSPF). Exclusive of supplemental heat requirements, there was an overall degradation in HSPF of 26.5% (from 2.642 to 1.943). About 52% of this degradation was due to frosting/defrosting losses with the remainder caused by cycling losses (off-cycle parasitics and start-up transients). A sample calculation of energy use penalties for a bin-month is given by Appendix A (Sect. A.2.1).

3.2.1 Effect of Cycling Rate Reduction

As mentioned in Sect. 2, the Honeywell thermostat was replaced in November 1982 with a GE model having a slightly lower cycling rate. Table 3.4 presents a comparison of heat pump performance between two months using different thermostats. The data in the table

Table 3.3. Effect of dynamic losses on heating seasonal performance factor (HSPF)

(1) Measured HSPF	1.937
(2) Measured HSPF without supplemental resistance heat	1.943
(3) HSPF (2) without off-cycle parasitic losses	2.030
(4) HSPF (2) without start-up transient losses	2.121
(5) HSPF (2) without defrost losses	2.163
(6) HSPF (2) without frosting losses	2.017
(7) HSPF (2) with no losses	2.642
(8) HSPF (7) with supplemental resistance heat	2.627

Table 3.4. Comparison of heat pump performance degradation with different thermostats

	December 1982 (GE thermostat; ~ 5 cph at 50% load)	February 1982 (Honeywell thermostat; ~ 6 cph at 50% load)
Ambient operating temperature, °C		
Transient	4.3	4.2
Normal	1.7	2.0
Defrost	−0.3	−0.6
Overall average	2.3	2.6
Degradation from steady-state capacity, %		
Transient	20.3	19.2
Normal	11.0	6.6
Defrost	57.3	55.9
Overall average	14.6	10.2
Total cycles	1627	2549
Average on-time per cycle, min	7.8	6.1
Transient time, % of total	26.7	31.3
Total defrosts	96	110
Defrost energy usage, % of total	15.7	12.0
Supplemental I^2R, kWh	3.3	8.9
Off-cycle parasitic, kWh[a]	35.2	16.0
COP	1.90	1.99

[a]Off-cycle parasitic power draw increased from 53.5 W to 80 W with installation of the hard-start kit in November 1982.

reveal several interesting points. Average on-time per cycle increased from 6.1 to 7.8 min. Capacity degradation in the transient mode was about 6% higher with the 5-cph thermostat than with the 6-cph thermostat, suggesting that cyclic capacity losses are not directly proportional to cycling rate. Degradation of normal-mode capacity was about 67% higher (from 6.6 to 11%) with the lower cycling rate thermostat, indicating that possibly the longer average on-time was conducive to greater frosting losses.

Figures 3.5 and 3.6 are plots of the energy use penalty, in percentage of total heat pump energy consumption, due to frosting and defrosting losses vs ambient operating temperature for the 1981–82 and 1982–83 heating seasons, respectively. Defrost degradations were not greatly different from one season to the next. Frosting degradation levels were similar for temperatures above −6°C. At lower temperatures, however, frosting losses were much higher in the 1982–83 season. These losses correspond to periods when the heat pump was running almost constantly. As illustrated in Table 3.5, during those periods the heating capacity became progressively lower and the energy consumption higher from hour to hour, indicating that perhaps the coil was not being defrosted thoroughly and was, therefore, becoming ice covered.

Energy use penalty, in percentage of total energy consumption, due to start-up transients and off-cycle parasitics is plotted vs ambient operating temperature in Figs. 3.7 and 3.8. Energy consumption caused by start-up transient losses was greater in the 1981–82 season at all temperatures because of the higher cycling rate prevalent during that time. Off-cycle

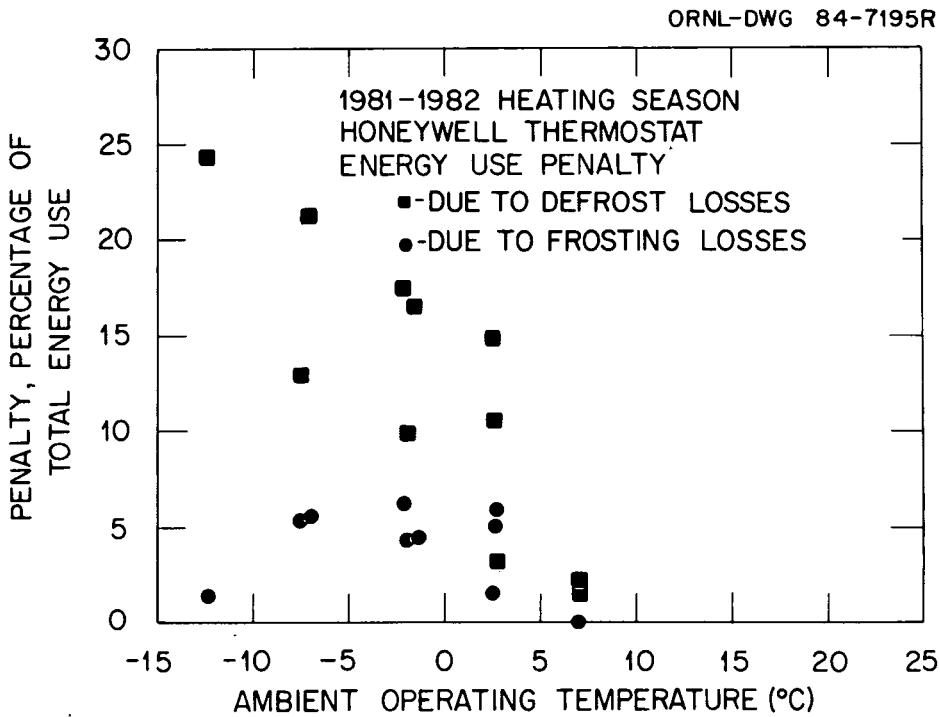

Fig. 3.5. Frosting/defrosting energy use penalty vs ambient operating temperature: 1981–82 heating season.

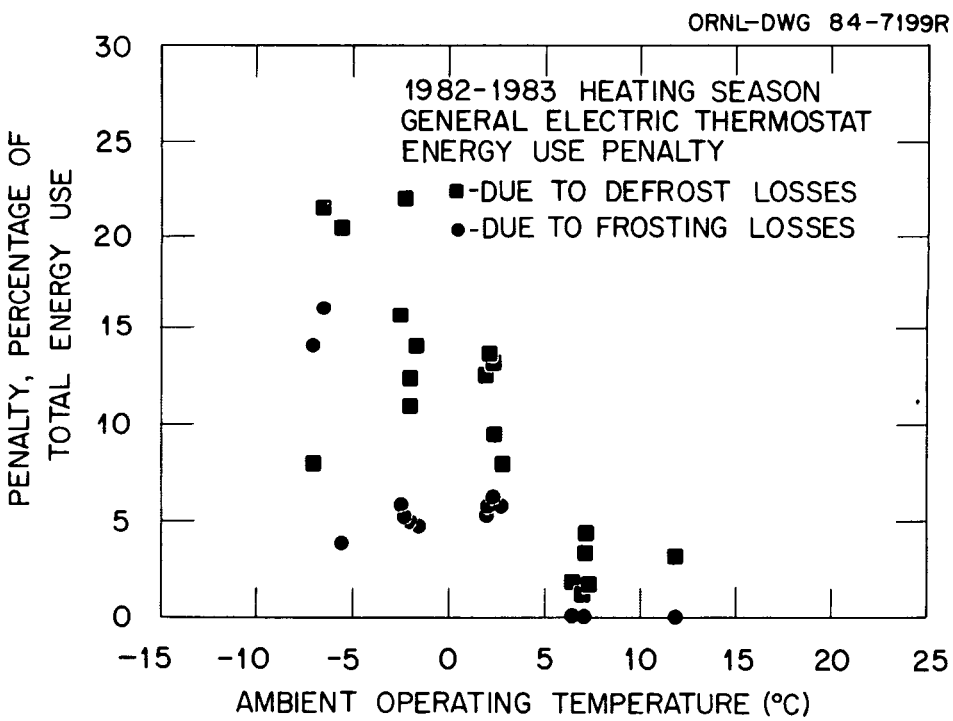

Fig. 3.6. Frosting/defrosting energy use penalty vs ambient operating temperature: 1982–83 heating season.

Table 3.5. Heating output and energy consumption at very cold ambient temperatures

Date	Time[a]	Heat output (Wh)	Energy use (Wh)	Temperature (°C)
December 14, 1982[b]	2:00-3:00 a.m.	5627	3041	−6.3
	5:00-6:00 a.m.	5548	3078	−7.3
January 18, 1983[c]	5:00-6:00 a.m.	5671	2882	−6.5
	8:00-9:00 a.m.	5553	3433	−6.4

[a]Hourly periods with no defrost occurrence.
[b]Heat pump on continuously from 1:00 through 6:00 a.m.
[c]Heat pump on continuously from 3:00 through 9:00 a.m.

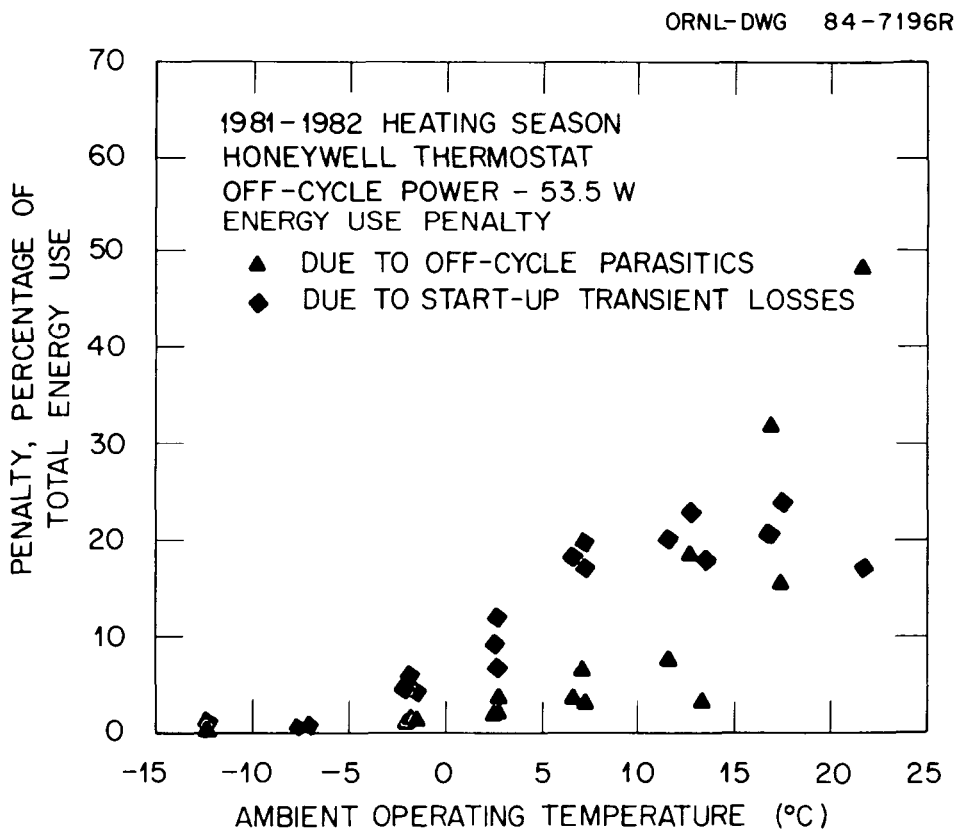

Fig. 3.7. Cycling energy use penalty vs ambient operating temperature: 1981–82 heating season.

parasitic energy consumption was higher in 1982-83 because of the increased off-cycle power rate caused by the addition of the hard-start kit. Table 3.6 gives an overall performance comparison between the 1981-82 and 1982-83 seasons. The start-up transient energy use fraction was lower in 1982-83 because of the lower cycling rate, while the frosting energy use fraction was higher. The increase in frosting energy use is most likely due to longer run

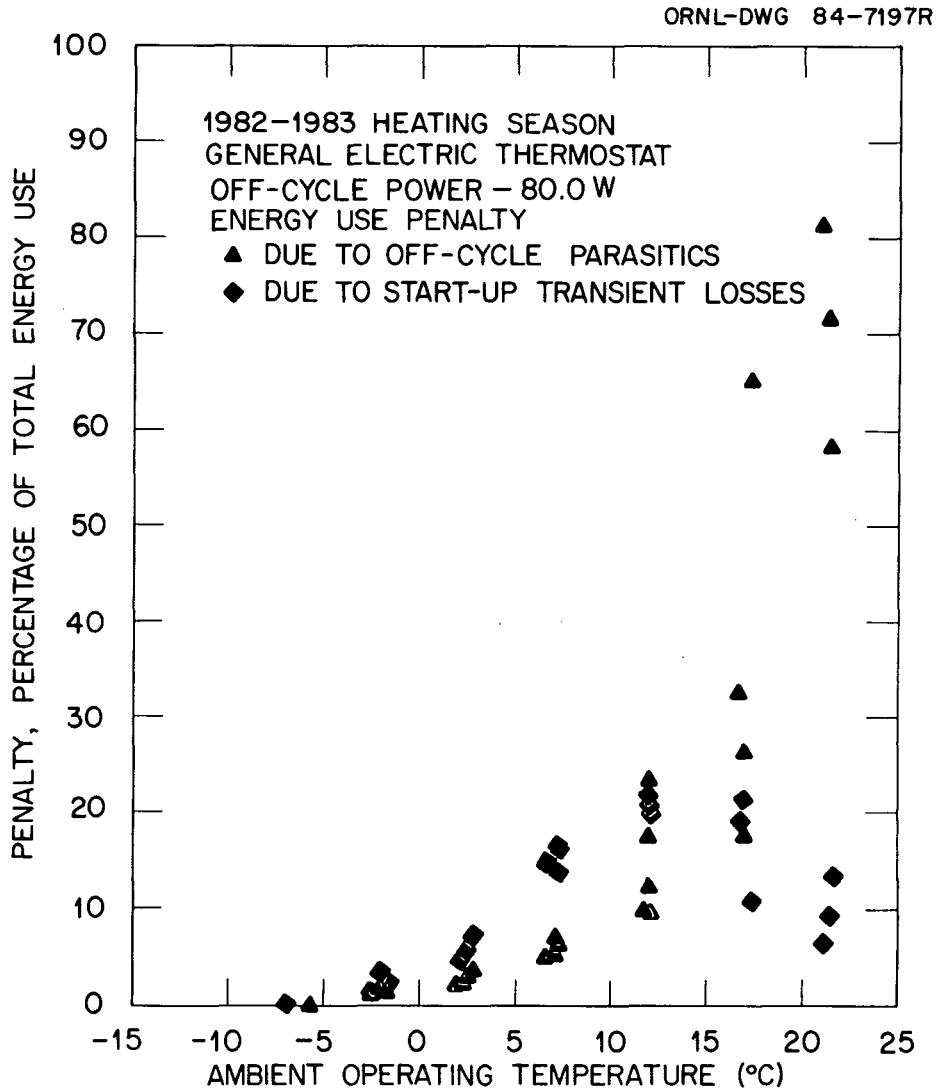

Fig. 3.8. Cycling energy use penalty vs ambient operating temperature: 1982–83 heating season.

times per cycle and the fact that a larger percentage of the run hours were spent in the temperature range most susceptible to frost formation. The overall HSPF was slightly higher in 1982-83 than in 1981-82, but so was the average operating temperature. Reducing the nominal cycling rate from 6 to 5 cph did not significantly improve the seasonal efficiency of the test heat pump. Possibly a greater reduction in maximum cycling rate (for example, from 6 to 3 cph, as assumed by the DOE test standards) would have had a more noticeable effect.

3.2.2 Defrost Cycle Characterization

As mentioned in Sect. 2.3, defrost-mode data collection begins with the onset of a defrost cycle and continues for about 1.25 min after defrost termination. Use of this scheme charges

Table 3.6. Comparison of dynamic losses and cycling rates for 1981–82 and 1982–83 heating seasons

Season	Delivered heating load (kWh)	Energy consumption (kWh)		Percent heat pump energy use due to losses				HSPF	Thermostat cycles	Run time per cycle (min)
		Supplemental heat	Heat pump	(1)[a]	(2)[a]	(3)[a]	(4)[a]			
1981-82[b]	3747.4	30.5	1929.5	3.4	9.3	10.6	3.0	1.908	5067	6.42
1982-83[c]	6866.8	7.6	3513.0	4.7	7.9	9.9	4.0	1.950	8067	7.41

[a](1) Off-cycle parasitic losses.
(2) Start-up transient losses.
(3) Defrosting losses.
(4) Frosting losses.
[b]Honeywell thermostat—6 cph at 50% load; off-cycle power rate = 53.5 W.
[c]GE thermostat—5 cph at 50% load; off-cycle power rate = 80.0 W.

the defrost mode with most of the recovery transient period immediately following, as shown in Fig. 3.9. This figure illustrates the air temperature rise across the indoor unit during a complete heating cycle with a defrost. The area between the entering and leaving temperature curves is proportional to the heating energy delivered by the heat pump during

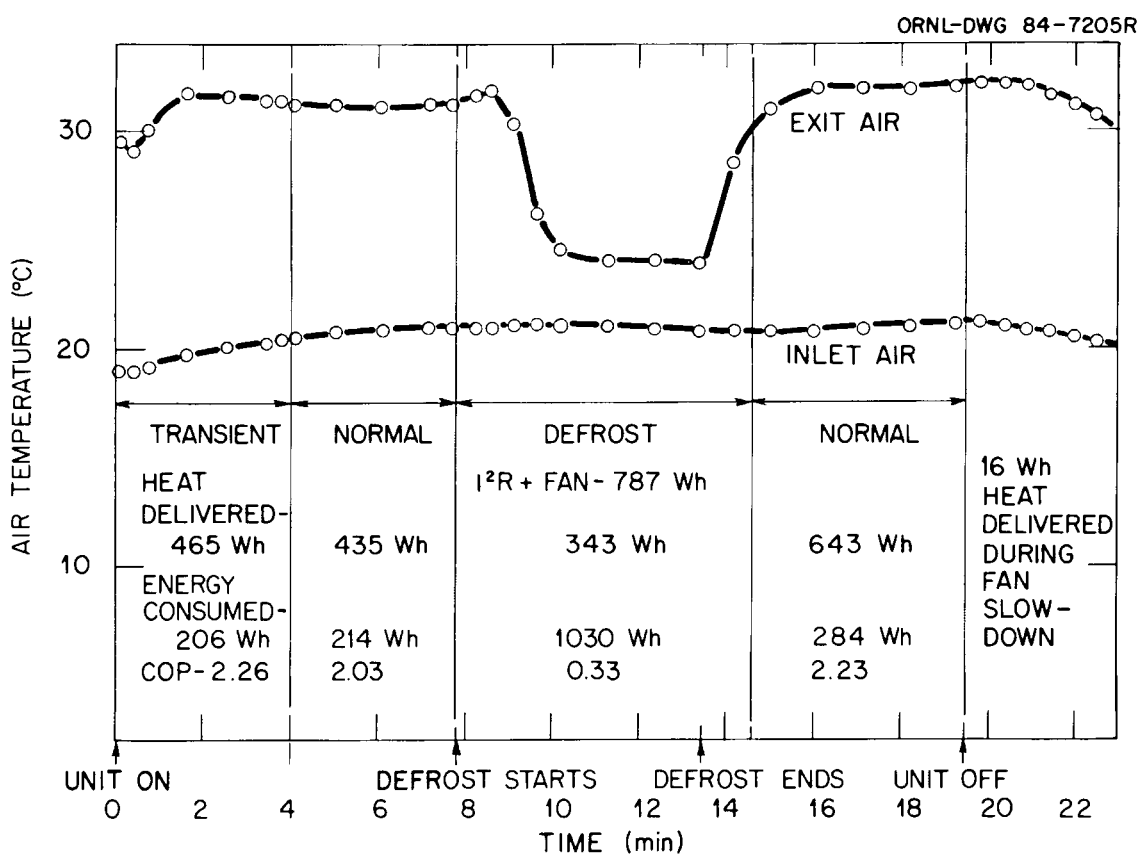

Fig. 3.9. Heat pump indoor unit inlet and exit air temperature vs time for a heating cycle with defrost.

the cycle. By observing the area between the curves for the defrost period, the relative amounts of heat delivered to the space during the defrost cycle and the recovery period can be determined. This was done for several cycles; the fraction of total defrost-mode space heat that was delivered during the recovery period (FQ_r) is plotted against defrost cycle time (not including recovery period time) in Fig. 3.10. The equation fitted to the data by linear regression analysis is

$$FQ_r = 0.380 - 0.029 \times \text{(defrost time)}, \ (r^2 = 0.924) ,$$

where r^2 is the correlation coefficient and defrost time is in minutes.

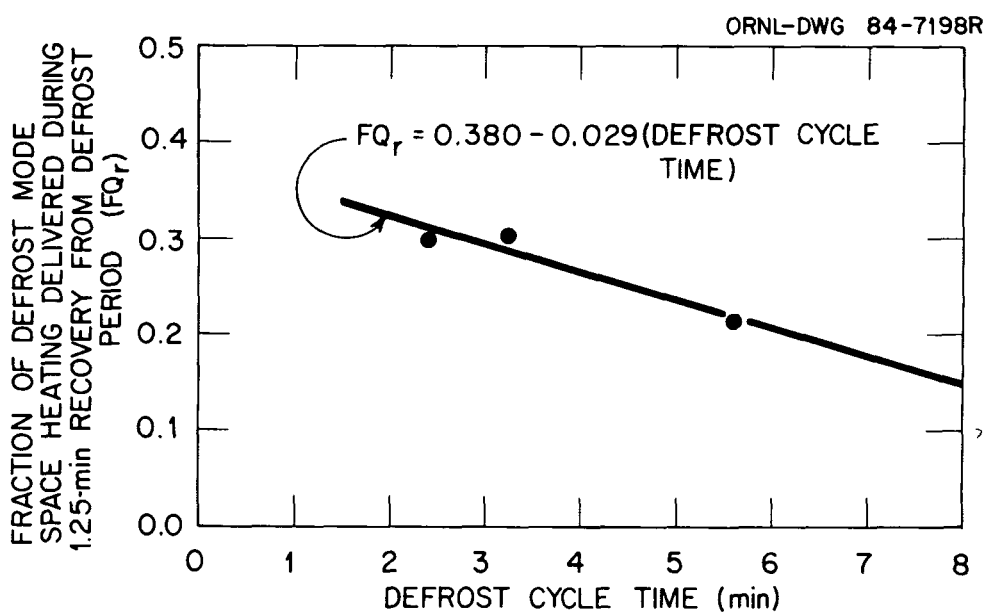

Fig. 3.10. Fraction of defrost cycle space heating delivered during recovery from defrost period vs defrost time.

By subtracting, the fraction of defrost-mode space heat delivered during the defrost cycle itself (FQ_d) is

$$FQ_d = 1 - FQ_r = 0.62 + 0.029 \times \text{(defrost time)} .$$

Table 3.7 gives average heat pump energy consumption, cooling capacity, and defrost time per cycle along with total defrost cycles for each month in the data set. Average defrost cycle cooling capacity is approximated by

$$\dot{Q}_c = (I^2R_d - HTLD_d \times FQ_d)/t_d$$

Table 3.7. Average defrost cycle parameters

Month	Defrost cycles	Average energy consumption (kW)		Average cooling capacity (kW)	Average defrost time[a] (min)
		I^2R[a]	Heat pump		
December 1981	111	8.23	2.51	5.28	5.72
February 1982	110	8.70	2.62	5.66	4.87
April 1982	19	8.39	2.52	4.18	2.41
December 1982	96	8.26	2.50	5.27	6.19
January 1983	164	8.07	2.76	4.66	4.68
February 1983	93	9.27	2.84	5.77	4.38
March 1983	41	9.05	2.88	5.38	3.55
April 1983	31	9.44	2.74	5.81	3.74
Total	665	8.53	2.67	5.26	4.88

[a]Does not include 1.25-min recovery period.

where

$\dot{Q}_c$ = average defrost cycle cooling capacity (kW),
I^2R_d = electric resistance heat used in defrost mode for the month (kWh),
$HTLD_d$ = net space heating delivered during defrost mode during the month (kWh),
t_d = total time spent in defrost mode during the month exclusive of the recovery period (h).

Details of the calculation methods and a sample calculation are given in Appendix A.

3.3 DYNAMIC LOSS ANALYSIS

3.3.1 Modal Coefficients of Performance

Coefficients of performance as measured for the transient and normal modes of operation and for overall operation are presented for a range of ambient operating temperatures in Figs. 3.11 and 3.12. Each point represents performance within a 5°C bin-month, with the plotted temperature of the point being the average outdoor temperature during operation within the bin-month. Steady-state, dry-coil COPs as measured in the laboratory and reported by Miller[6] for a heat pump identical (same model) to the field test unit are also presented. Fig. 3.11 is from operation during December 1981, when transient data represented the first 4 min of each on period. Figure 3.12 represents operation during February 1983, when only the first 2-min period of operation in each cycle was assigned to transient performance.

The variation of normal-mode COP from steady-state, dry-coil COP is due primarily to frosting losses; other minor variations may be due to slight differences in the two units as manufactured, field-vs-laboratory differences in installation, and uncontrolled ambient conditions in the field. In Fig. 3.11 the effect of frosting is clearly evident in the ambient

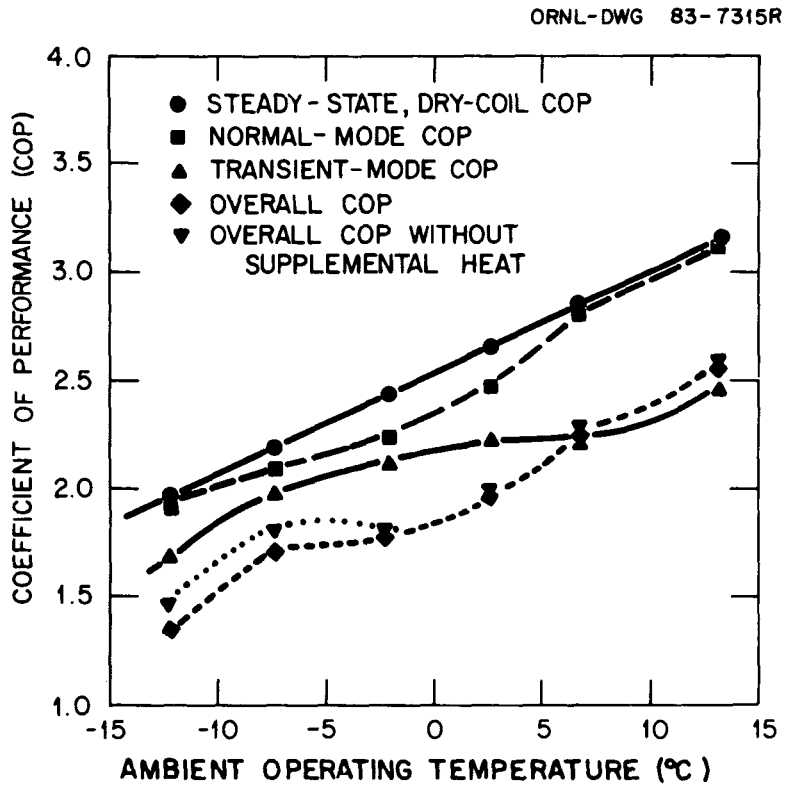

Fig. 3.11. Modal COP vs ambient operating temperature for 4-min transient period.

temperature range of −10 to +5°C, with the maximum degradation of COP of approximately 8% occurring at about 0°C.

Transient-mode COP is degraded from normal-mode COP by the reduced heat output rate at the beginning of each on period and by any increase in power input rate during start-up. As shown in Fig. 3.11, the cycling degradation is greatest at warmer ambient temperatures when the total cycling period and the off-time per cycle are long and the on-time per cycle is short.

Overall COP reflects the composite degradation of performance due to frosting losses, cycling losses (excluding off-cycle energy use), the very poor heating performance during defrosting, and the use of supplemental electric resistance heat as required at low ambient temperatures.

Normal and transient COPs as presented in Fig. 3.12 for 2-min transient measurements are both lower than those for 4-min measurements as shown in Fig. 3.11, especially at higher temperatures. A 2-min measurement period is too short to include all of the transient effects of start-up. The transient data cover only the poorest period of transient performance and, therefore, provide a lower COP than that resulting from a longer transient measurement period. Since a portion of the transient performance is included in the normal data, the resulting normal COP is also lower. Frosting loss effects are not evident from the 2-min transient measurement data. Overall COPs are similar in Figs. 3.11 and 3.12, indicating that overall heat pump performance was essentially unchanged and the modal COP differences were due to data allocation techniques.

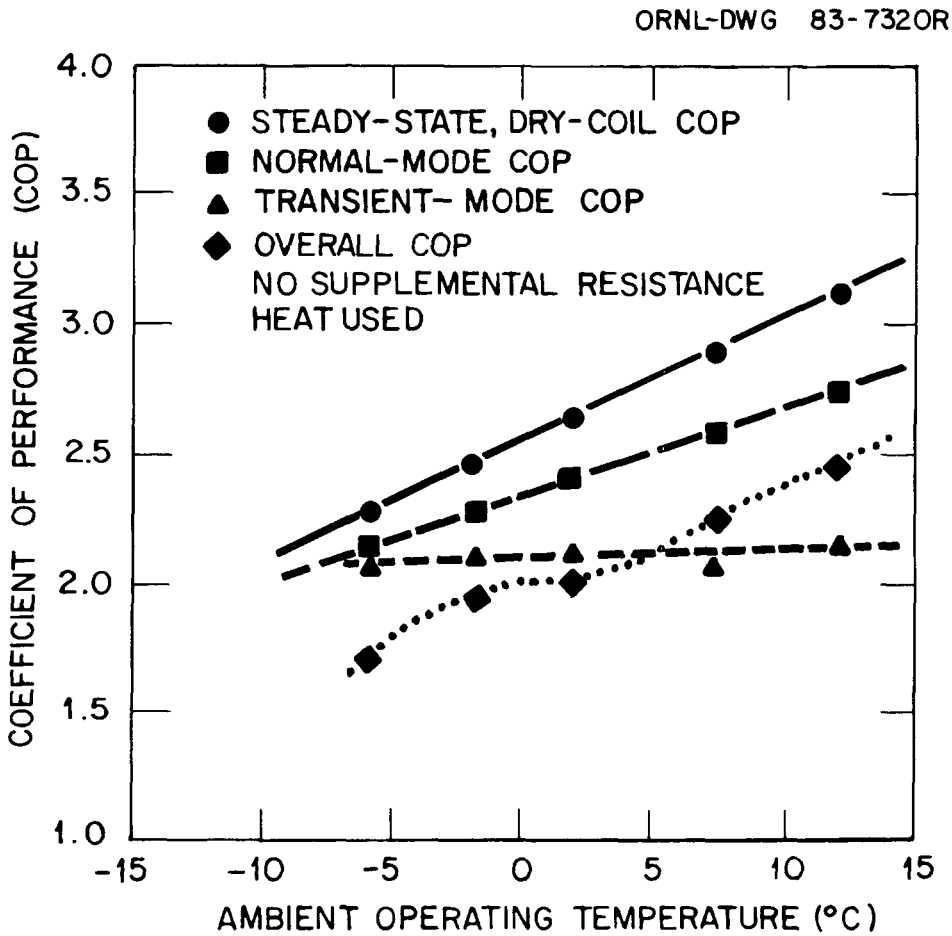

Fig. 3.12. Modal COP vs ambient operating temperature for 2-min transient period.

An alternative presentation of the data for 4-min start-up transient time is given in Fig. 3.13, which more clearly shows the contributions of the various dynamic losses to the overall COP degradation. The effect of off-cycle energy use is included in this figure (in the cycling losses) and is very pronounced at high ambient temperatures. Curves 1-4 in Fig. 3.13 are approximate representations of the data taken for 4-min transient time intervals in December 1981 and November and December 1983.

3.3.2 Degradation of Capacity and COP at Part Load

An indication of the overall degradation of capacity and COP, due to both frosting and cycling losses (excluding defrosting and off-cycle power), at part load is given in Fig. 3.14. The ordinate for this figure is the ratio of cyclic to steady-state capacity or COP. The ordinate value of each data point reflects the average capacity or COP for a bin-month divided by the steady-state, dry-coil capacity or COP as reported by Miller[6] at the average operating temperature for the bin-month. The abscissa for the figure is heating load factor, defined as the total nondefrosting heat delivered in a bin-month divided by the product of

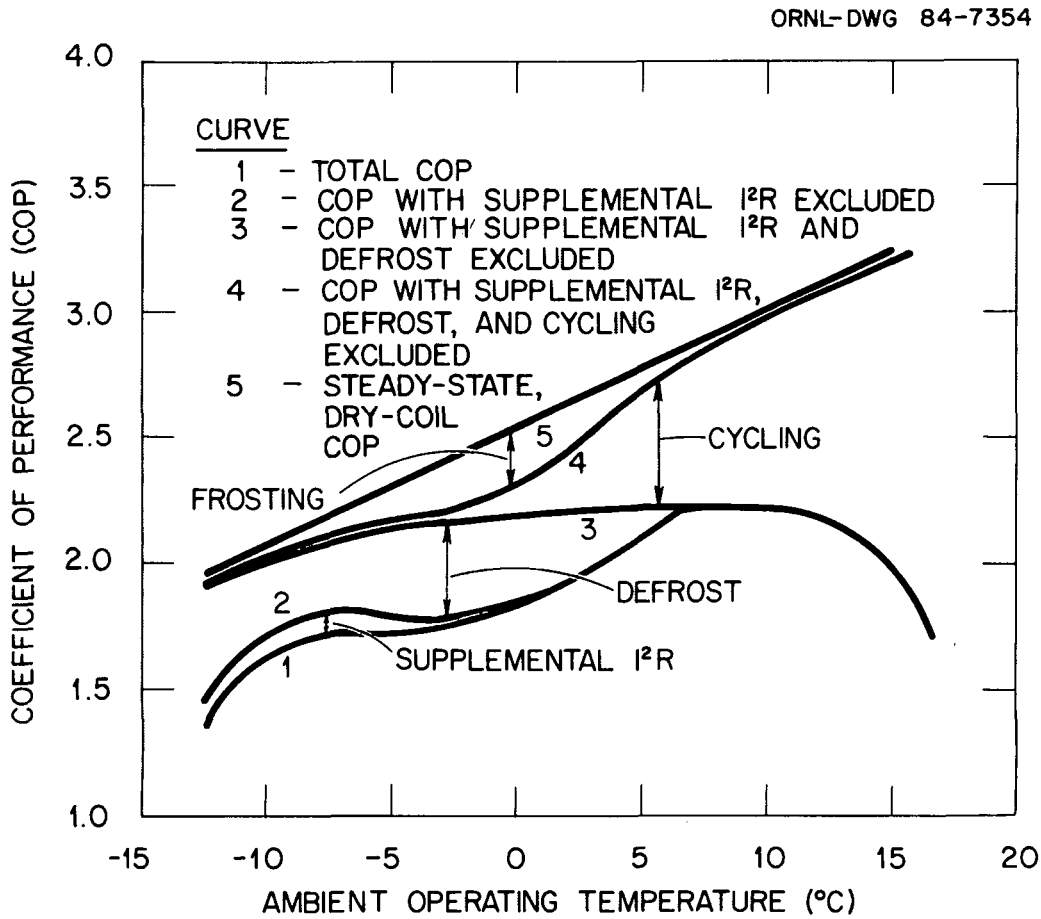

Fig. 3.13. Effects of dynamic losses on heating COP.

steady-state, dry-coil capacity at the bin average operating temperature and the non-defrosting bin hours for the month.

Data points shown in Fig. 3.14 are for both 2-min and 4-min transient measurement operation. The curves were hand fitted to the capacity ratio (CAPRAT) and COP ratio (COPRAT) points.

Both CAPRAT and COPRAT decrease rather steadily as heating load factor decreases, with no clear indication of increased frosting degradation in the heavy frost accumulation temperature range of −10 to +5°C. The greater degradation of COP than that of capacity indicates an increase in power consumption under frosting-plus-cycling operation, concomitant with the lower capacity. The indicated percentage increase in power consumption is equal to (CAPRAT/COPRAT − 1) × 100, or less than 5% over the range of load factor.

If capacity and COP ratios are redefined as the measured nondefrosting capacity and COP, respectively, for each temperature bin-month divided by the measured normal-mode capacity and COP, respectively, for that bin-month, cyclic degradation can be separated from frosting effects. This assumes that measured normal-mode performance represents steady-state performance at the frosting condition of that bin-month. Similarly, the heating load factor is redefined as the total nondefrosting heat delivered in a bin-month divided

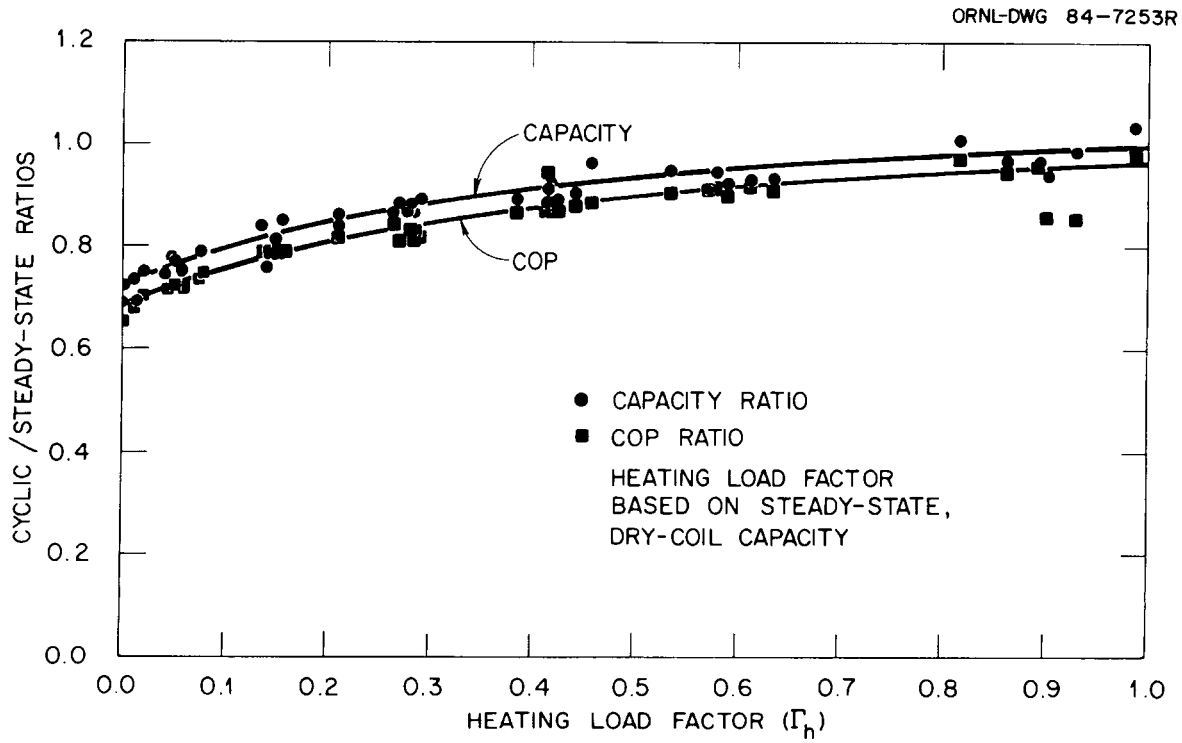

Fig. 3.14. COPRAT and CAPRAT vs heating load factor (Γ_h) based on steady-state, dry-coil capacity.

by the product of normal-mode capacity and nondefrosting bin hours for the bin-month. Figure 3.15 presents the redefined capacity and COP ratios, plotted against the redefined heating load factor, with each data point representing 1 bin-month of field test operation.

Since a 4-min transient delay time seemed to be more appropriate and the available 4-min transient data included few hours of operation at temperatures greater than 5°C, it was decided to supplement the available data with data from two weeks in November and December 1983. Table 3.8 gives average operating temperatures, percent on-times, capacity and COP ratios, and heating load factors for this period (based on normal-mode capacity). These data are included in Fig. 3.15.

There is little difference between capacity ratio and COP ratio as determined from data collected with a 2-min transient measurement interval. A tendency for capacity ratio to become smaller than COP ratio at very low values of heating load factor is evident, indicating a decrease in power consumption during transient-mode operation.

The data collected with a 4-min transient measurement interval probably presents a more accurate portrayal of cyclic performance, as discussed in Sect. 3.3.1. As shown in Fig. 3.15, there is a marked degradation in performance at lower values for heating load factor. COP ratio is lower than capacity ratio, indicating an increase in overall power consumption of up to 6% over that for normal-mode operation.

The National Bureau of Standards developed a test and rating procedure to be used for estimating the heating seasonal performance of heat pumps.[7] In that procedure, cyclic

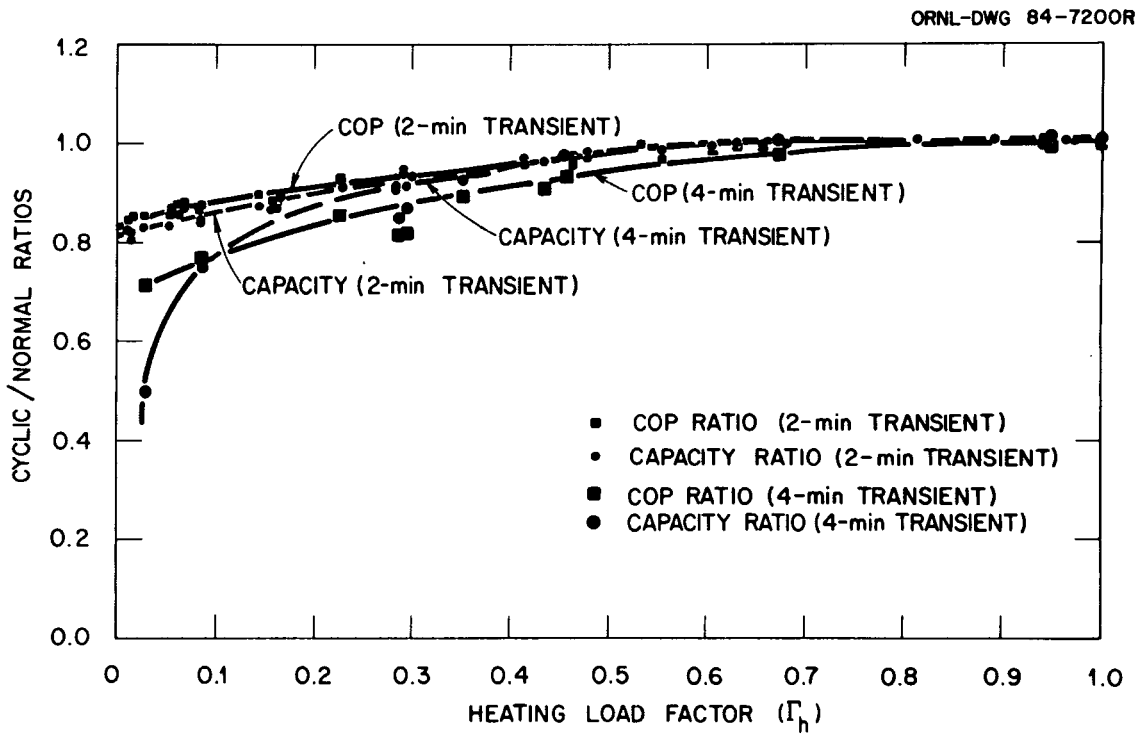

Fig. 3.15. COPRAT and CAPRAT vs heating load factor (Γ_h) based on normal-mode capacity.

Table 3.8. Percent on, CAPRAT, COPRAT, and heating load factor (Γ_h) vs ambient operating temperature for November 28, 1983, through December 11, 1983

Bin-month (°C range)	Average ambient operating temperature (°C)	Percent on	CAPRAT[a]	COPRAT[a]	Γ_h[a]
T < 0°C	−2.1	53.6	1.00	0.99	0.536
0-5°C	2.7	38.5	0.92	0.90	0.355
5-10°C	2.1	26.4	0.85	0.85	0.223
10-15°C	11.8	12.8	0.72	0.74	0.093
T > 15°C	16.3	5.5	0.49	0.69	0.030

[a]Based on normal-mode capacity and COP.

degradation of heat pump performance is characterized by the cyclic degradation factor, C_d, defined as follows.

$$C_d = (1 - \mathrm{COP}_{cyc(47)}/\mathrm{COP}_{ss(47)})/(1 - HLF) ,$$

where

$\mathrm{COP}_{cyc(47)}$ = cyclic COP for 20% on-time measured at 47°F,
$\mathrm{COP}_{ss(47)}$ = steady-state COP measured at 47°F,
HLF = heating load factor resulting from a 20% on-time test.

The C_d thus defined in ref. 7 included the effect of off-cycle power. Interpolating in the field data in Table 3.8 at 20% on-time, *HLF* is about 0.162 and the cyclic COP ratio is about 0.8, yielding a C_d of about 0.24 (for the 4-min transient time). The corresponding value for C_d for the 2-min transient data is about 0.1.

3.3.3 Analysis of Cycling Loss During Heating

The overall degradation in performance due to cycling during part-load operation was quantified in the preceding section. That treatment of the subject is useful in predicting the seasonal performance of a heat pump system but does little toward providing an understanding of why the losses occur and what might be done to reduce them.

The overall degradation is a composite result of a loss in output energy and an increase in input energy for each thermostat-controlled on-off cycle experienced by the heat pump. Energy consumption for the crankcase heater and the control circuit should be included in a complete analysis, but are excluded in the following discussion, which attempts to elucidate the variation of cyclic losses with the various cycle parameters.

From data collected during each temperature bin and month, the average cycle period, on-time, and off-time were calculated as follows:

$$P = (BH - DH) \times 60/N ,$$

$$t_{on} = 60 \times t_{op}/N ,$$

$$t_{off} = P - t_{on} ,$$

where, for each bin-month,

P	=	average cycle period (min),
BH	=	bin hours,
DH	=	defrost-mode operating hours,
t_{on}	=	average time on per cycle (min),
t_{op}	=	normal-mode plus transient-mode operating time (h),
t_{off}	=	average time off per cycle (min),
N	=	number of cycles.

In addition, the average per-cycle loss in output (the difference in actual measured output and that which would have resulted from normal operation during the entire run time) and increase in input (the difference in measured input and that which would have resulted from delivery of the measured output at normal COP) were estimated as follows:

$$OLPC = (\dot{Q}_n \times T_{op} - Q) \times 3600/N ,$$

$$IIPC = (E - \frac{Q}{\mathrm{COP}_n}) \times 3600/N ,$$

where

$OLPC$	=	output loss per cycle (kJ),
$\dot{Q}_n$	=	normal-mode capacity (kW),
Q	=	total nondefrost delivered energy (kWh),
$IIPC$	=	input increase per cycle (kJ),
E	=	normal-mode plus transient-mode input (kWh),
COP_n	=	normal-mode COP.

3.3.3.1 Cycling rate

Figure 3.16 shows average cycling rate in cycles per hour as a function of ambient temperature for each temperature bin-month. Although there is considerable scatter in the data, the effect of changing thermostats is evident. With each thermostat, cycling rate approaches zero at low temperatures, when the unit essentially operates full-time to meet the building heating load, and at high temperatures, when no heating is required and the unit is idle. Peak cycling rates occur when the ambient temperature is in a range of 0 to 5°C. On-time and off-time per cycle are shown in Figs. 3.17 and 3.18, respectively.

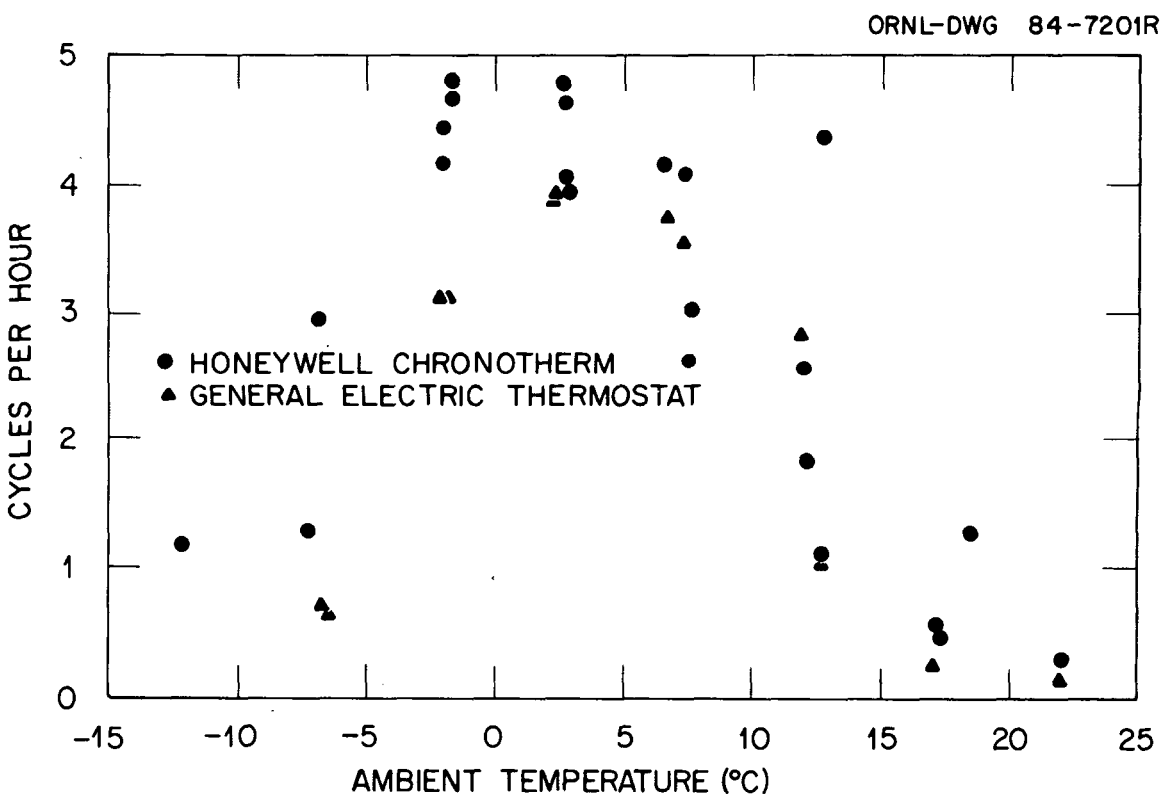

Fig. 3.16. Cycles per hour vs ambient temperature.

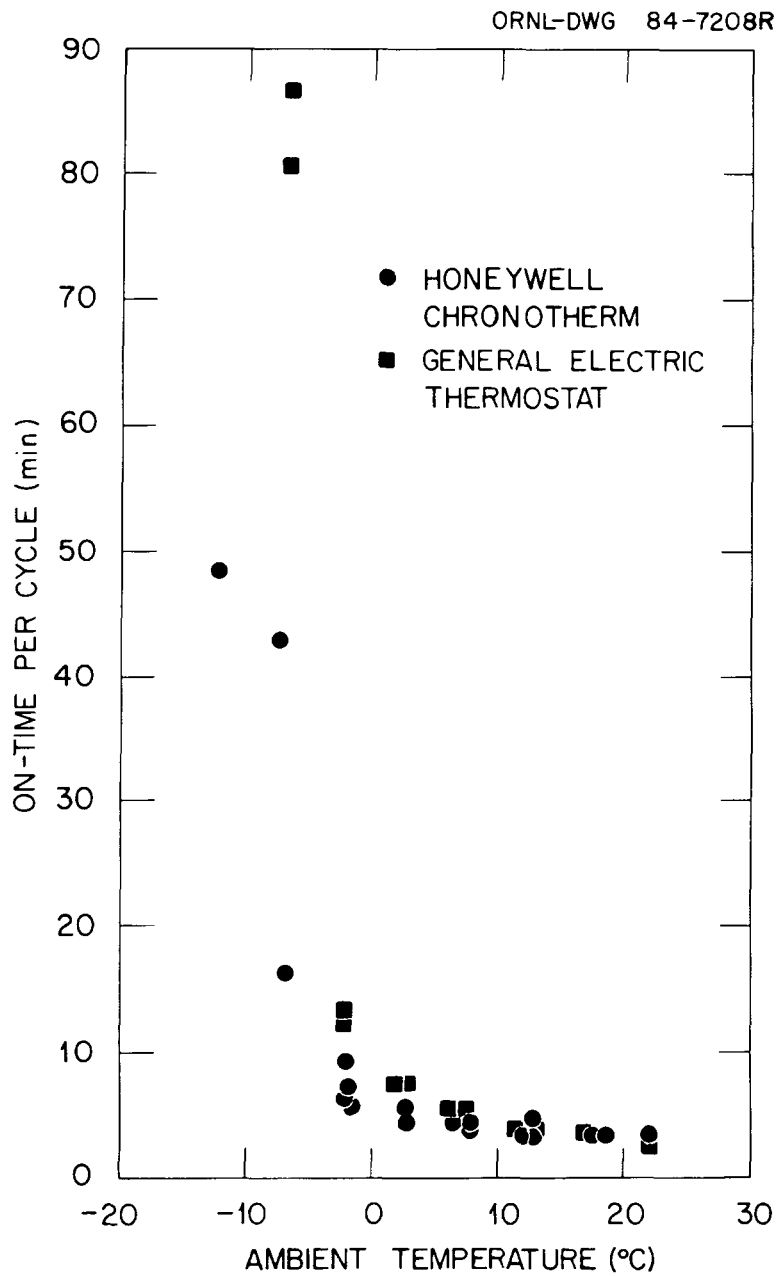

Fig. 3.17. On-time per cycle vs ambient temperature.

3.3.3.2 Output loss per cycle

Figure 3.19 shows calculated values of per-cycle loss in output as a function of ambient operating temperature. A least-squares linear-fit line through the plotted points has the equation

$$OLPC\ (\text{kJ}) = 69.78 + 16.85 \times T\ (°\text{C})$$

with a correlation coefficient (r^2) of 0.934.

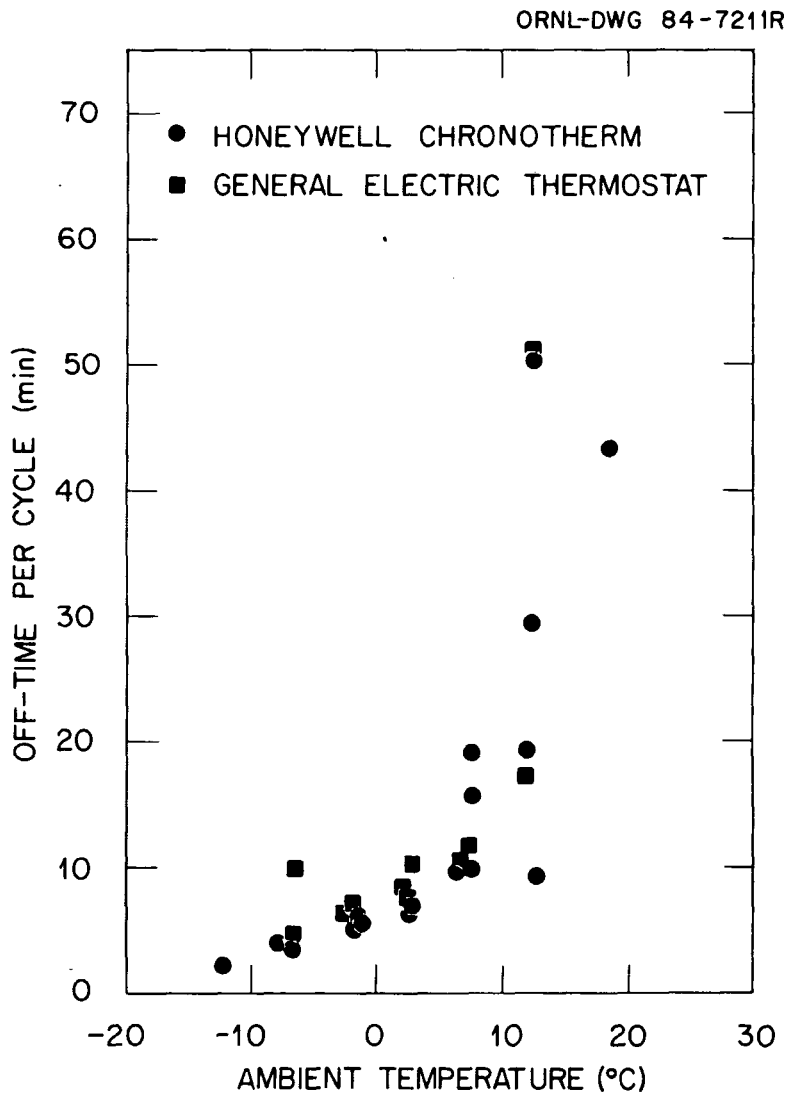

Fig. 3.18. Off-time per cycle vs ambient temperature.

The calculated loss data also correlate well with percent on ($100 \times t_{on}/P$), as shown in Fig. 3.20. Here, the least-squares linear-fit line through the data has the equation

$$OLPC = 359.52 - 5.08 \times (\text{percent on})$$

with a correlation coefficient (r^2) of 0.922.

Given that a reasonably good linear relationship was found for loss as a function of ambient temperature, it is not surprising that a similarly good linear relationship was found for loss as a function of percent on. To a first approximation, percent on is linearly (although inversely) related to ambient temperature because building heating load and heat pump capacity vary approximately linearly with temperature.

The loss in output per cycle is due to the reduced heat production rate immediately following start-up. At the beginning of the on portion of the cycle, a finite period of time

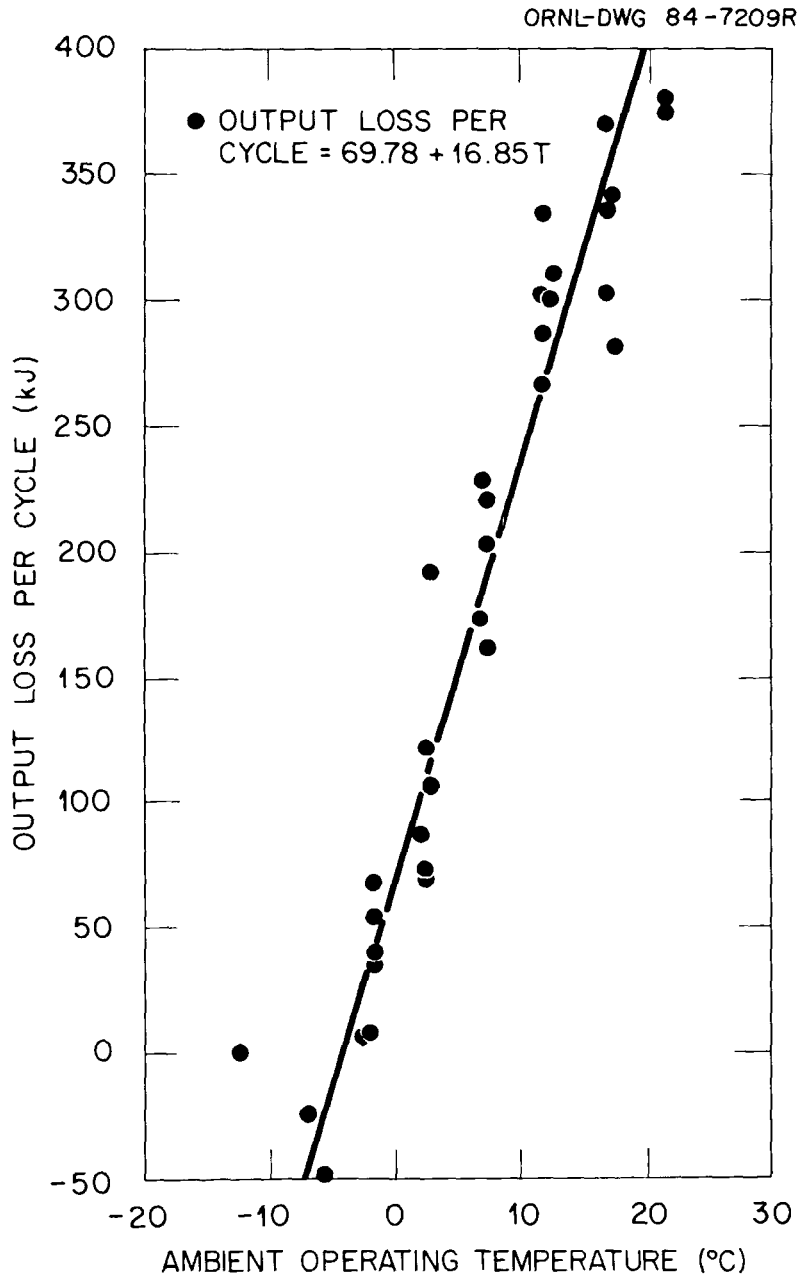

Fig. 3.19. Output loss per cycle vs ambient operating temperature.

elapses before the heat pump reaches steady-state operation and produces its full heating capacity. During this transient period, system operating pressures are being established, the refrigerant charge is being redistributed within the system, and the masses of the various system components are being brought to their steady-state temperature levels. No mechanism is evident that would cause the loss per cycle to increase so significantly with increasing temperature or decreasing percent on as indicated in Figs. 3.19 and 3.20. Rather, it is believed that the loss per cycle is primarily a function of one or more cycle parameters that vary with ambient operating temperature. Cycle period can be ruled out because the

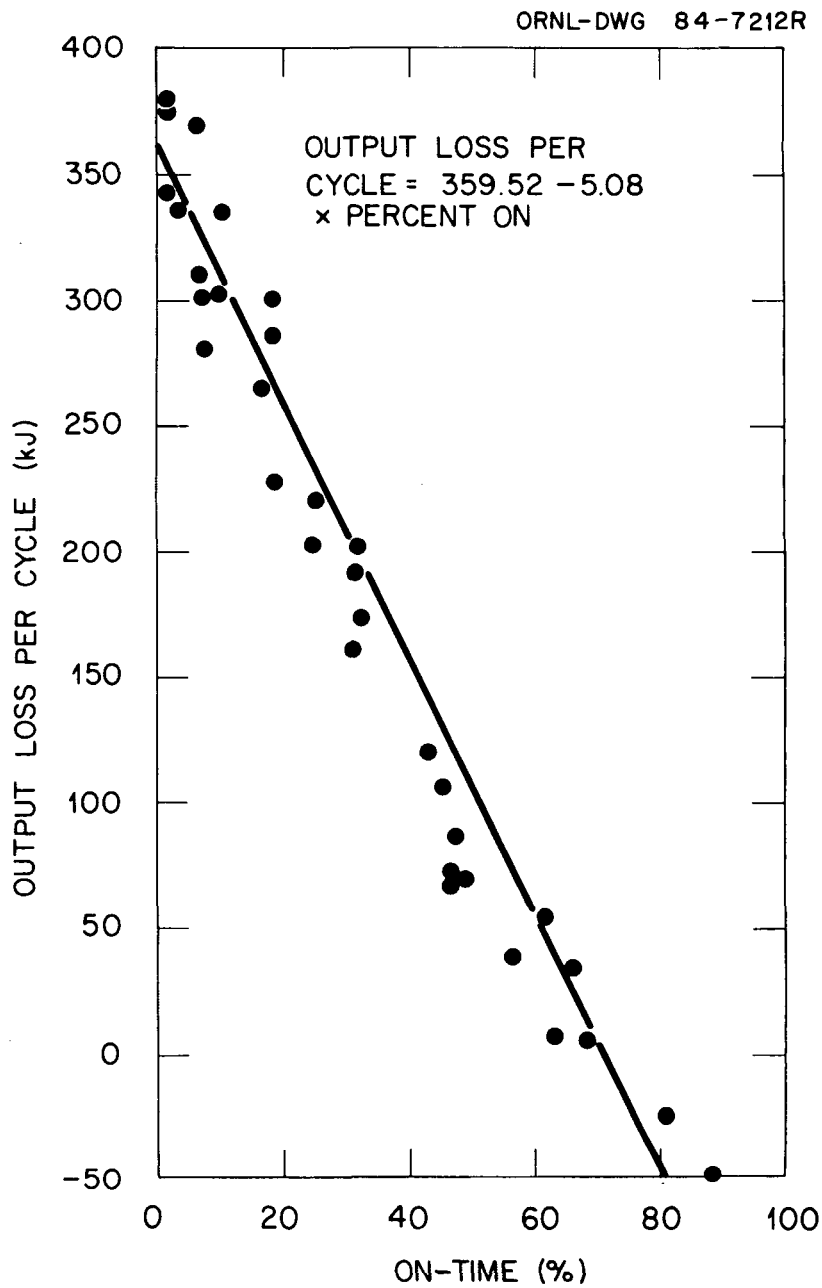

Fig. 3.20. Output loss per cycle vs percent on-time.

period becomes large at both extremes of the temperature range; any strong effect of period is not in consonance with the linearity in Fig. 3.19. On-time should not influence transient loss per cycle unless on-time is shorter than the period of time required to reach steady-state operating conditions.

The one remaining cycle parameter, off-time, is believed to be the key to explaining the variation of output loss per cycle. Figure 3.21 presents output loss per cycle as a function of

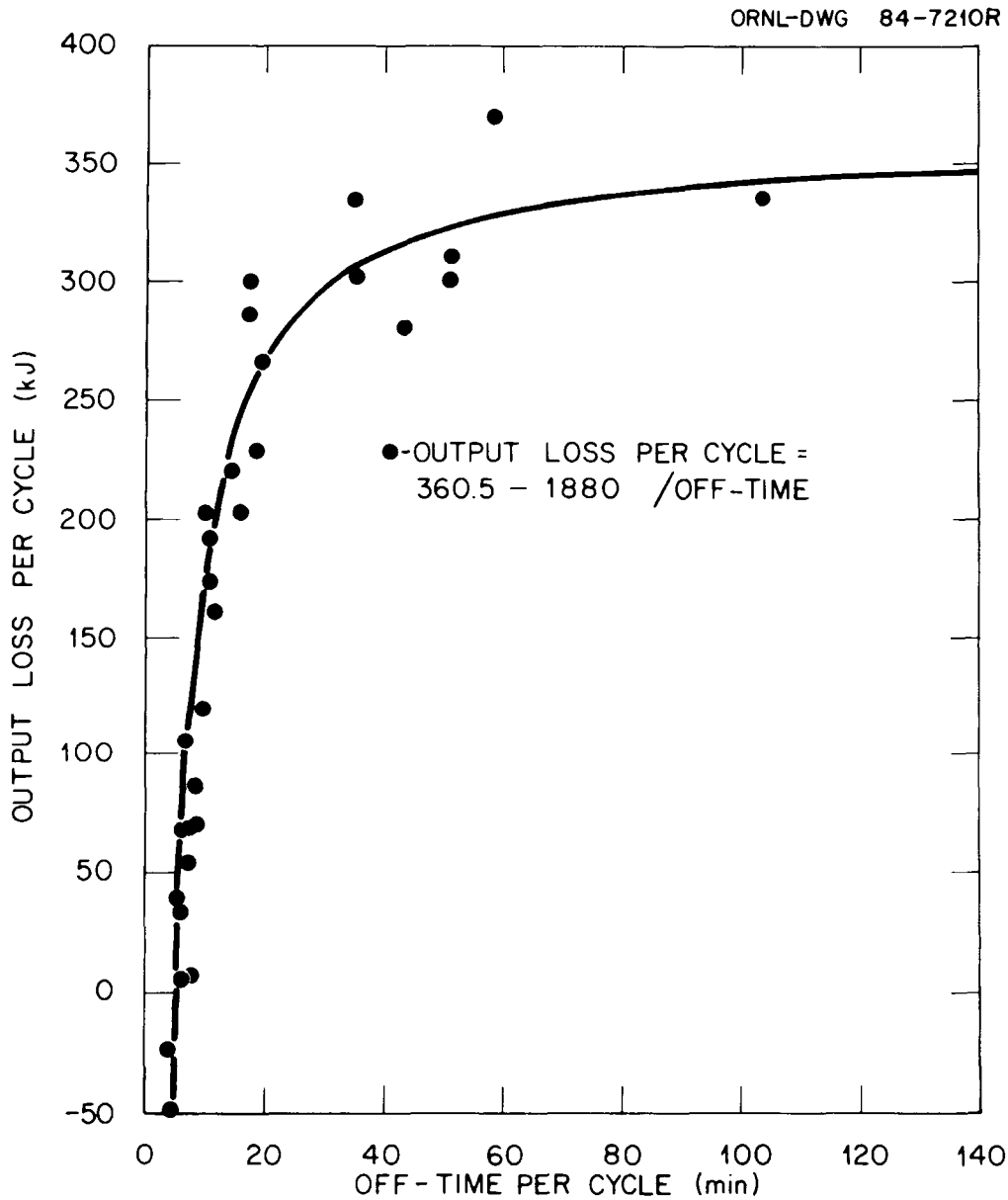

Fig. 3.21. Output loss per cycle vs off-time per cycle.

off-time per cycle. Initially, loss increases rapidly with increasing off-time. Then, for off-times greater than approximately 20 min, loss increases at a much lower rate. The line on the figure represents a least-squares fit to the data as follows:

$$OLPC = 360.5 - 1880/(\text{off-time}) ,$$

with a correlation coefficient (r^2) of 0.888. However, the line and correlation should not be allowed to obscure what may be a two-stage phenomenon. The first stage, when loss increases rapidly with off-time, could reflect the effect of refrigerant migration from the warm indoor portion of the system to the cold outdoor portion. After the bulk of refrigerant

migration has occurred, some low-loss-rate mechanism may continue for an extended time period.

No clear explanation for the apparent negative losses per cycle at low values for off-time (or low ambient temperatures or high percent on) is offered. The negative losses imply an increase in output per cycle due to cycling when off-times are short. As was pointed out in an earlier section, most of the data were collected using a 2-min transient measurement interval, which was not sufficient to account for the total transient performance period. This tends to understate the output loss per cycle and could, along with other (but unrecognized) biases in the data, account for the apparent negative losses.

3.3.3.3 Input increase per cycle

Calculated values of the increase in per-cycle energy input are shown as a function of ambient operating temperature and as a function of off-time per cycle in Figs. 3.22 and 3.23, respectively. Although there is considerably greater scatter in the data than in that for output losses, the same general trends are evident. Increase in input is larger for higher ambient temperature and longer off-time. A possible cause for these trends is ingestion of some liquid refrigerant by the compressor at start-up, due to evaporator flooding by the migration of refrigerant during long off-times.

3.3.4 Analysis of Defrost Time as a Function of Frosting Potential

The defrost control scheme for the field test unit is of the timed-initiation, demand-termination type. A timer that operates with the compressor initiates a defrost cycle after approximately 80 min of operation if, at that instant, the outside coil is below approximately 0°C. If the coil is above freezing temperature, defrosting does not occur and another 90-min timer period starts. When the coil is below freezing at the end of a timer cycle, the unit operates in the defrosting mode until the outside coil is warmed to approximately 10°C, or for a timed 10-min period if the coil does not reach 10°C. The unit then returns to heating mode operation.

During defrosting operation, the unit operates in the air-conditioning mode but with the outdoor blower idle and the supplemental resistance heaters energized to overcome the indoor air cooling effect. The net result is that, during defrosting, the energy input rate is high and the net heat delivery rate to the indoor air is low. Typically, only about one-third of the energy input is delivered as heat to the indoor air, and two-thirds is used to warm the outdoor components and melt the accumulated frost.

The duration of each defrosting operation reflects, to a first approximation, the efficiency-penalizing effect of defrosting since the energy delivery rate to the outdoor components for metal warming and frost melting, the input energy rate, and the rate of delivery of heat to indoor air are all relatively constant. It would be expected that defrosting duration is a function of both the mass of accumulated frost to be melted and outdoor temperature.

If the mass flow rate of air over the outdoor coil is assumed constant during the operating period preceding defrost (data from ref. 6 suggest that it is not), the accumulated frost mass should be approximately proportional to the difference in the humidity ratio (mass of water vapor per unit mass of air) of the outdoor air entering the coil and the

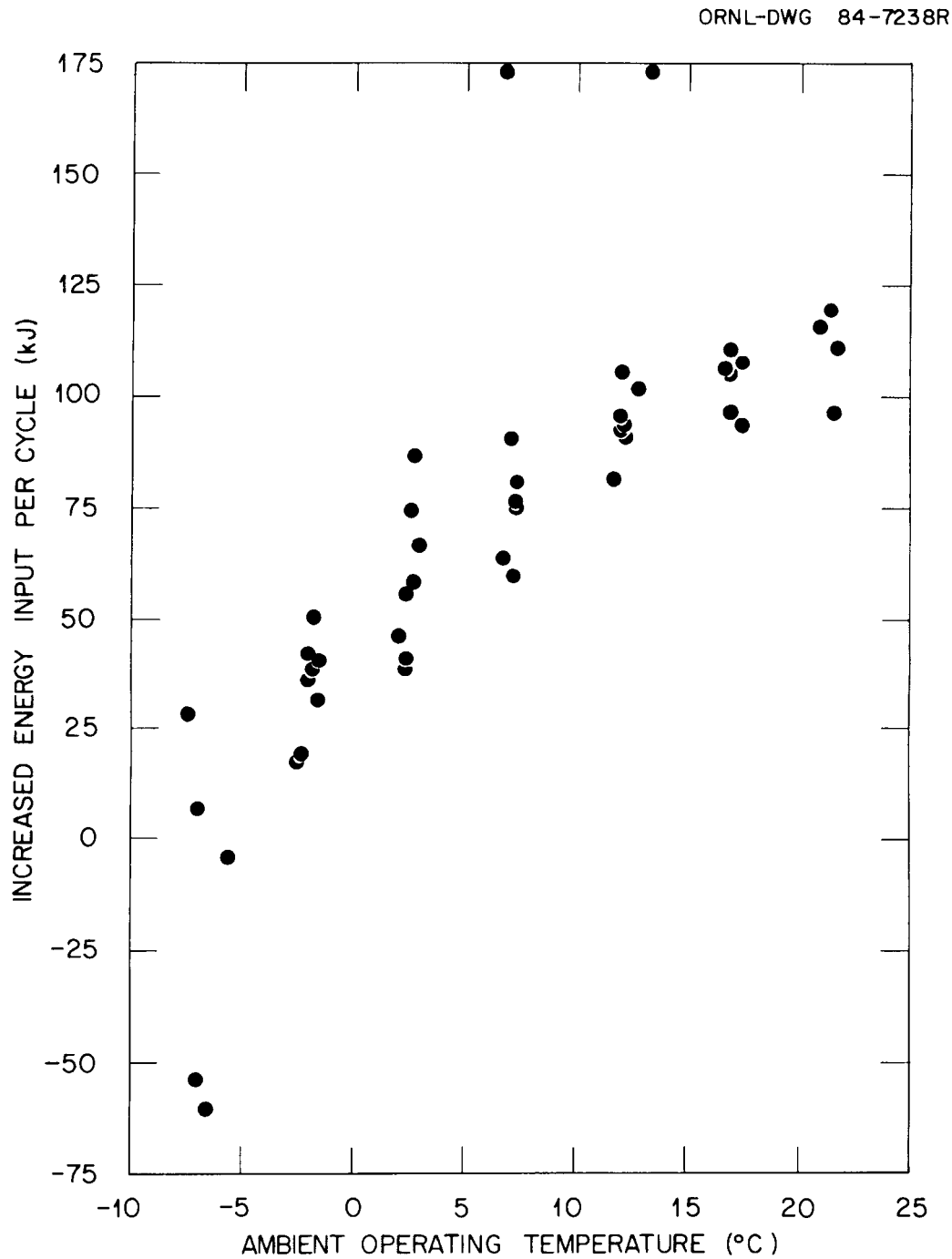

Fig. 3.22. Increased input per cycle vs ambient operating temperature.

saturated humidity ratio of air at the coil surface temperature. This difference, referred to as frosting potential,[8] is essentially the mass of water removed from a unit mass of outdoor air as it is cooled from ambient temperature and relative humidity to the tube surface temperature.

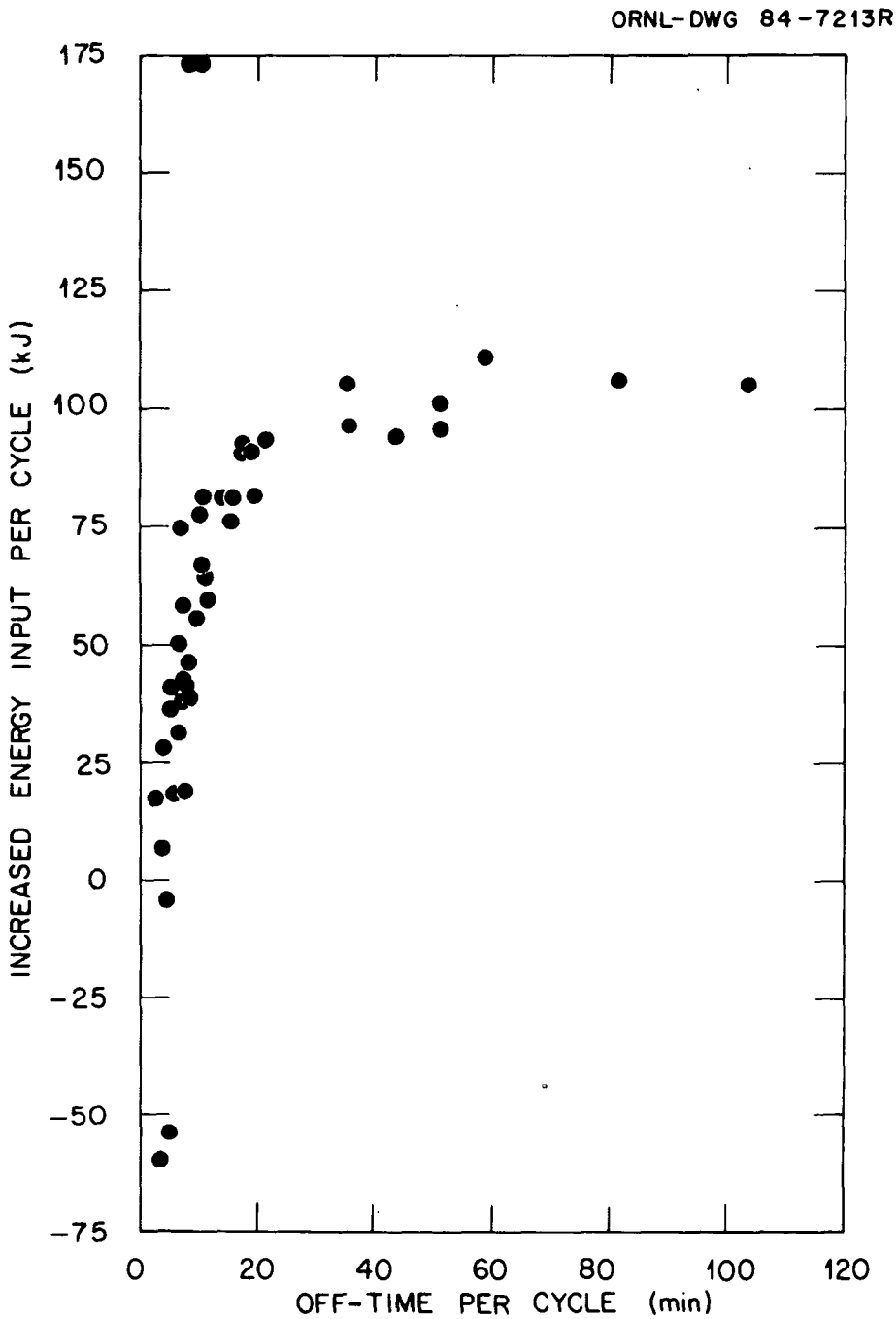

Fig. 3.23. Increased input per cycle vs off-time per cycle.

To facilitate evaluation of the effect of frosting potential on defrost time, data for six of the eight heating months (April 1982 and 1983 being excluded) were divided into relative humidity sub-bins five percentage points wide. For example, a sub-bin might represent all hours having 70–75% relative humidity in the −5 to 0°C temperature bin-month during December 1982.

Plots of defrost time versus frosting potential for 3 temperature bin-months of interest are shown in Figs. 3.24, 3.25, and 3.26. Defrost time as shown includes a constant 1.25 min for recovery, as discussed in Sect. 2.3. Ambient relative humidity used to calculate frosting potential was as measured by the weather station at the Knoxville municipal airport, located approximately 11 km (7 miles) from the test site. (Relative humidity was regularly measured and recorded at the test site. However, the on-site measurements are not believed

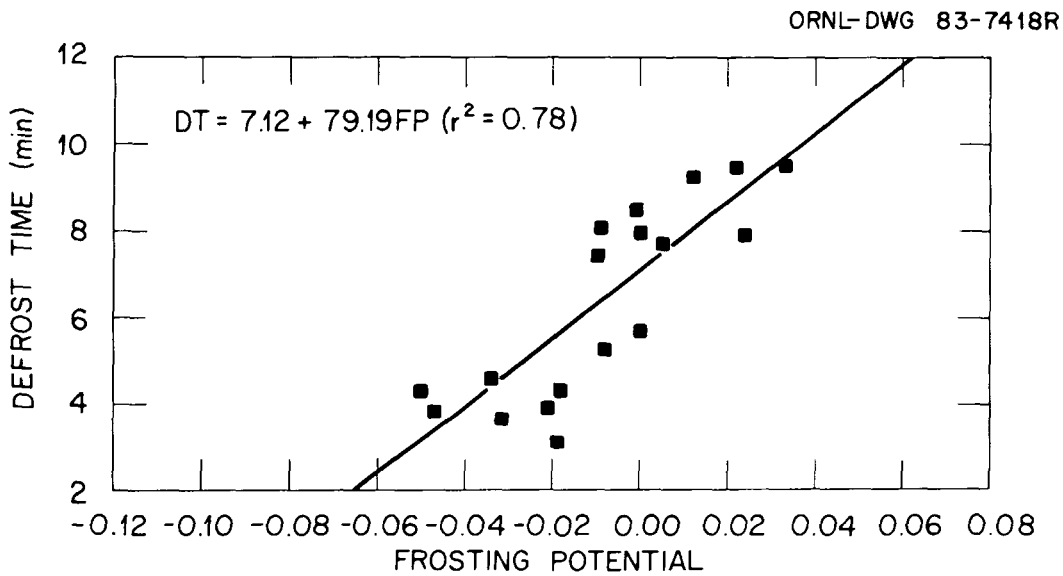

Fig. 3.24. Defrost time vs frosting potential ($-10°C < T < -5°C$).

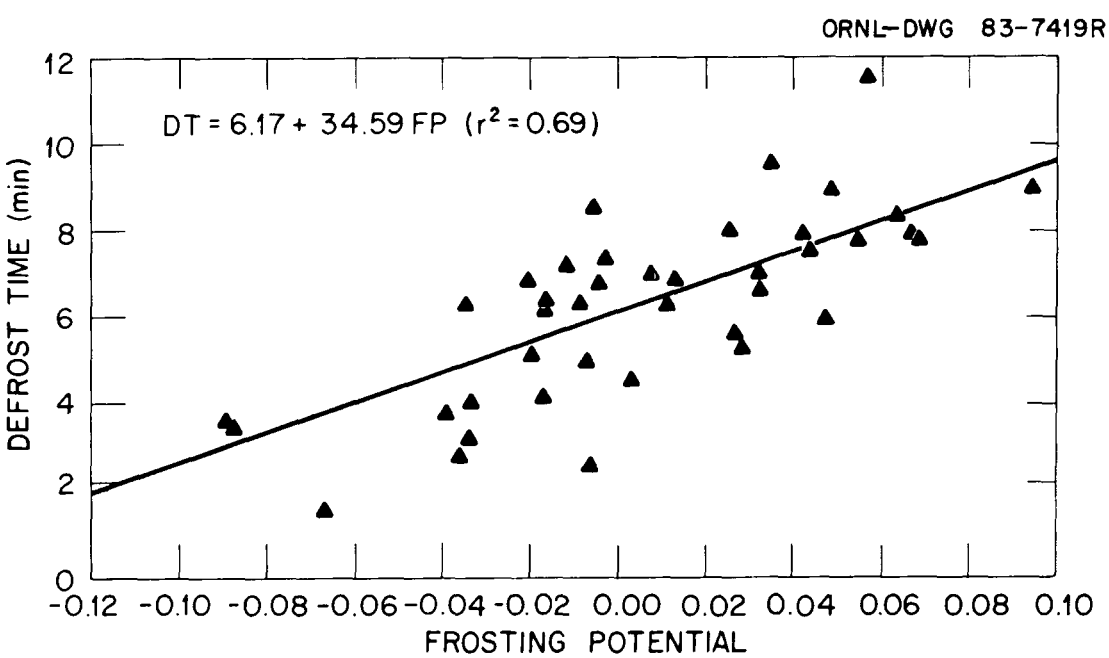

Fig. 3.25. Defrost time vs frosting potential ($-5°C < T < 0°C$).

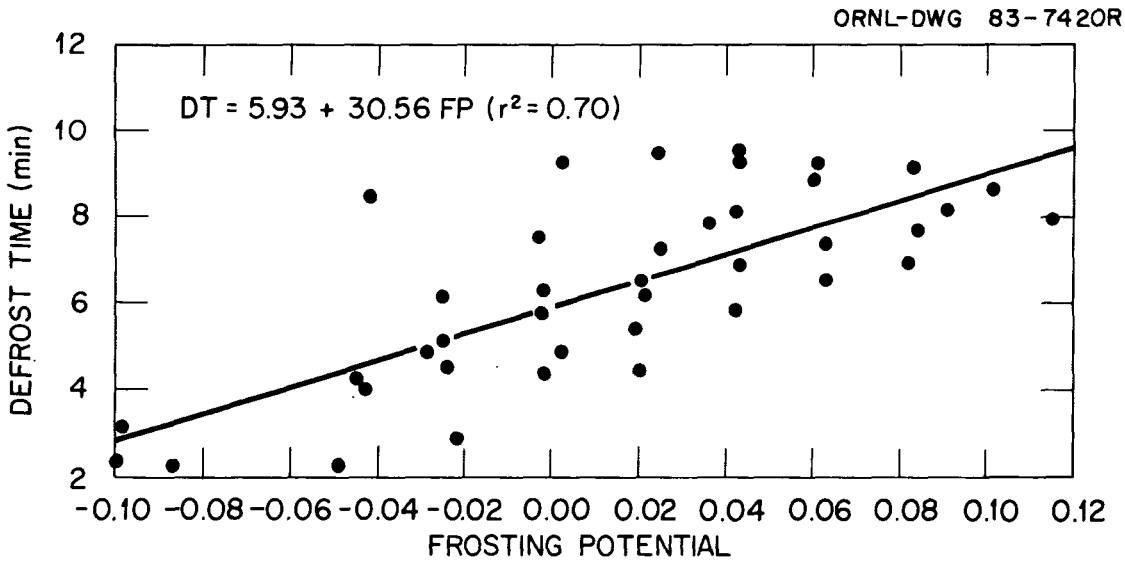

Fig. 3.26. Defrost time vs frosting potential (0°C < T < 5°C).

to be as reliable as the airport measurements.) Depression of tube wall temperature from ambient temperature used in the calculations was assumed to vary linearly from 4.4°C at 4.4°C ambient to 1.7°C at −17.8°C. This relationship is as reported in ref. 8 for an outdoor coil of "normal" configuration and is in close agreement with measurements made on a heat pump similar to the test unit at −1.1 and 1.7°C by Miller.[6]

The lines shown in Figs. 3.24, 3.25, and 3.26 are least-squares linear fits to the data points, weighted to reflect the number of defrost cycles represented by each sub-bin data point. Regression equations and correlation coefficients for the lines are included in the figures. As with much of the field-measured data reported herein, the degree of scatter is much greater than would be expected from laboratory testing under carefully controlled conditions, and, as a result, the correlation coefficients are low. However, the trends are clear. Defrost time increases essentially linearly with frosting potential and is a stronger function of frosting potential at lower outdoor temperatures.

It should be noted that data from ref. 6 indicate decreasing air flow across the outdoor coil during the frosting period, especially at high relative humidities (and, thus, frosting potential). Such a variation in air flow should cause a reduction in required defrost time from that predicted by a linear relationship with frosting potential. However, examination of the data portrayed in Figs. 3.24, 3.25, and 3.26 does not suggest a nonlinear relationship between defrost time and frosting potential.

An approximate relationship of defrost time to frosting potential and outdoor temperature, derived from the regression equations for the three figures and using the average operating temperature within each of the three bins, is as follows.

$$DT = 5.39 + 7.15/(T + 11.12) + [24.7 + 60.5/(T + 8.10)] \times FP ,$$

where

DT = defrost time (min),
T = outdoor air temperature (°C),
FP = frosting potential $\left[\frac{\text{kg } H_2O}{\text{kg dry air}}\right]$.

This relationship is plotted for the range of applicability of the data in Fig. 3.27. For positive values of frosting potential, where frost accumulation would be expected, defrost time decreases as outdoor temperature increases. This is as would be expected because the fraction of the energy pumped to the outdoor coil that is utilized for frost melting (rather than being lost to the outdoor air) increases with temperature. However, two paradoxical features appear in the region of negative frosting potential. First, the linear relationship of defrost time with frosting potential appears to persist even though there should be no frost accumulation to be melted in this region. Second, defrost time at a given negative value of frosting potential is essentially constant over the warmer temperatures but decreases rather sharply at the colder temperatures. No explanation is available for either of these paradoxes.

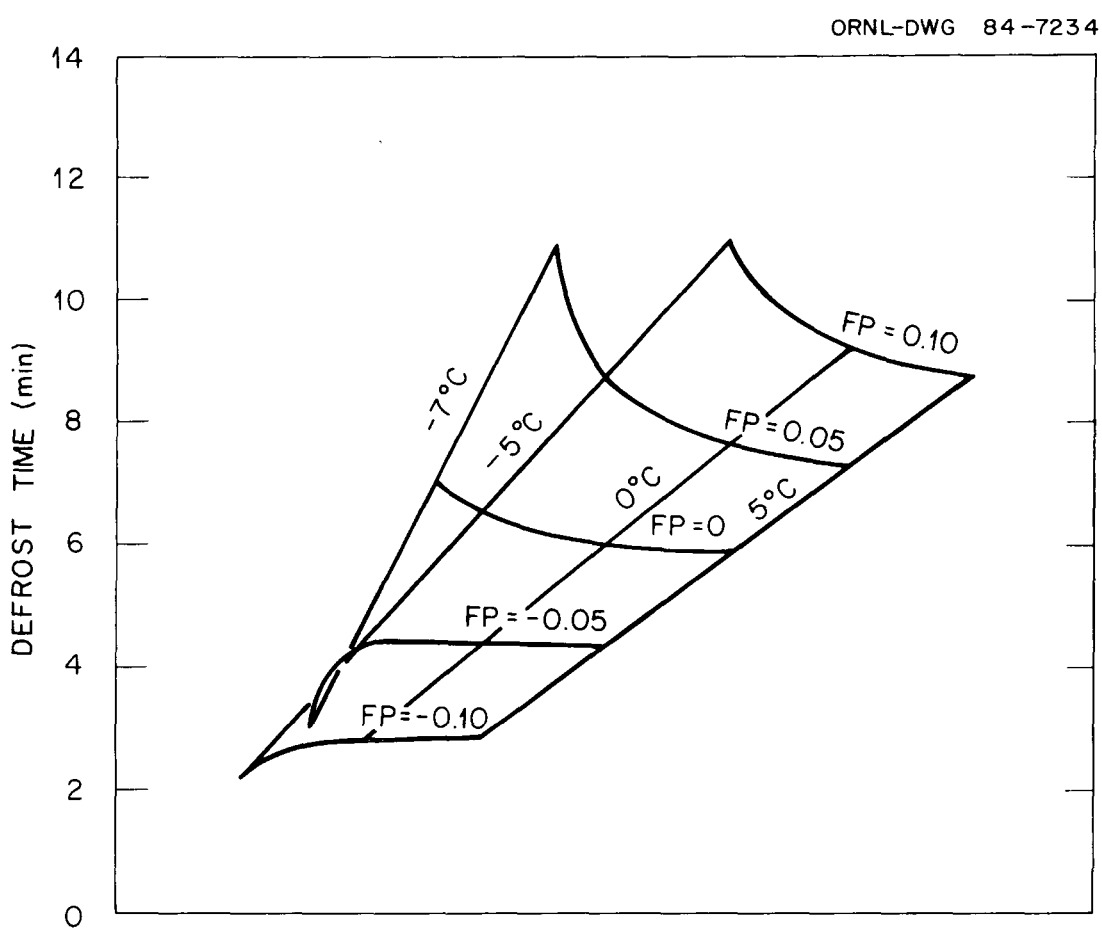

Fig. 3.27. Defrost time vs frosting potential and outdoor air temperature.

3.4 EFFECT OF DESUPERHEATER OPERATION ON CYCLING, FROSTING, AND DEFROSTING LOSSES

As indicated in Sect. 2, the desuperheater was operated during alternate months in the 1981-82 test year, including January and March. This section discusses the effect of the desuperheater operation on heating mode dynamic losses.

Figure 3.28 is a plot of modal COP versus ambient operating temperature for March 1982 (2-min transient delay time), superimposed on the data from Fig. 3.12 for nondesuperheater operation. As the figure shows, transient, normal, and overall COPs for desuperheater operation agree reasonably well with those without the desuperheater. A similar plot for 4-min transient delay times, Fig. 3.29, shows almost the same level of agreement. Figure 3.29 shows that the effect of supplemental resistance heat on the space heating COP of the unit is greater with the desuperheater, as is to be expected.

Normal-mode space heating capacity vs ambient operating temperature is plotted in Fig. 3.30, showing that desuperheater operation reduces space heating capacity by 5-20%. This reduction results in greater use of supplemental I^2R for space heating. For example, for temperatures between −10 and −5°C the heat pump used an average of 0.4 kWh/h of supplemental space heat without the desuperheater. With the desuperheater, average supplemental space heat use was 1.0 kWh/h. The difference of 0.6 kWh/h is approximately equal to the capacity reduction shown in Fig. 3.30.

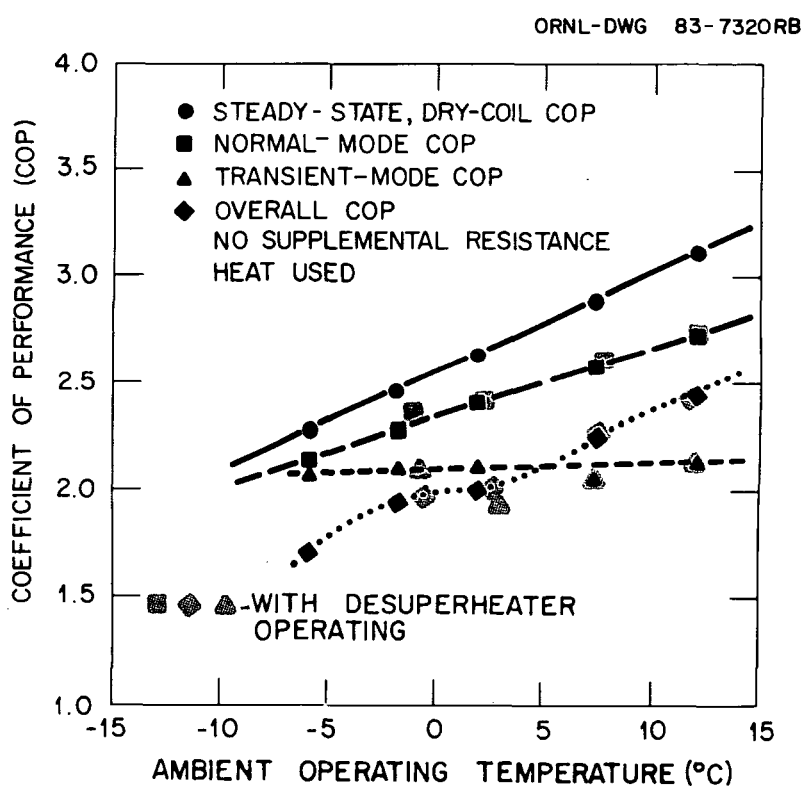

Fig. 3.28. Heat pump modal COP vs ambient operating temperature with and without desuperheater (2-min delay time for start-up transient).

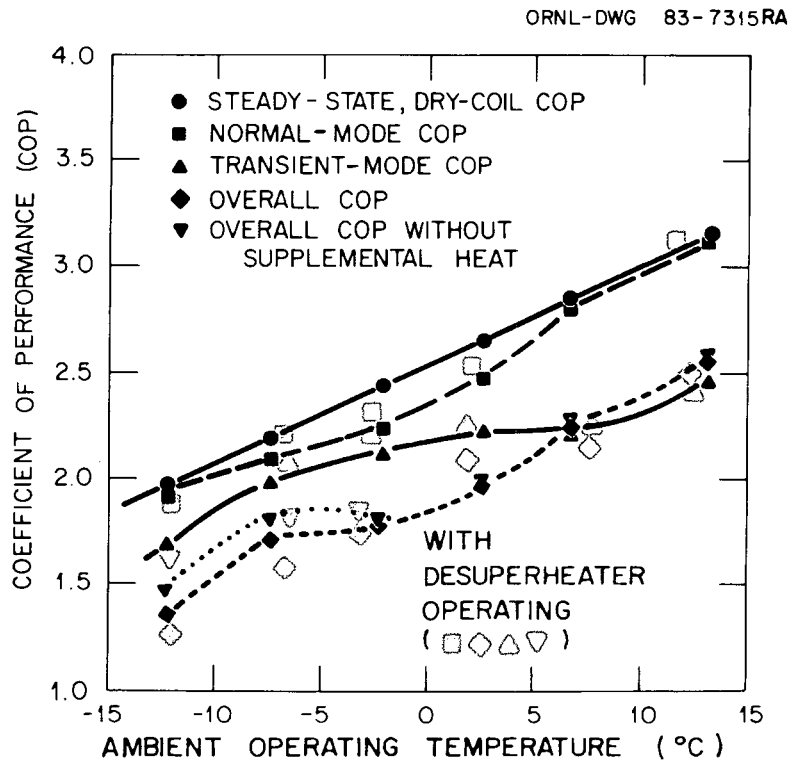

Fig. 3.29. Heat pump modal COP vs ambient operating temperature with and without desuperheater (4-min delay time for start-up transient).

It would be expected that this capacity reduction should be manifested by increased percentage run time at a given temperature for desuperheater operation. However, percent on-time plotted against outdoor air temperature in Fig. 3.31 shows no clear difference between that for desuperheater and nondesuperheater operation.

Capacity and COP ratios based on normal-mode space heating capacity for desuperheater operation are superimposed on those for nondesuperheater operation (from Fig. 3.15) in Fig. 3.32. Here again, no real difference is discernible. Thus, there is no reason to suspect that the C_d for desuperheater operation is any different from that previously determined for nondesuperheater operation.

Space heating output loss per cycle (as defined in Sect. 3.3.3) for desuperheater operation is plotted against off-time per cycle in Fig. 3.33 superimposed on nondesuperheater operation results. As before, no clear effect of the desuperheater can be seen. Similar results are seen in Fig. 3.34 for the input energy increase per cycle.

Defrost time per cycle versus frosting potential for desuperheater operation is superimposed on similar data for nondesuperheater operation in Figs. 3.35–3.37. For low outdoor air temperature ranges (Figs. 3.35 and 3.36) there seems to be a slight tendency for defrost times to be longer when the desuperheater is operating. This is reasonable in light of the fact that, in defrost, the desuperheater is competing with the outdoor coil for the available heat output, leaving less available for frost melting. For the temperature range above 0°C,

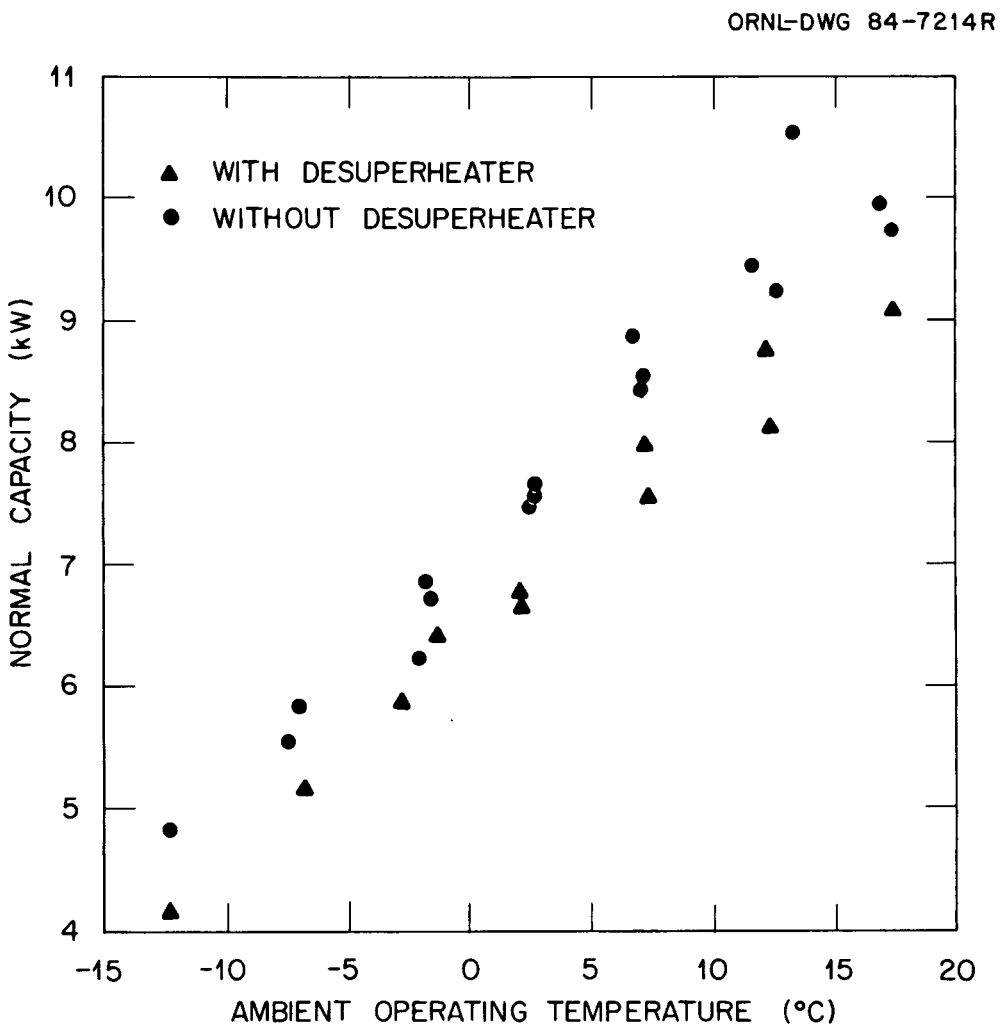

Fig. 3.30. Normal-mode space heating capacity vs ambient operating temperature with and without desuperheater.

there appears to be no significant difference in defrost times whether or not the desuperheater is operating.

Overall energy consumption penalty including frosting, defrosting, and cycling as a percentage of total energy consumption (exclusive of I^2R supplemental heat) is plotted against ambient operating temperature in Fig. 3.38 for the 1981-82 heating season. For operation both with and without the desuperheater, the overall penalty ranges from about 20 to about 30%, rising sharply for temperatures above 13°C. There seems to be essentially no difference in degradation with or without the desuperheater.

From the foregoing data and analyses, it appears that having the desuperheater operating with the heat pump had no detectable effect on space heating dynamic losses. Supplemental space heating requirements were significantly higher, however.

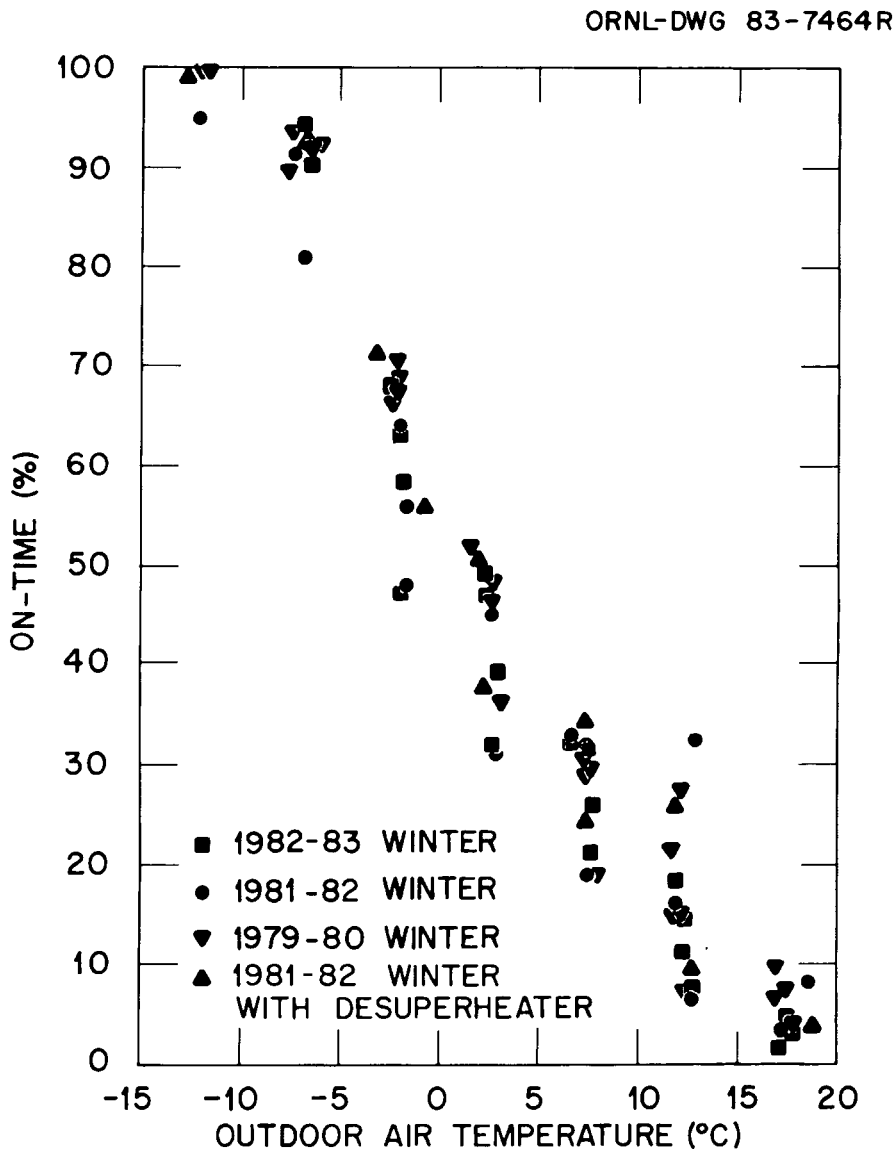

Fig. 3.31. Percent on-time vs outdoor air temperature.

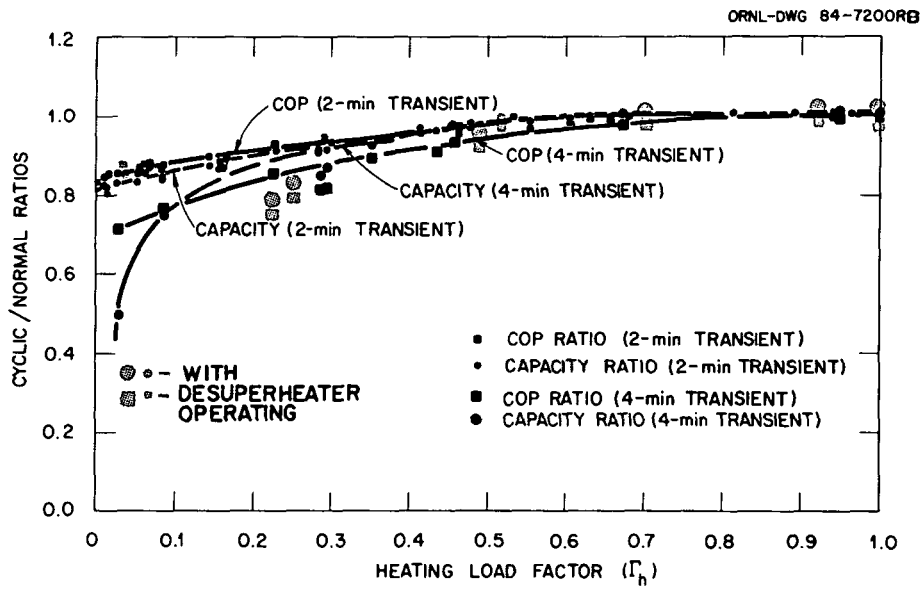

Fig. 3.32. COPRAT and CAPRAT vs heating load factor (Γ_h) with and without desuperheater.

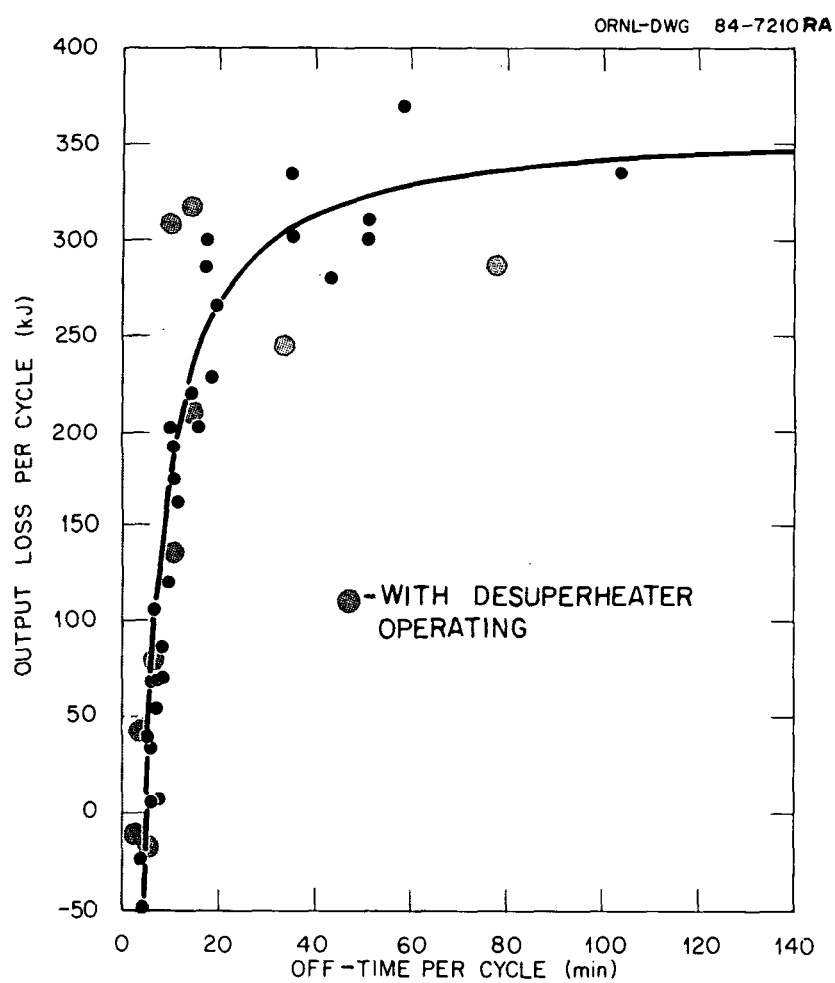

Fig. 3.33. Output loss per cycle vs off-time per cycle with and without desuperheater.

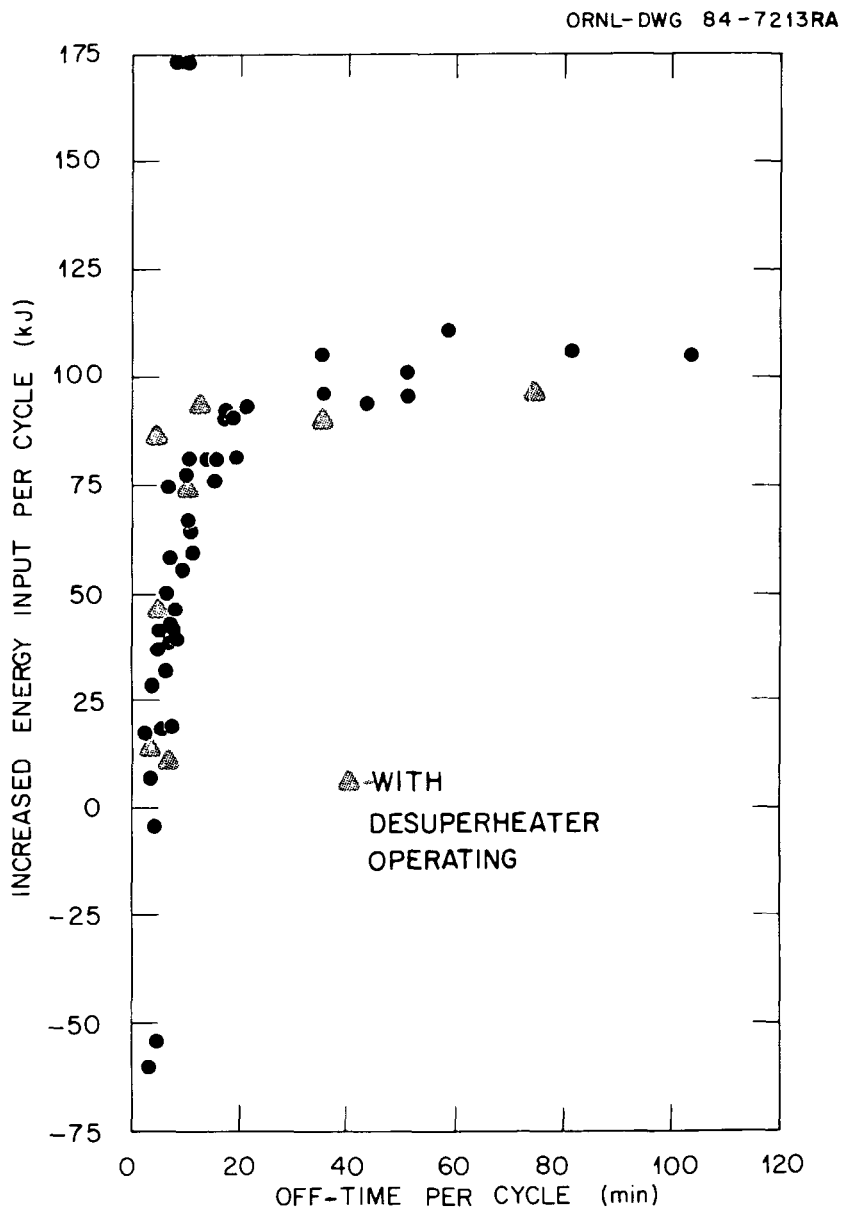

Fig. 3.34. Increased energy input per cycle vs off-time per cycle with and without desuperheater.

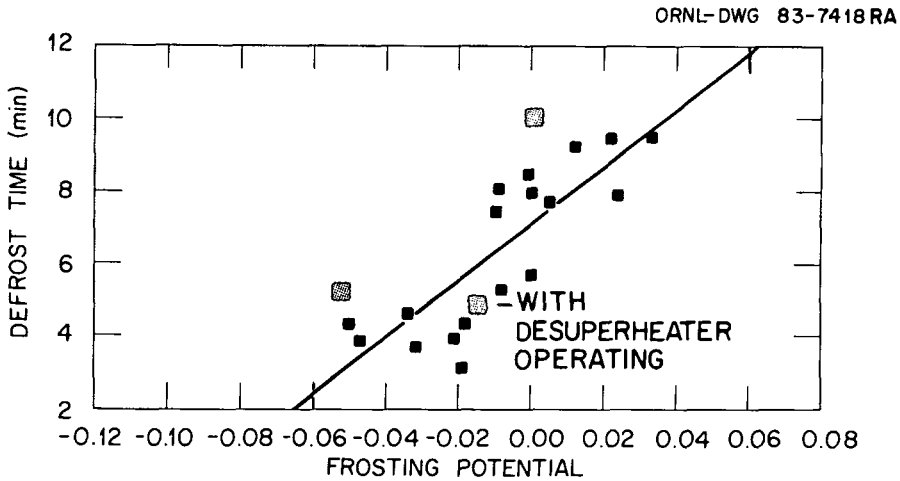

Fig. 3.35. Defrost time vs frosting potential with and without desuperheater ($-10°C < T < -5°C$).

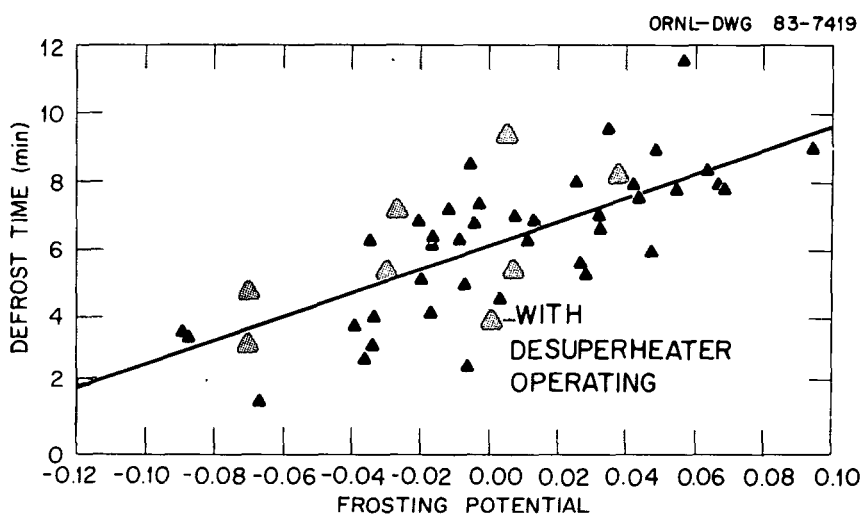

Fig. 3.36. Defrost time vs frosting potential with and without desuperheater ($-5°C < T < 0°C$).

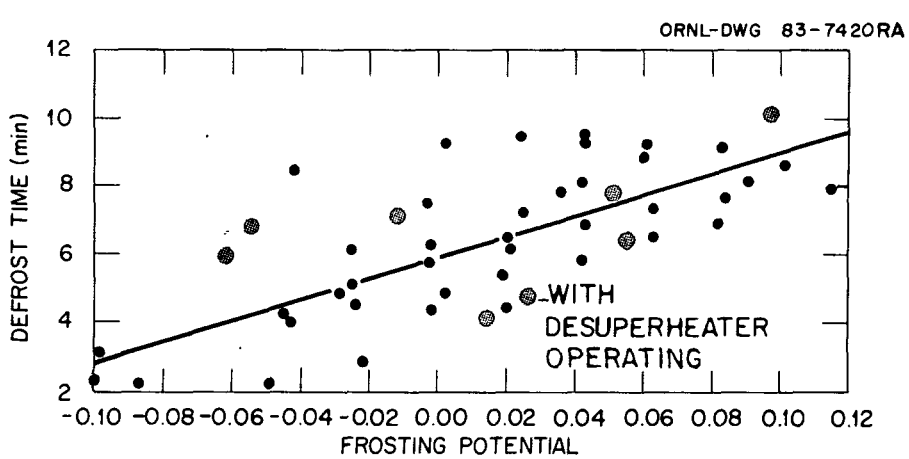

Fig. 3.37. Defrost time vs frosting potential with and without desuperheater ($0°C < T < 5°C$).

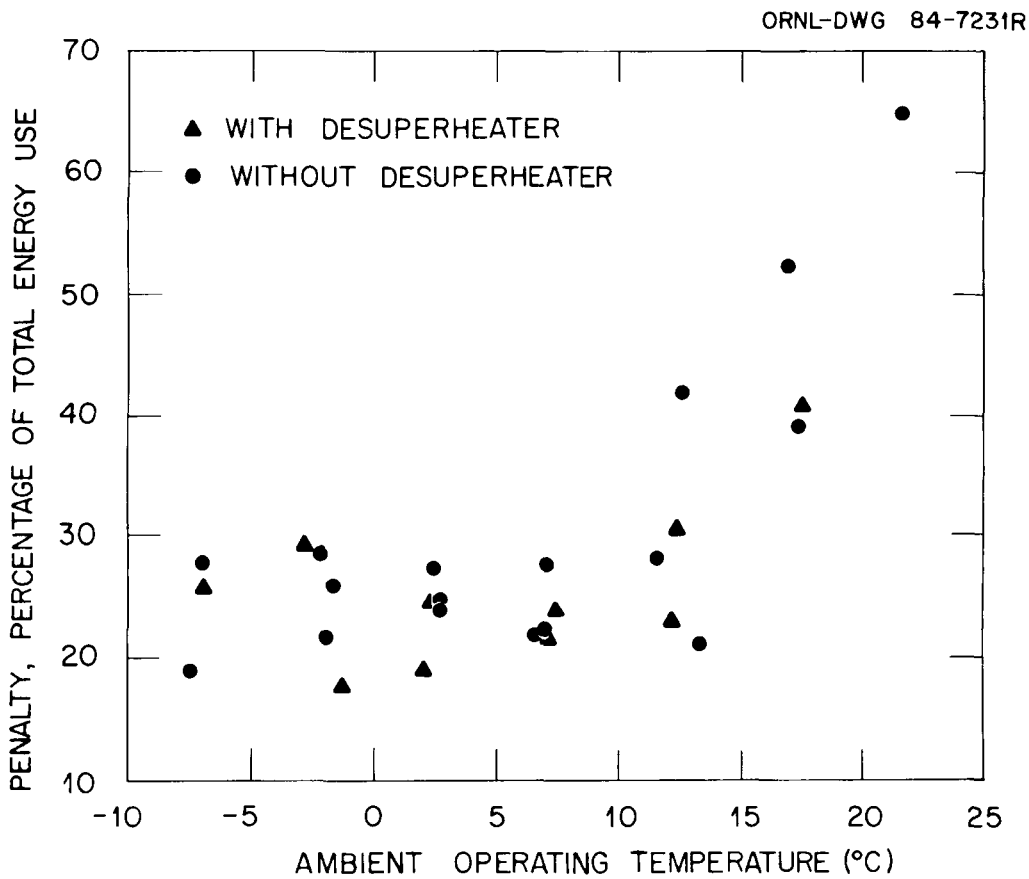

Fig. 3.38. Overall energy consumption penalty vs ambient operating temperature with and without desuperheater.

4. COOLING SEASON PERFORMANCE

Cooling season test results covering seven summer months during 1982 and 1983 and analyses of those results are discussed in this section. Table 4.1 provides a description of the seven monthly data sets on which the test results and analyses are based. Detailed tabulations of data and results are included in Appendix A, Tables A.3 and A.4, in 5°C-wide bin-months. Steady-state performance, energy use penalties due to cycling, and the effect of cycling rate on seasonal performance are discussed in the following sections.

Table 4.1. Cooling season monthly data sets

Month	Days included in data set	Data hours[a]	Hours with no heat pump operation
June 1982	June 1-30	714	329
July 1982[b]	July 12-28	383	68
August 1982	August 18-September 2	381	168
September 1982[b]	September 1-October 14[c]	991	700
June 1983	June 13-July 10	641	309
July 1983	July 11-20, 25-31	361	129
August 1983	August 1-4, 9-26	502	174

[a]Total hours minus those hours with missing or suspect data.
[b]Desuperheater active.
[c]There is a 2-d overlap in the August and September 1982 data sets.

4.1 MANUFACTURER'S RATINGS AND ON-SITE STEADY-STATE TESTS

There is no ORNL laboratory measurement of steady-state cooling performance analogous to that used in the heating performance analysis. Manufacturer's product data and on-site measurements were available, however. Table 4.2 summarizes the results of several on-site tests over the 1980, 1982, and 1983 summers. Data from the manufacturer are listed in Table 4.3. The data from the tables are plotted against outdoor air temperature in Figs. 4.1 and 4.2.

As noted in Table 4.3, the manufacturer's data used are for a 16.1°C indoor wet-bulb temperature in order to match the average wet-bulb temperature for the on-site tests. These data were then adjusted, as noted, to account for the differences between site-measured fan power draw and that used by the manufacturer for rating purposes. Linear regression of the adjusted data gives the following equations for capacity and COP:

$$\text{Capacity} = 12.57 - 0.089 \times T \tag{4.1}$$

and

$$COP = 4.46 - 0.052 \times T , \tag{4.2}$$

with capacity in kilowatts and T in degrees Celsius.

Obviously, the steady-state performance in 1982 and 1983 has been degraded from both the 1980 measured performance and the manufacturer's claimed performance, especially at higher temperatures. The reason for this degradation is not known. Installation of the

Table 4.2. Results of on-site steady-state cooling tests

Date	Cooling capacity (W)	Energy consumption (W)		COP	Outdoor temperature (°C)	Indoor temperature[a] (°C)	
		Compressor + outdoor fan	Indoor fan			wet bulb	dry bulb
June 20, 1980	10,424	3,037	404	3.03	26.5	15.8	22.2
July 9, 1980	9,379	3,411	405	2.46	35.2	17.2	23.3
May 13, 1982	9,704	3,006	408	2.84	27.0	17.8	24.4
May 28, 1982	9,823	2,861	415	3.00	25.6	16.1	22.8
July 1, 1982	9,589	2,880	411	2.91	27.8	15.6	22.8
August 19, 1982	8,869	3,003	405	2.60	29.8	16.7	23.3
June 29, 1983	8,907	2,935	410	2.66	29.1	16.1	23.3
August 29, 1983	8,173	3,104	407	2.33	31.3	16.1	24.4
October 5, 1983	9,710	2,903	410	2.93	24.5	16.1	24.4

[a]Measured at return air grill.

Table 4.3. Manufacturer's rated steady-state cooling performance data

Outdoor temperature (°C)	Compressor power[a] (kW)	Total capacity[a,b] (kW)	COP[b]	Adjusted capacity[c] (kW)	Adjusted COP[c]
29.4	2.75	9.74	2.71	9.93	2.92
32.2	2.85	9.54	2.58	9.73	2.78
35.0	2.95	9.29	2.45	9.48	2.63
37.8	3.05	9.00	2.31	9.19	2.48

[a]Based on 16.1°C indoor wet-bulb temperature.
[b]Based on specified 600-W indoor fan and 250-W outdoor fan.
[c]Adjusted for site-measured 410-W indoor fan and 240-W outdoor fan.

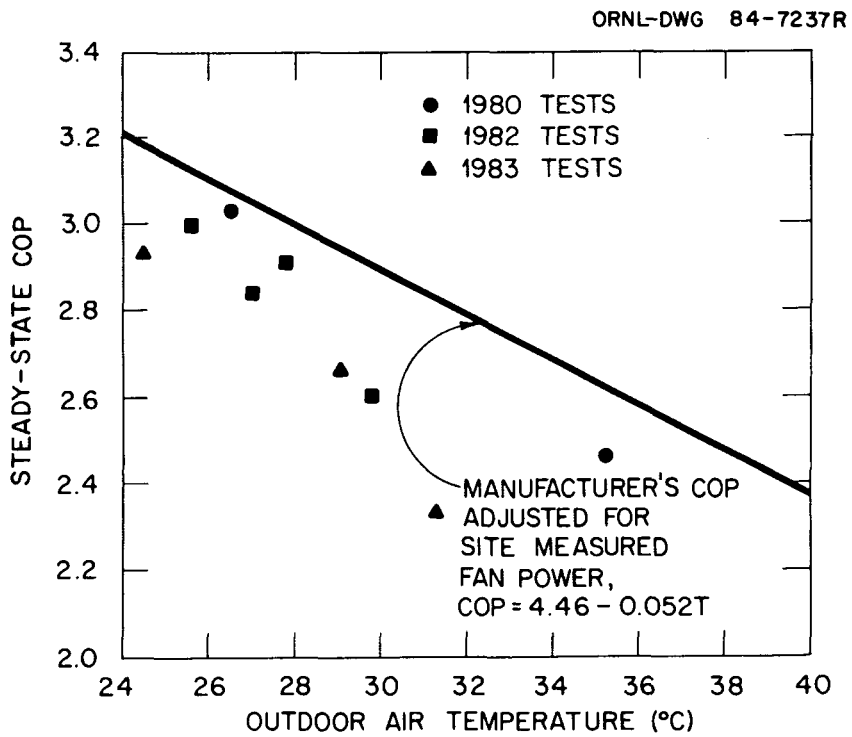

Fig. 4.1. Steady-state cooling COP vs outdoor air temperature.

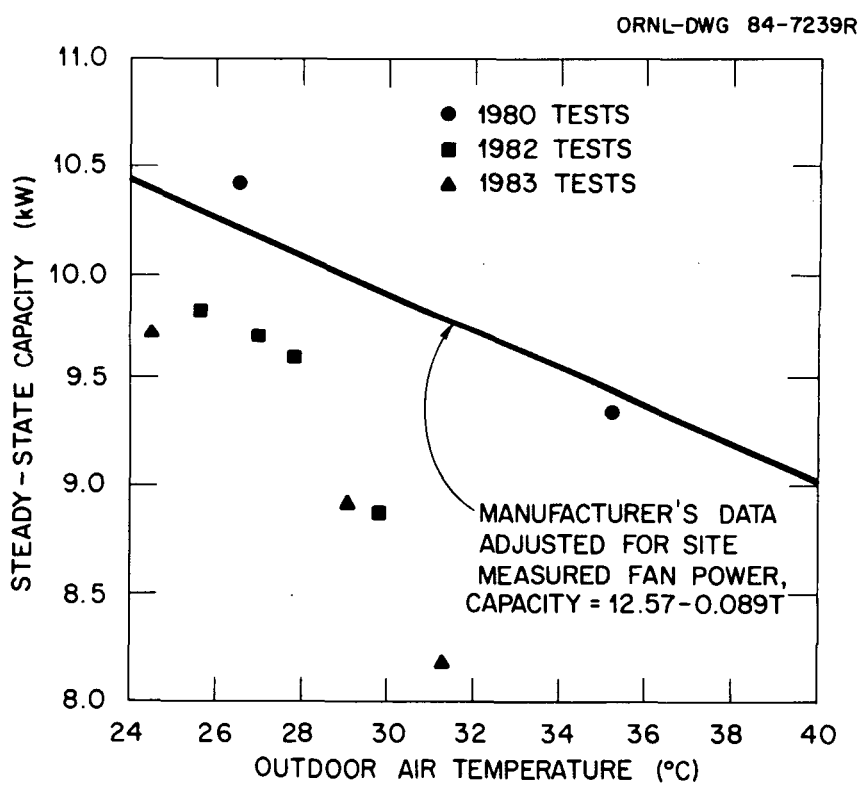

Fig. 4.2. Steady-state cooling capacity vs outdoor air temperature.

desuperheater (during November 1980) may have had some effect. Whatever the reason, it apparently did not similarly affect heating performance, as illustrated in Figs. 3.3 and 3.4.

Plotting fractional on-time (F_r) vs outdoor air temperature, as is done in Fig. 4.3 for the 1980, 1982, and 1983 cooling seasons, shows that the heat pump had to run longer to meet

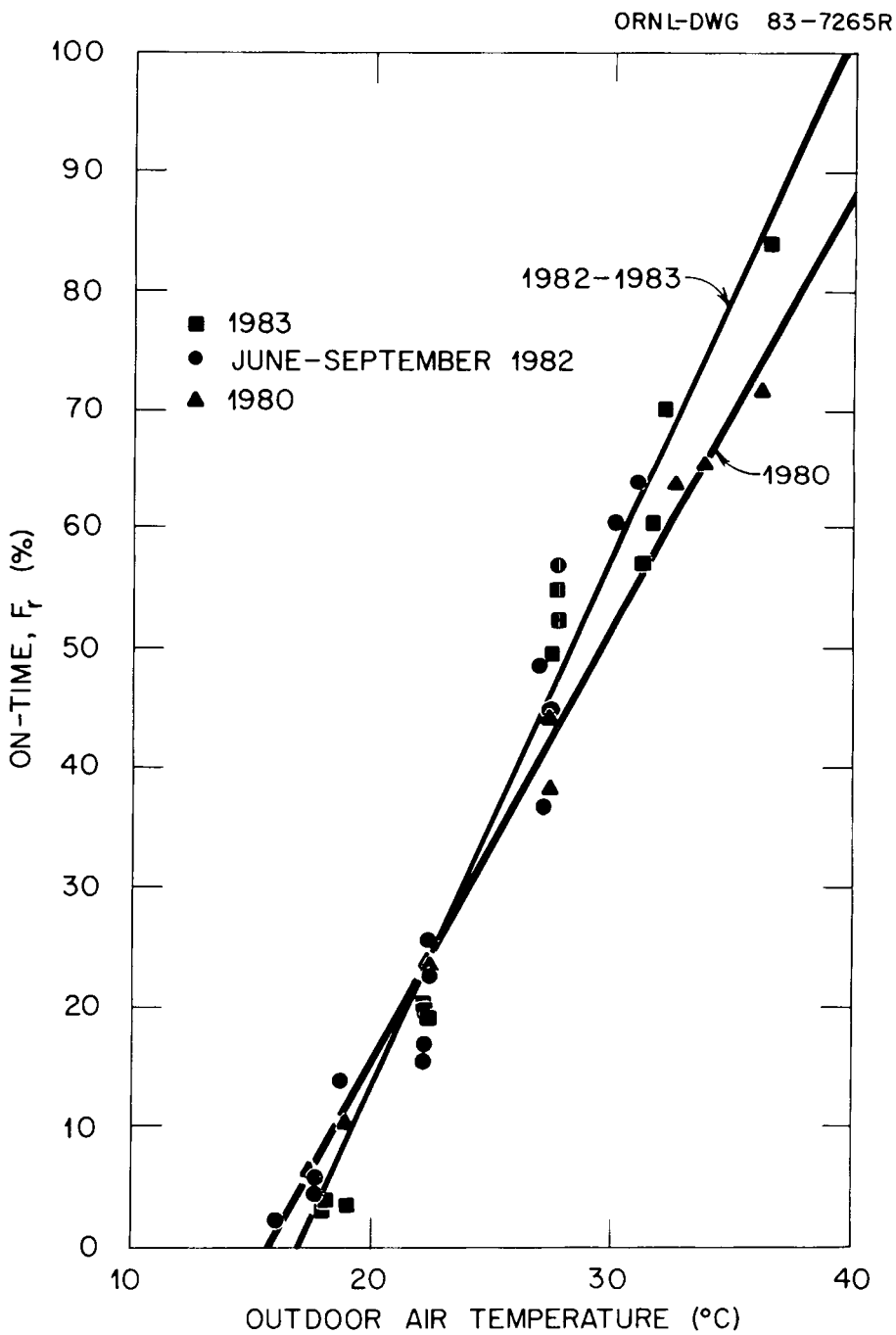

Fig. 4.3. Percent on-time vs outdoor air temperature.

the load at high temperatures in 1982 and 1983 than it did in 1980, mirroring the trend shown in Figs. 4.1 and 4.2. At low temperatures, F_r tended to be about the same or slightly less than in 1980. Linear regressions of the data in Fig. 4.3 gave the following equations:

For 1980

$$F_r(\%) = 3.63 \times T - 57.46 \quad (r^2 = 0.99) ,$$

and for 1982 and 1983

$$F_r(\%) = 4.42 \times T - 74.94 \quad (r^2 = 0.96) .$$

Plotting cyclic to steady-state capacity and COP ratios (CAPRAT and COPRAT) vs cooling load factor (Γ_c), using both manufacturer's data and 1980 on-site tests as the steady-state base (Figs 4.4 and 4.5, respectively), yielded poor correlations. Correlations obtained using the 1980 tests as the base were somewhat better than those obtained using the manufacturer's data. In neither case do the CAPRATs or COPRATs appear to approach 1.0 as Γ_c approaches 1.0.

Linear regression analyses of the 1982 and 1983 on-site steady-state test results yielded the following equations for steady-state capacity and COP.

$$\text{Capacity (kW)} = 15.86 - 0.237 \times T \quad (r^2 = 0.92) ,$$

$$\text{COP} = 5.277 - 0.0906 \times T \quad (r^2 = 0.92) .$$

CAPRAT and COPRAT vs Γ_c using the above equations for steady-state performance are plotted in Fig. 4.6. The data correlate much better than before, but CAPRAT and COPRAT significantly exceed 1.0 at $\Gamma_c = 1.0$.

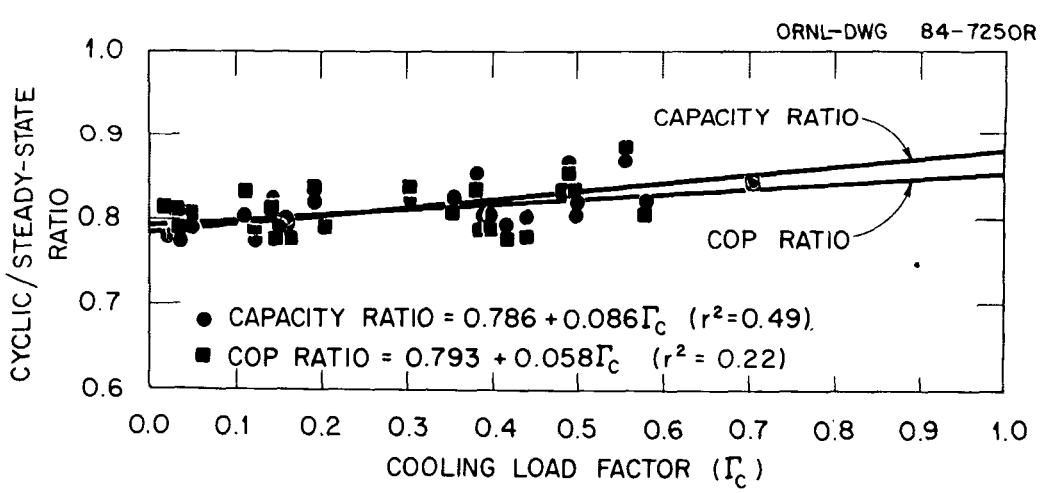

Fig. 4.4. COPRAT and CAPRAT vs cooling load factor (Γ_c) based on manufacturer's steady-state rating.

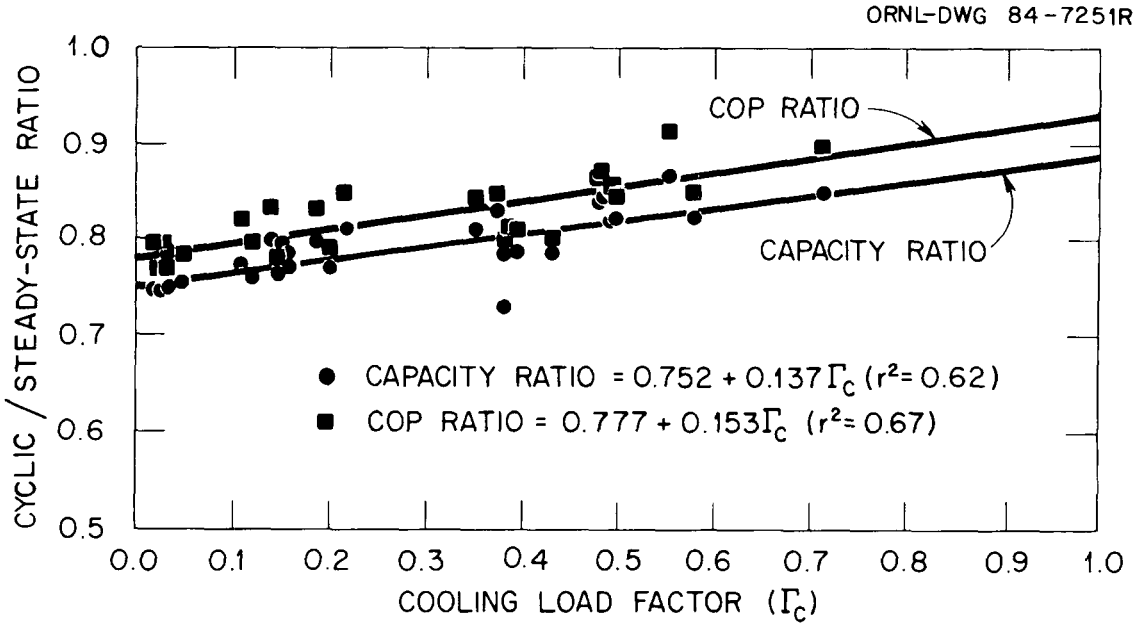

Fig. 4.5. COPRAT and CAPRAT vs cooling load factor (Γ_c) based on 1980 on-site tests.

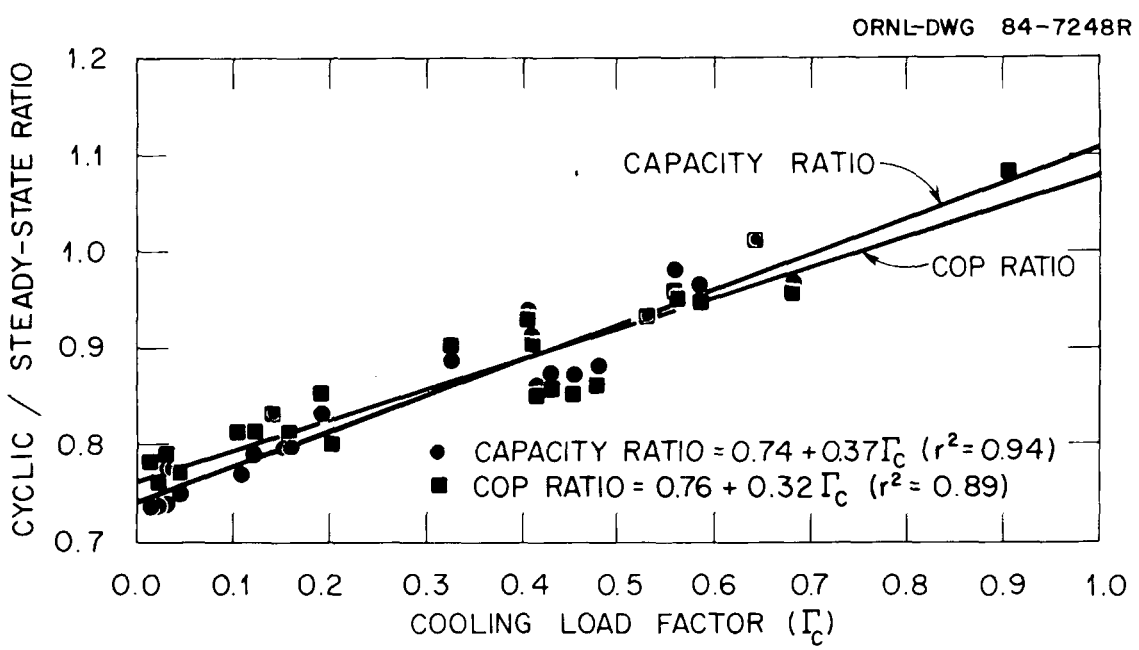

Fig. 4.6. COPRAT and CAPRAT vs cooling load factor (Γ_c) based on 1982 and 1983 on-site tests.

4.2 DERIVED STEADY-STATE PERFORMANCE

Reasoning that the cyclic-to-steady-state ratios of capacity and COP should approach 1.0 as Γ_c approaches 1.0, we decided to derive equations for steady-state performance that would force such a result and compare them with the site-measured performance. The approach taken was to determine relationships for steady-state capacity and COP such that the following relationships held.

For CAPRAT,

$$\text{CAPRAT} = \text{Cap}_{cyc}/\text{Cap}_{ss} = A + (1 - A) \times \Gamma_c \ .$$

Similarly, for COPRAT,

$$\text{COPRAT} = \text{COP}_{cyc}/\text{COP}_{ss} = B + (1 - B) \times \Gamma_c \ .$$

In Fig. 4.6, where CAPRAT, COPRAT, and Γ_c are determined using the 1982 and 1983 on-site tests as the steady-state basis, both CAPRAT and COPRAT are approximately equal to 0.75 at $\Gamma_c = 0.0$. It was decided, therefore, to let both A and B be 0.75. The CAPRAT and COPRAT curve desired is illustrated in Fig. 4.7.

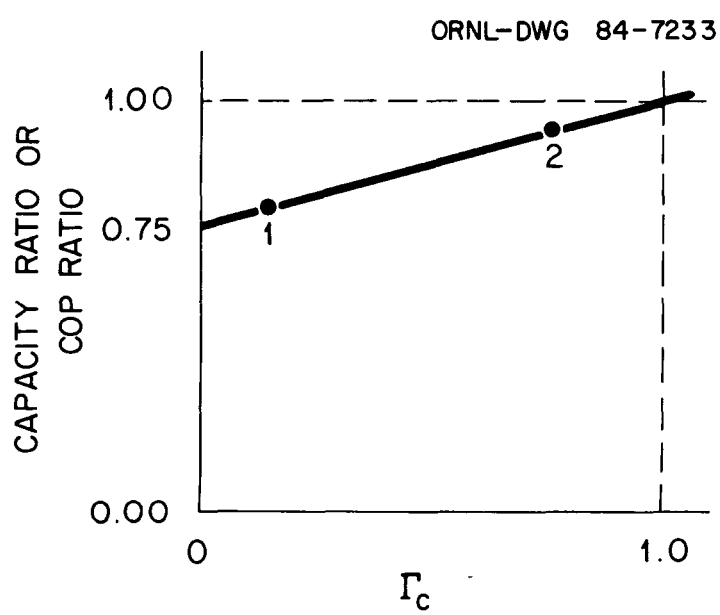

Fig. 4.7. COPRAT and CAPRAT vs cooling load factor (Γ_c), idealized.

4.2.1 Determination of Steady-State Capacity Curve

Data for point 1 in Fig. 4.7 are taken from the June 1982 bin containing all hours where outdoor air temperature is less than 20°C. Point 2 data come from the August 1983 bin containing all hours where outdoor air temperature is greater than 35°C. The data are listed in Table 4.4.

Table 4.4. Data for points 1 and 2 in Fig. 4.7

Point no.	Bin-month	Cyclic capacity (kW)	Cyclic COP	Average operating temperature (°C)	Bin hours	Total cooling delivered (kWh)
1	June 1982 T < 20°C	8.50	2.77	18.6	235	87.43
2	August 1983 T > 35°C	7.83	2.14	36.3	19	125.12

For point 1:

$$\mathrm{CAPRAT}_1 = (\mathrm{Cap}_{cyc}/\mathrm{Cap}_{ss})_1 = 0.75 + 0.25 \times \Gamma_c ,$$

where $\Gamma_c = [(\text{actual cooling load})/(\mathrm{Cap}_{ss} \times \text{bin hours})]_1$.

Substituting the data from Table 4.4,

$$8.50/(\mathrm{Cap}_{ss})_1 = 0.75 + 0.25 \times 87.43/[(\mathrm{Cap}_{ss})_1 \times 235] .$$

Solving for $(\mathrm{Cap}_{ss})_1$:

$$(\mathrm{Cap}_{ss})_1 = 11.209 \text{ kW} .$$

Similarly, for point 2:

$$(\mathrm{Cap}_{ss})_2 = 8.245 \text{ kW} .$$

Using an equation for steady-state capacity, Cap_{ss}, of the form

$$\mathrm{Cap}_{ss} = a + b \times T ,$$

we have for point 1

$$11.209 = a + b \times 18.6 ,$$

and for point 2

$$8.245 = a + b \times 36.3 .$$

The equation for Cap_{ss} thus becomes

$$\mathrm{Cap}_{ss} = 14.324 - 0.168 \times T . \tag{4.3}$$

4.2.2 Determination of Steady-State COP Curve

The steady-state COP curve was derived from Eq. 4.3 and the average site-measured full-hour power draw of the heat pump as a function of ambient temperature.

Average full-hour power draws for each month along with the average temperature at which they were measured are given in Table 4.5. Linear regression gives the following equation for the power draw as a function of outdoor temperature.

$$\text{Power}_{ss} = 2.515 + 0.0327 \times T, \text{ kW} \quad (r^2 = 0.92) \tag{4.4}$$

Now, since

$$\text{COP}_{ss} = \text{Cap}_{ss}/\text{Power}_{ss} ,$$

we can obtain from Eqs. 4.3 and 4.4:

$$\begin{aligned} &\text{at T} = 20°\text{C}, \text{ COP}_{ss} = 3.46; \\ &\text{at T} = 25°\text{C}, \text{ COP}_{ss} = 3.04; \\ &\text{at T} = 30°\text{C}, \text{ COP}_{ss} = 2.66; \\ &\text{at T} = 35°\text{C}, \text{ COP}_{ss} = 2.31. \end{aligned}$$

For these points, the equation for COP_{ss} from linear regression is

$$\text{COP}_{ss} = 4.974 - 0.0766 \times T \quad (r^2 = 0.998) . \tag{4.5}$$

Table 4.5. Measured average full-hour cooling mode power draw

Month	Average operating temperature (°C)	Power draw (kW)
June 1982	25.9	3.373
July 1982	29.4	3.466
August 1982	27.7	3.455
September 1982	27.4	3.356
June 1983	28.0	3.431
July 1983	29.7	3.509
August 1983	31.6	3.541

4.2.3 Discussion of Derived Steady-State Performance

Figure 4.8 is a plot of CAPRAT and COPRAT vs Γ_c using Eqs. 4.3 and 4.5 as the base steady-state performance. As the figure shows, the correlations are reasonably good. The obvious question to be raised, however, is, Are Eqs. 4.3 and 4.5 reasonable representations of the heat pump steady-state cooling performance? Figures 4.9 and 4.10 are plots of Eqs. 4.5

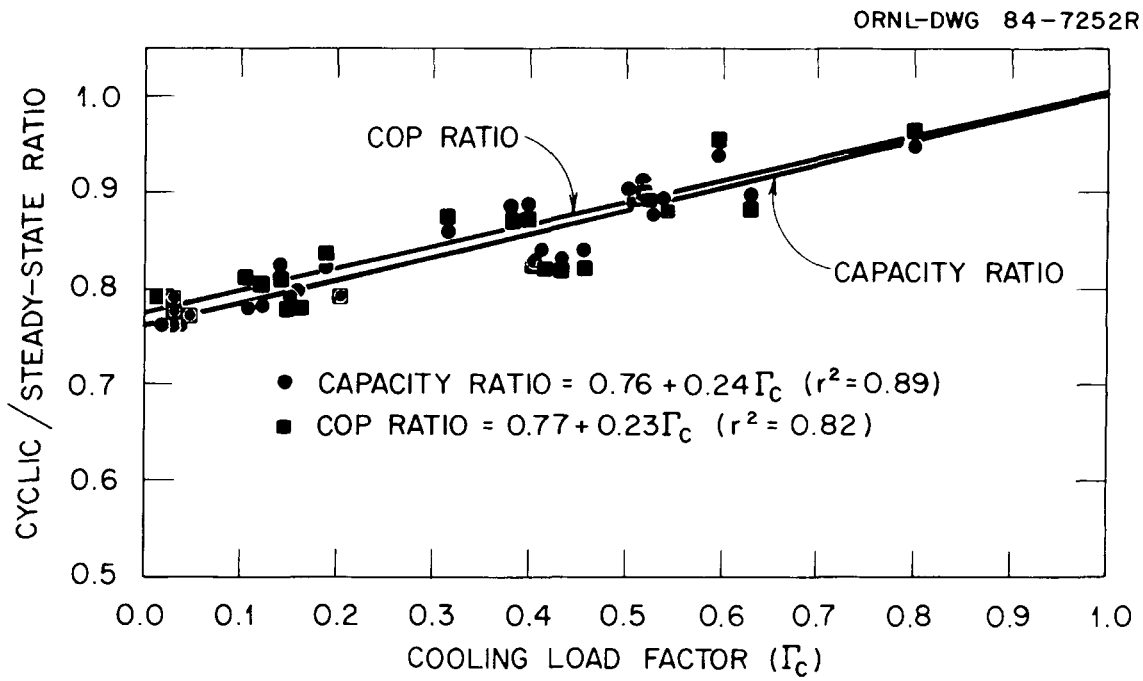

Fig. 4.8. COPRAT and CAPRAT vs cooling load factor (Γ_c) based on derived steady-state performance (Eqs. 4.3 and 4.5).

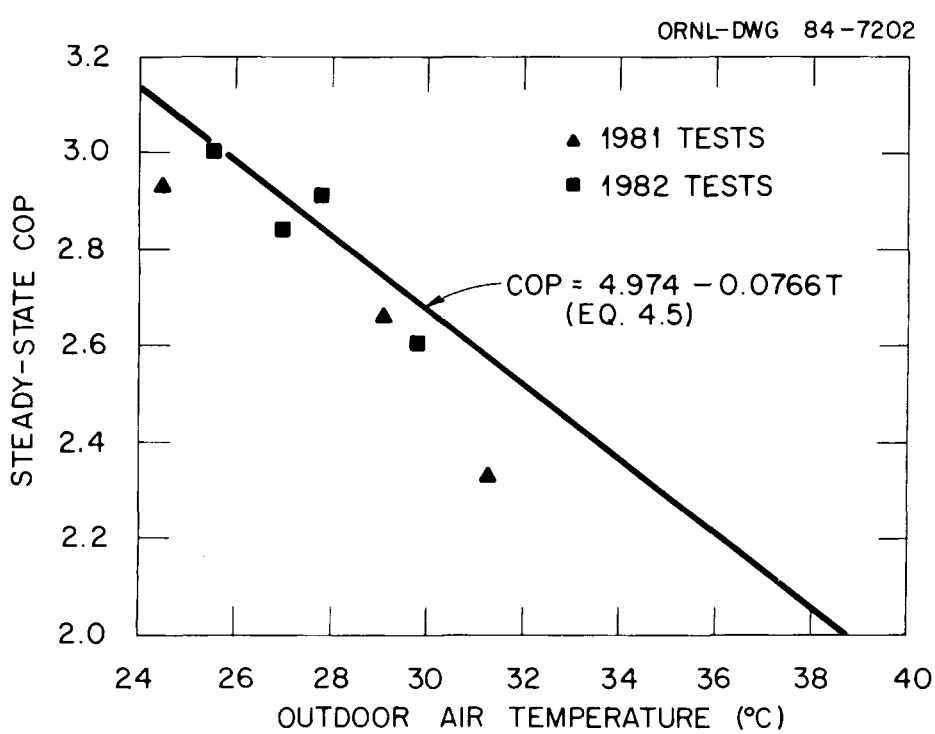

Fig. 4.9. Derived steady-state COP (Eq. 4.5) vs outdoor air temperature, with on-site test results.

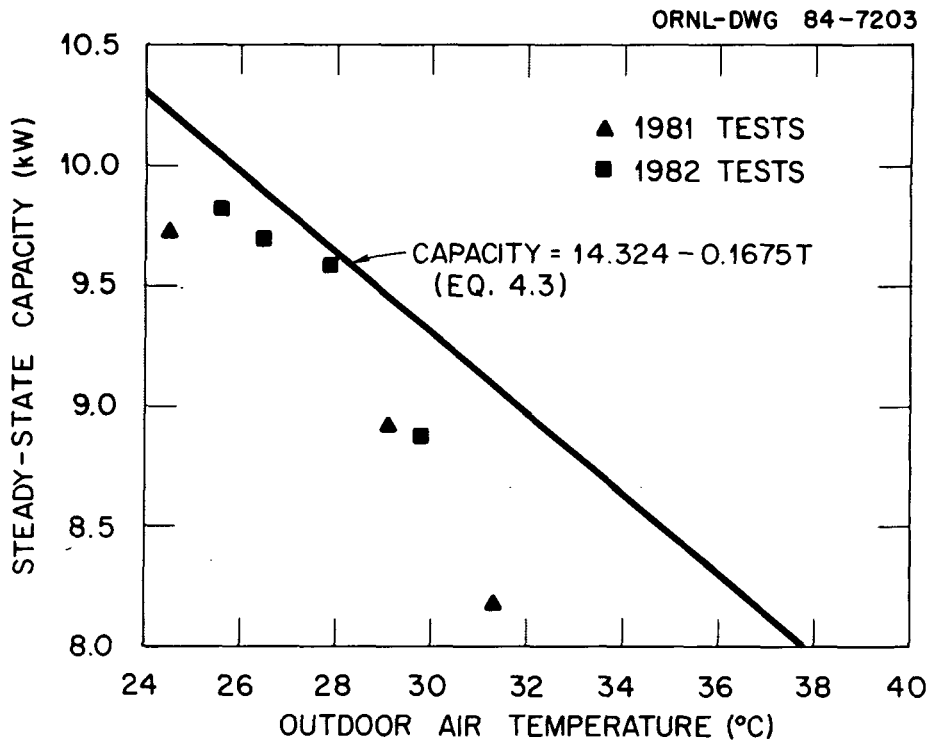

Fig. 4.10. Derived steady-state capacity (Eq. 4.3) vs outdoor air temperature, with on-site test results.

and 4.3, respectively, along with data from the 1982 and 1983 on-site tests. The figures show that both the capacity and COP equations yield values that, for any given temperature, are generally higher than those measured on-site. Repeating the derivations for an intercept point of 0.8 yielded the following equations:

$$\mathrm{Cap}_{ss} = 13.236 - 0.138 \times T \ , \tag{4.6}$$

$$\mathrm{COP}_{ss} = 4.628 - 0.0672 \times T \ . \tag{4.7}$$

These are plotted in Fig. 4.11 for comparison with site-measured performance and are seen to approximate the measured performance more closely than Eqs. 4.3 and 4.5. Plotting CAPRAT and COPRAT vs Γ_c (using Eqs. 4.6 and 4.7 for steady-state performance) as in Fig. 4.12 shows, however, that the correlations thus obtained are not as good as those from using Eqs. 4.3 and 4.5.

It is not clear which of the previously described sets of equations best represents the 1982 and 1983 steady-state performance of the test unit. Analysis of the data indicates, however, that CAPRAT and COPRAT decrease essentially linearly with Γ_c from 1.0 at Γ_c = 1.0 to between 0.75 and 0.8 at Γ_c = 0.0, exclusive of off-cycle energy use effects. This indicates a C_d for cooling of between 0.20 and 0.25.

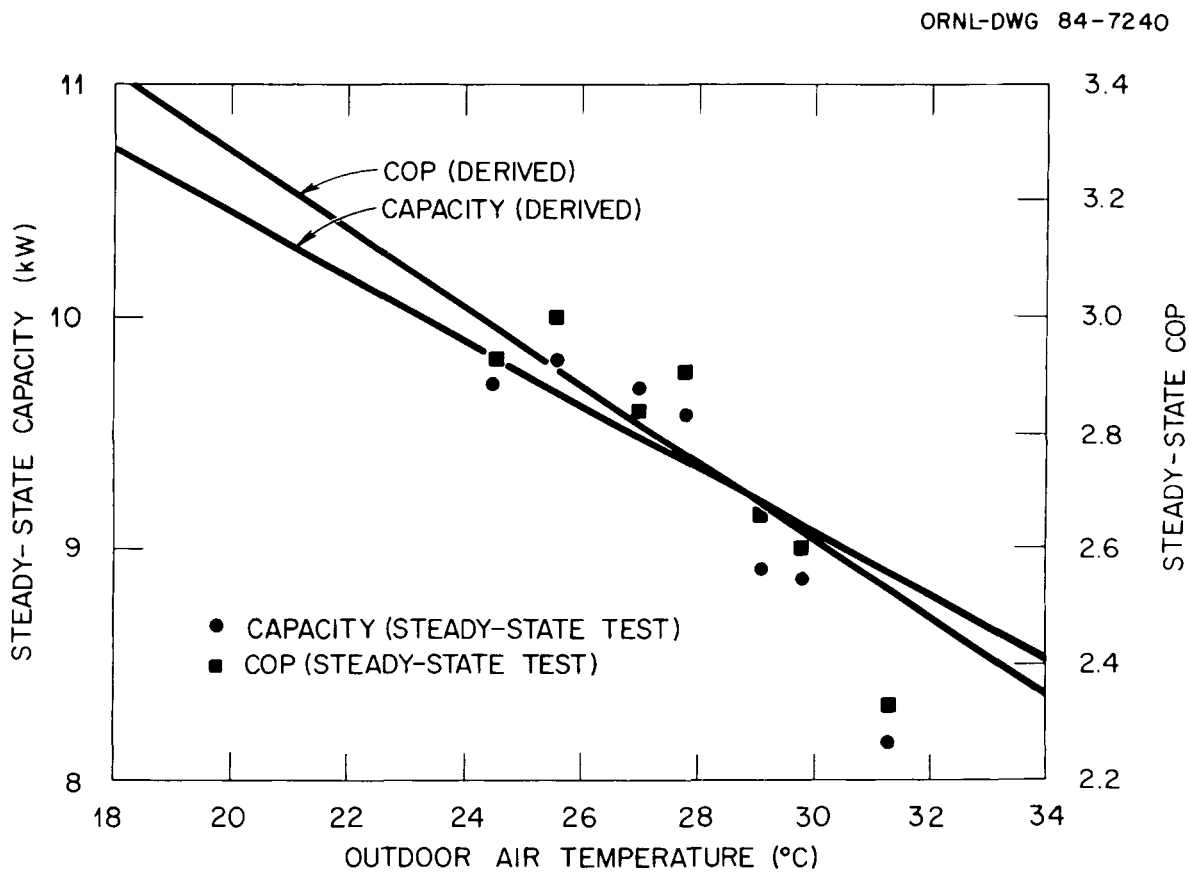

Fig. 4.11. Derived steady-state COP and capacity (Eqs. 4.6 and 4.7) vs outdoor air temperature, with on-site test results.

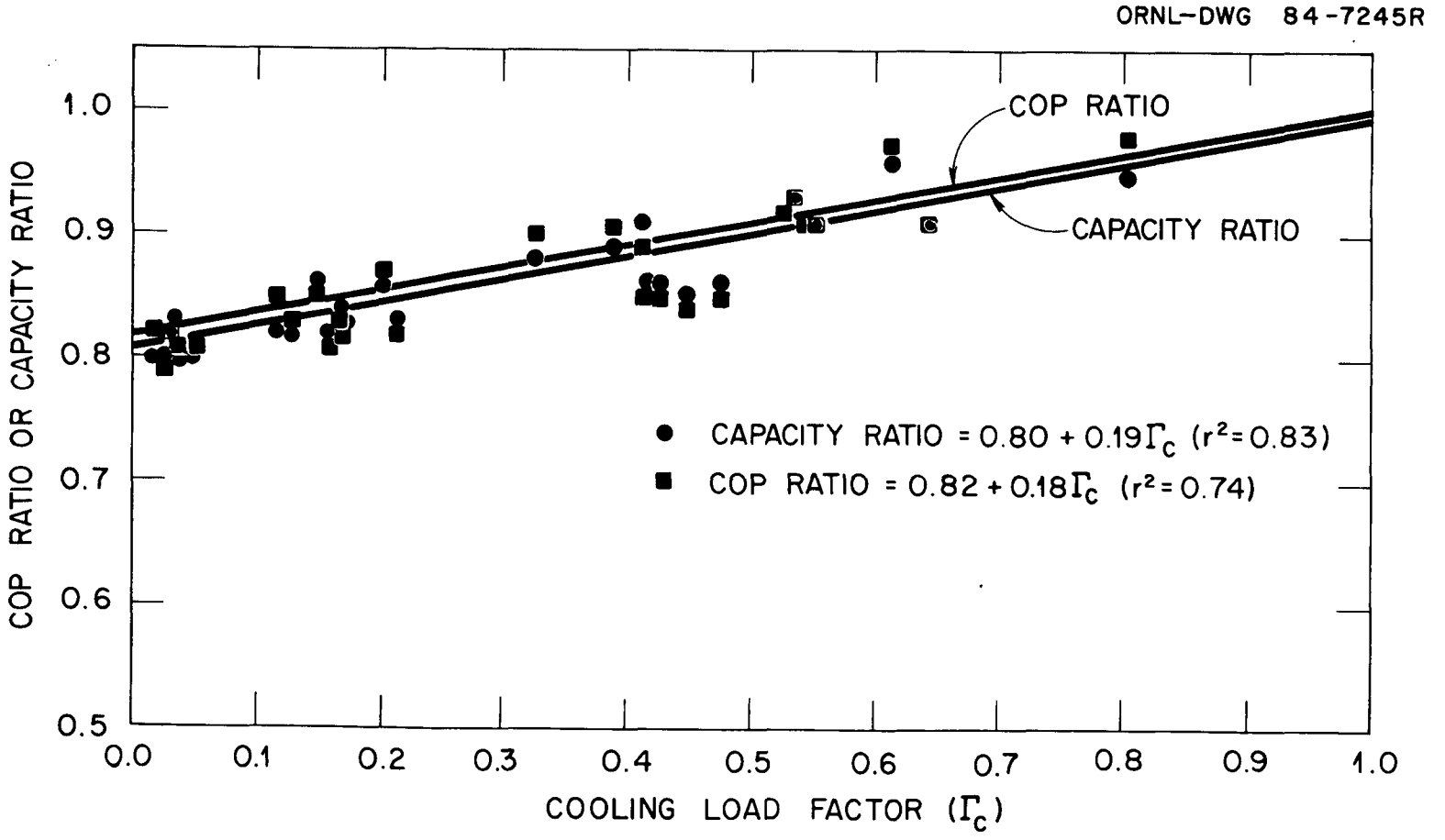

Fig. 4.12. COPRAT and CAPRAT vs cooling load factor (Γ_c) based on derived steady-state performance (Eqs. 4.6 and 4.7).

4.3 OVERALL SUMMER CYCLING TEST RESULTS

Given in Table 4.6 are overall energy consumption penalties for each month due to off-cycle energy use and start-up transients. Also included in the table are cooling load delivered, steady-state energy use required to meet the load, measured energy use, COP (overall and neglecting off-cycle energy), average ambient temperature (overall and operating*), and average run time per cycle. Steady-state energy use and start-up transient energy use penalty are based on steady-state performance as described by Eqs. 4.6 and 4.7. Hereinafter, COP and energy use (unless otherwise specified) are to be understood as neglecting off-cycle energy use effects in order to compare all months on an equal basis.

Table 4.6. Cooling season monthly dynamic losses, loads, and average temperatures

Month	Cooling load (kWh)	Off-cycle energy use (kWh)	Start-up transient energy use penalty[a] (kWh)	Steady-state energy use required[a] (kWh)	Total energy use (kWh)	COP		Average temperature (°C)	
						(1)[b]	(2)[c]	Overall	During operation
June 1982	1516.6	28.6	91.1	517.3	637.0	2.38	2.49	22.18	25.07
July 1982	1287.0	12.5	37.5	460.0	510.0	2.52	2.59	25.05	26.98
August 1982	769.8	15.5	34.9	264.3	314.8	2.45	2.57	22.82	25.34
September 1982	970.5	46.8	47.9	327.3	422.0	2.30	2.59	19.70	24.50
June 1983	1408.2	37.4	81.4	501.3	620.1	2.27	2.42	23.10	26.90
July 1983	1007.1	18.9	54.6	370.0	443.5	2.27	2.37	25.05	28.05
August 1983	1508.3	25.3	74.9	566.0	666.2	2.26	2.35	25.52	28.80
Total	8467.5	185.0	422.3	3006.2	3613.6	2.34	2.47		
Percent[d]		5.1	11.7	83.2	100.0				

[a]Based on Eqs. 4.6 and 4.7.
[b]Overall.
[c]Neglecting off-cycle energy use.
[d]Percent of total energy use.

Monthly COPs for July through September of 1982 are seen to be significantly greater than for the other months. Figures 4.13 and 4.14 are plots of average ambient operating temperature and COP (transient and normal), respectively, vs average outdoor air temperature for time periods ranging from 3 to 7 d. Average operating temperature is generally higher and COP is generally lower for 1983 and June 1982 than for July through September of 1982. At least some of this COP vs operating temperature variation can be explained by weather pattern differences.

Table 4.7 contains average minimum, maximum, and mean outdoor temperatures for each month, the number of days when the temperature exceeded 32.2°C, and average indoor temperature and latent-to-total cooling ratios. As the table shows, the much warmer weather in the summer of 1983 forced the heat pump to deliver its load at higher operating

*Average ambient temperature observed during heat pump operation.

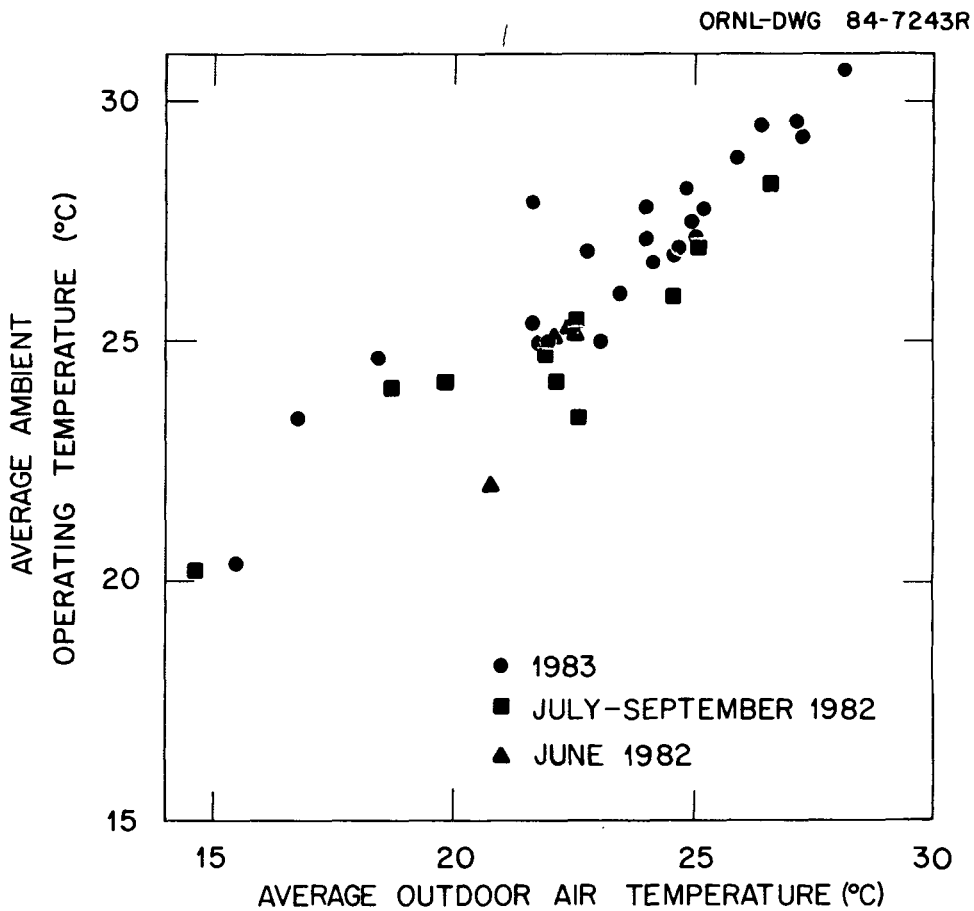

Fig. 4.13. Average ambient operating temperature vs average outdoor air temperature.

temperatures. Also of interest is the fact that July-September 1982 had higher latent-to-total cooling ratios and average relative humidity than did the other months, while the average indoor temperature was about the same for all months. For a given indoor temperature, higher latent-to-total cooling ratios result in increased COP and capacity. This trend is mirrored in Figs. 4.15 and 4.16, which plot average COP vs latent-to-total cooling ratio for the 25-30 and 30-35°C temperature bin-months, respectively.

It is interesting to compare July 1982 with July 1983. Though both months had the same average outdoor air temperature, July 1983 had a wider temperature swing. The average operating temperature in July 1983 was higher than that of July 1982, at least in part because of this wider swing. June 1982 and August 1982 both had similar outdoor temperature conditions, as indicated in Table 4.7. Despite this, June 1982 had a lower COP than did August 1982. The much lower latent-to-total cooling ratio in June probably contributed to this.

Weather effects do not seem to explain all of the differences, however. The COPs for August and September of 1982 are no better than that for July of the same year, though both months enjoyed milder outdoor temperatures and higher latent-to-total cooling ratios.

In addition, June 1983 had a lower COP than July 1982 despite milder outdoor temperature conditions and similar latent-to-total cooling ratios.

Other possible factors affecting cooling efficiency include differences in cycling rate and effects of the desuperheater on the heat pump's cooling performance.

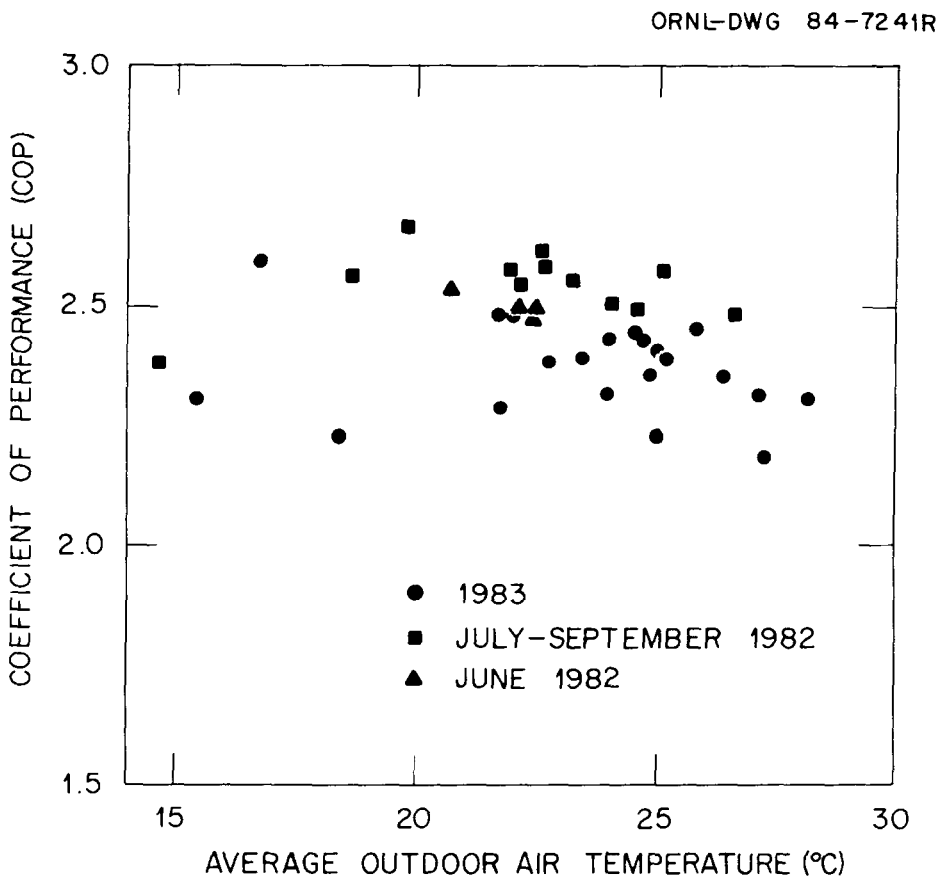

Fig. 4.14. Average COP vs average outdoor air temperature.

Table 4.7. Average ambient conditions, indoor temperatures, and latent-to-total cooling ratios

Month	Average outdoor relative humidity[a] (%)	Average temperature (°C)				Days temperature exceeded 32.2°C[a]	Average indoor temperature (°C)	Latent-to-total cooling ratio
		Mean[a]	Maximum[a]	Minimum[a]	During operation[a]			
June 1982	58	22.18	27.72	17.33	25.07	0	25.8	0.185
July 1982	69	25.05	30.72	20.61	26.98	3	26.3	0.201
August 1982	82	22.82	29.61	19.39	25.34	0	26.6	0.219
September 1982	78	19.70	25.83	15.67	24.50	0	26.0	0.225
June 1983	64	23.10	30.17	17.72	26.90	4	26.3	0.196
July 1983	65	25.05	32.50	19.94	28.05	12	26.6	0.186
August 1983	68	25.52	32.78	19.83	28.80	14	26.3	0.191

[a]From Knoxville airport weather data summary.

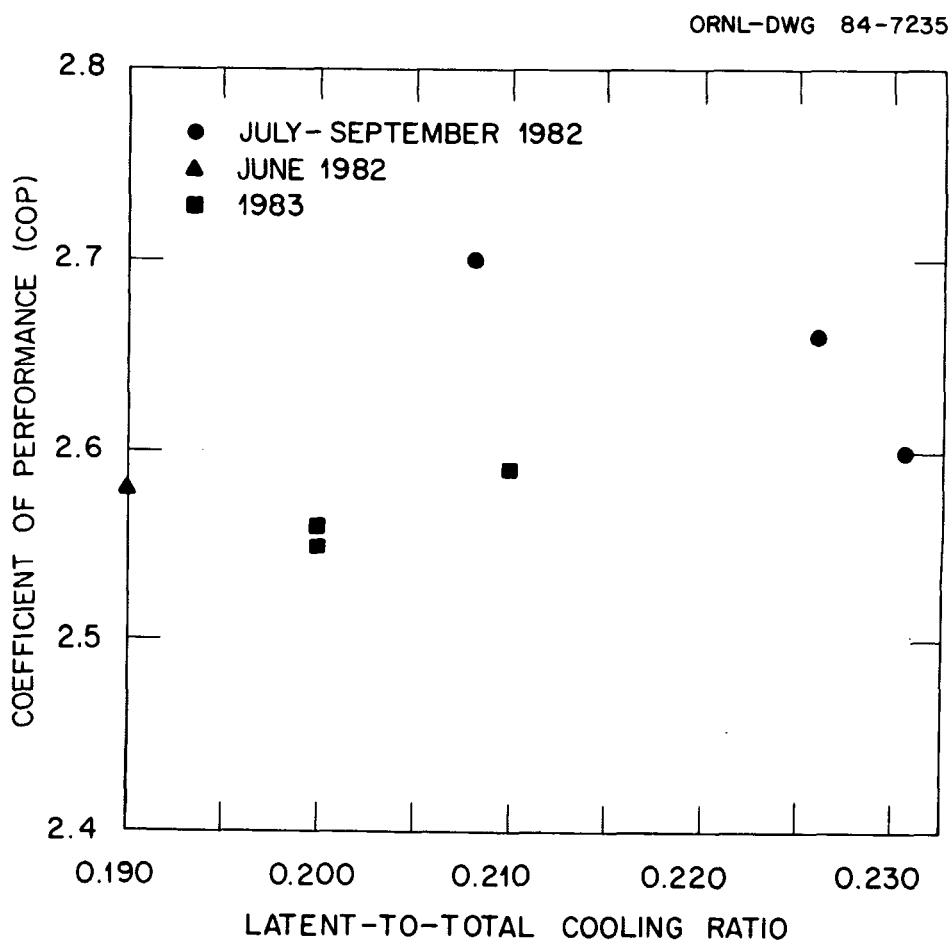

Fig. 4.15. Average COP vs average latent-to-total cooling ratio (25°C < T < 30°C).

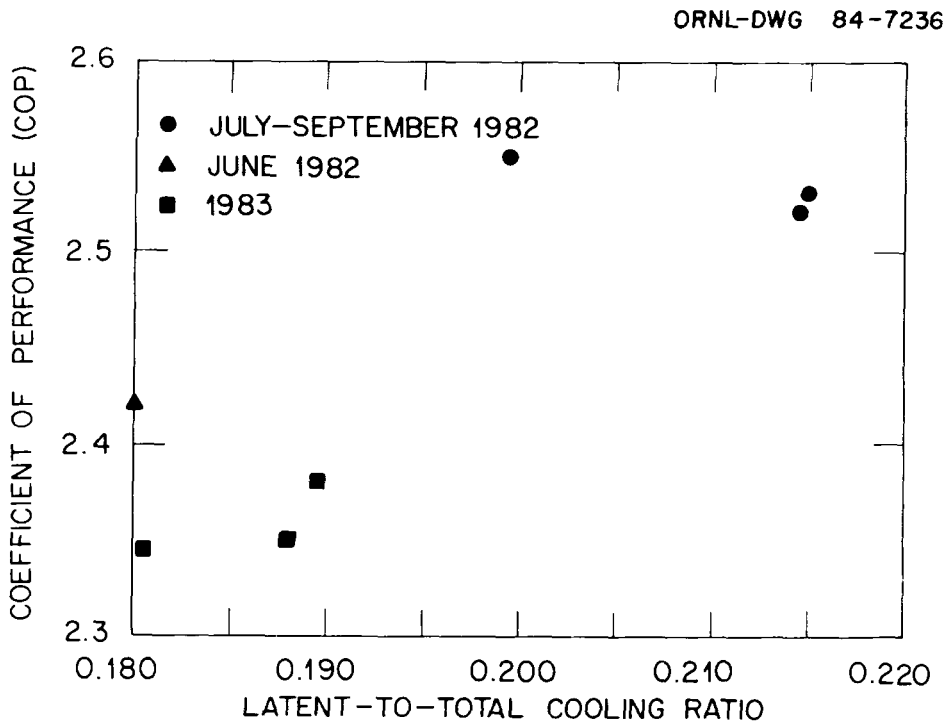

Fig. 4.16. Average COP vs average latent-to-total cooling ratio (30°C < T < 35°C).

4.3.1 Effect of Cycling Rate

Table 4.8 gives a listing of average cycling rate, on-time per cycle, and off-time per cycle along with the percentage of energy use due to start-up transient effects. An inspection of Tables 4.6 and 4.8 reveals that, with the exception of September 1982 (which had a large number of low-temperature, no-load hours), the months with lower average cycling rates had lower COPs and higher transient energy use penalties. This is counter to what one would intuitively expect. The thermostat change in November 1982 resulted in a lower cycling rate during the summer of 1983, while the effect of the data logic interface on the heat pump control system caused the cycling rate to be lower in June 1982 than during the rest of that summer.

Table 4.8. Average monthly thermostat cycle parameters and energy use penalties due to start-up transients

Month	Cycles	Run time per cycle (min)	Off-time per cycle (min)	Percentage of energy use due to start-up transient[a]	Average cycles per hour
June 1982	141.5	78.25	224.51	15.0	0.20
July 1982	137.5	65.32	101.81	7.5	0.36
August 1982	96.0	56.90	181.23	11.6	0.25
September 1982	117.5	59.76	446.28	12.8	0.12
June 1983	108.0	95.68	260.43	14.0	0.17
July 1983	79.0	94.01	180.17	12.9	0.22
August 1983	99.0	112.96	191.28	11.7	0.20

[a]Exclusive of off-cycle energy use.

Start-up transient energy use penalty as a percentage of total energy use for each 5°C bin-month is plotted against ambient operating temperature in Fig. 4.17. For June 1982 and all of 1983, this percentage is greater than that for July–September 1982 at temperatures higher than 22°C. The data for 1983 and June 1982 cluster reasonably tightly at various temperatures. However, there is a large degree of scatter in the rest of the 1982 data. Since cycling losses seemed to correlate well with off-time for heating, the possibility of a similar correlation for cooling was investigated. The result is plotted in Fig. 4.18.

Figure 4.18 shows a strong dependence of start-up energy use penalty for about the first 200 min with a lessening dependence at longer times. Data for July–September 1982 line up

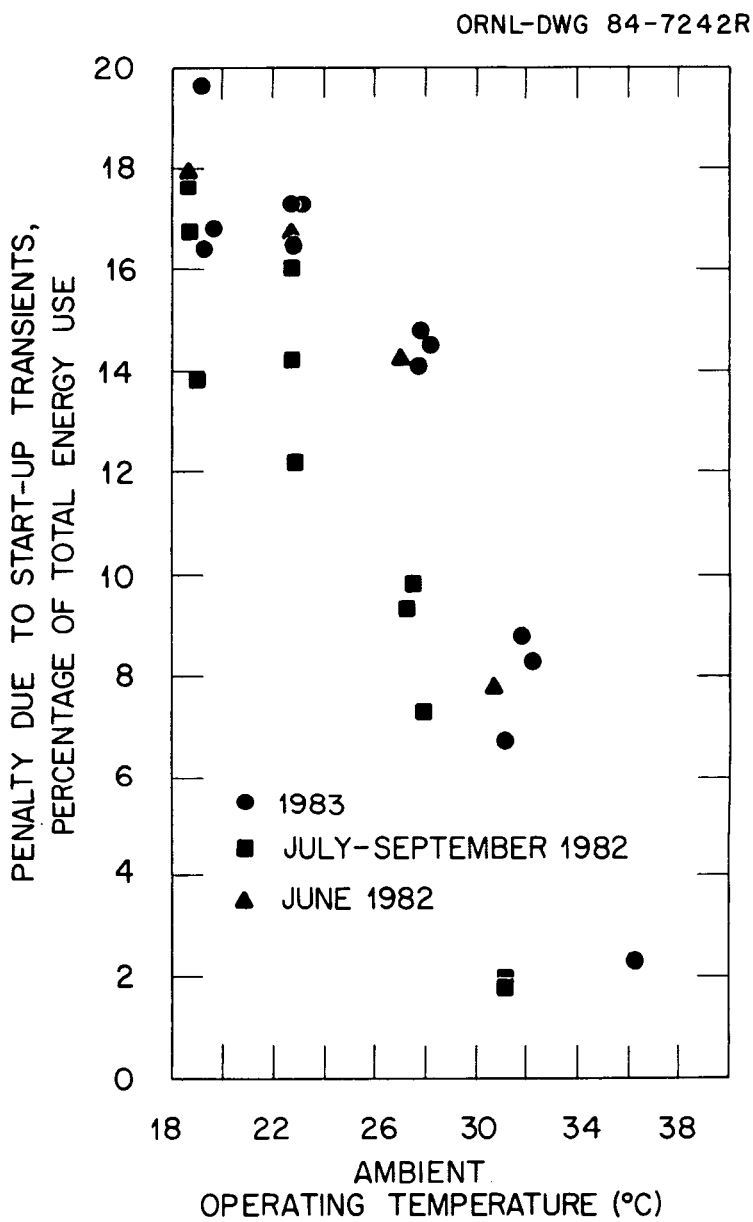

Fig. 4.17. Energy use penalty due to start-up transients vs ambient operating temperature.

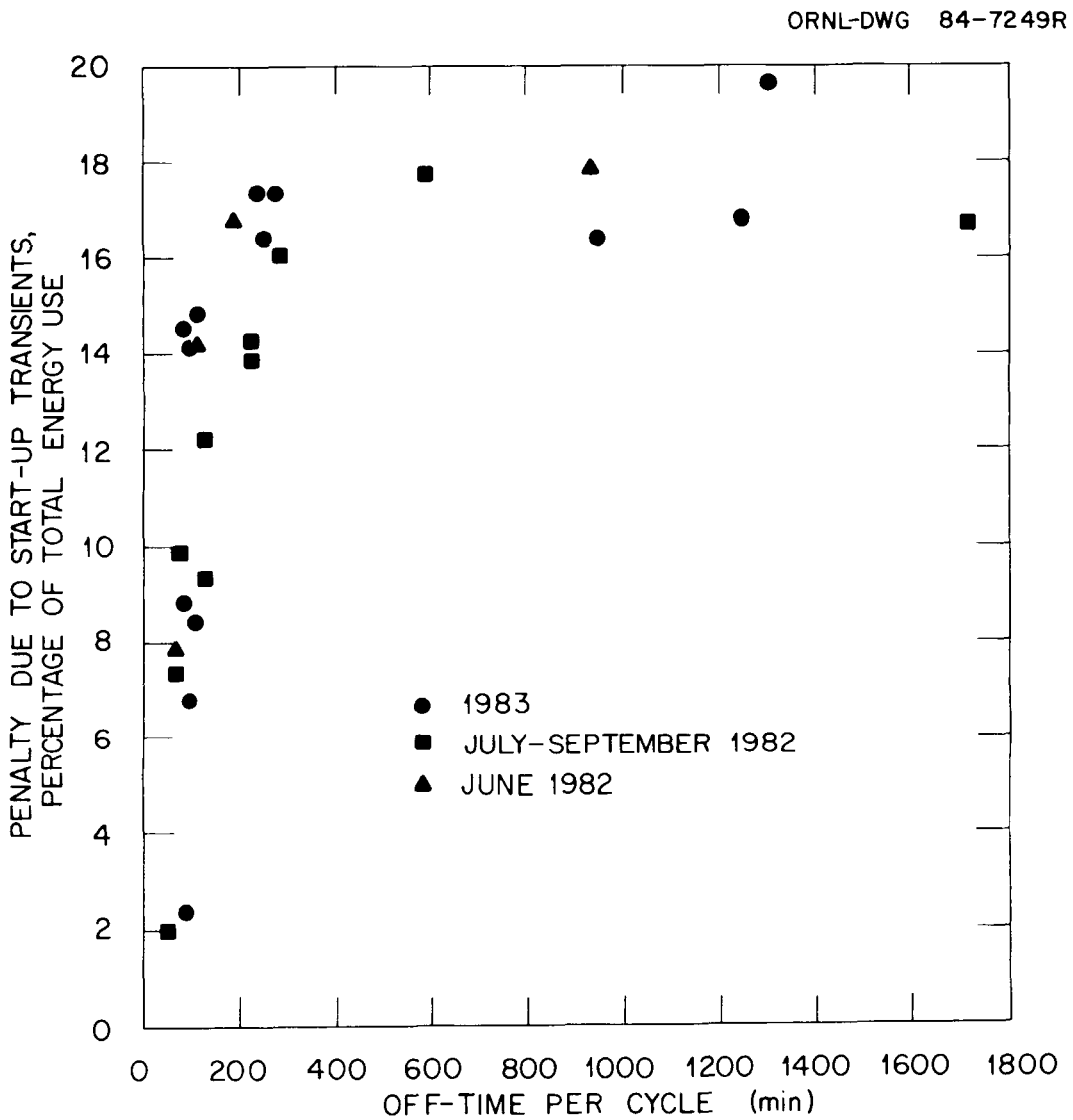

Fig. 4.18. Energy use penalty due to start-up transients vs off-time per cycle.

much better when plotted against off-time per cycle than when plotted against temperature. Start-up transient penalties for June 1982 and the summer of 1983 appear higher than those for the rest of 1982 for off-times between about 100 and 300 min. At shorter and longer times the start-up penalties are roughly the same for all months.

The off-times discussed above represent average off-times per cycle. Included in these averages are the long nighttime and other no-load periods when the heat pump does not run at all. These periods are a significant fraction of the total number of hours in each month, as shown in Table 4.1, and result in extremely long average off-times per cycle for the lower temperature bins. Replotting the start-up transient penalty vs off-time neglecting these no-load hours gives Fig. 4.19. The general shape of this curve is the same as that for Fig. 4.18, though the off-times do not exceed 150 min per cycle. In this case, however, there is no distinguishable difference in start-up penalty between months with different cycling rates.

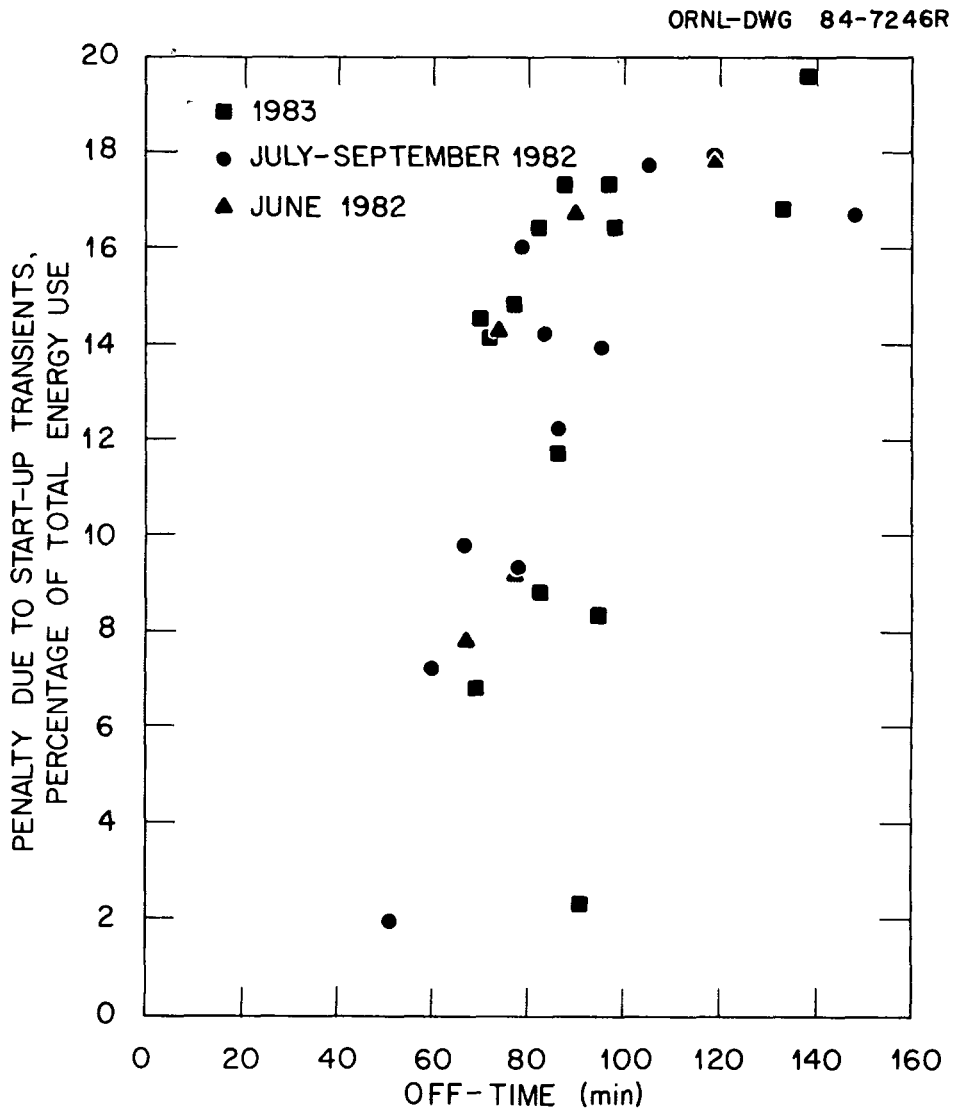

Fig. 4.19. Energy use penalty due to start-up transients vs off-time per cycle (neglecting no-load hours).

Start-up transient penalty is replotted in Fig. 4.20 against percent on (again neglecting no-load hours). The penalty decreases essentially linearly with increasing percent on, as would be expected. Additionally, the penalties for July-September of 1982 (the months with the highest cycling rates) appear to be somewhat lower than those for the other months for about 30% on-time or greater.

More research into the effect of cycling rates on cooling performance is needed. The data taken in this experiment seem to indicate that more frequent cycling than was experienced in 1983 may be beneficial for overall efficiency. Average cooling cycling rates experienced were very low (less than 0.5 cph) throughout the tests. It is not clear from these tests what effect much higher cycling rates (1-2 cph, i.e., those considered more typical) would have on performance.

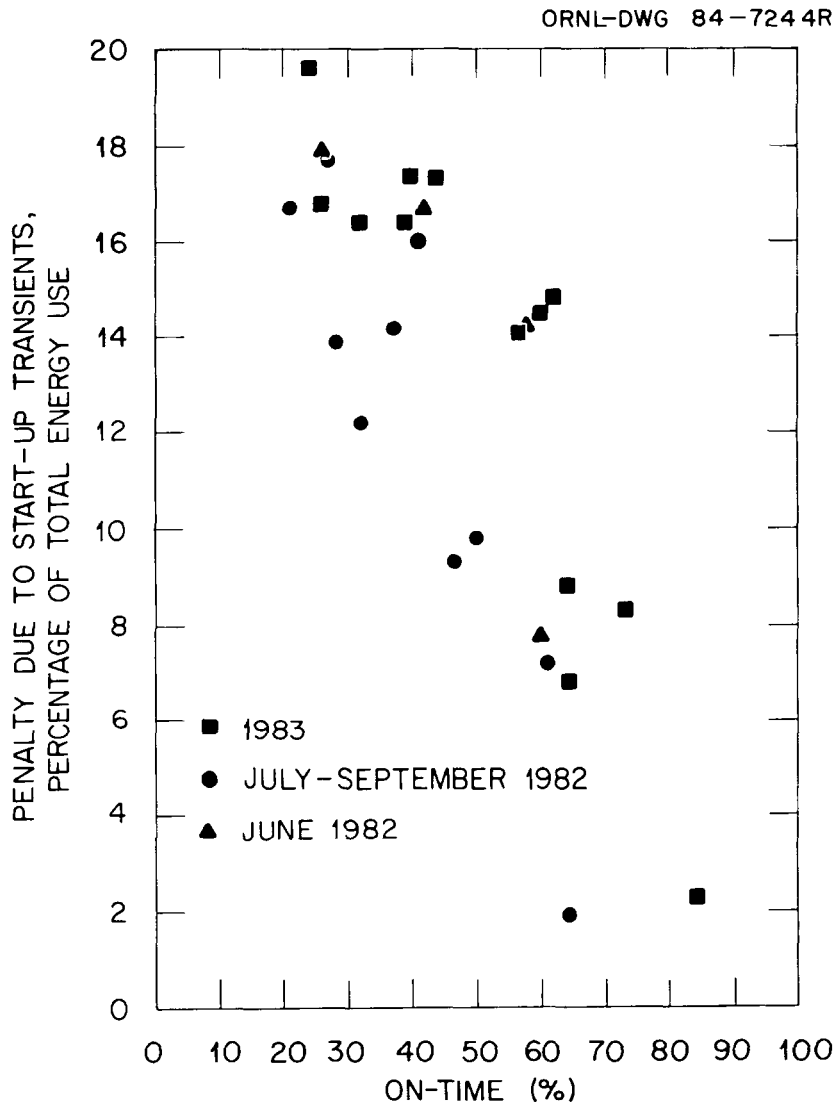

Fig. 4.20. Energy use penalty due to start-up transients vs percent on-time (neglecting no-load hours).

4.3.2 Effect of Desuperheater Operation

The desuperheater water heater was active during July and September 1982 and idle during June and August 1982 and throughout 1983. It was questioned whether the desuperheater may have had some effect on heat pump cooling performance since the COPs for July and September 1982 were slightly greater than that of August 1982.

Figure 4.21 is a plot of normal-mode COP vs ambient operating temperature for the months in question. The normal-mode COPs for August are generally the same as those for July and September. From these data it appears that there is little or no measurable effect on steady-state cooling operation when the desuperheater is active. The reason that the COP in August is not somewhat better than that of July probably has more to do with the fact

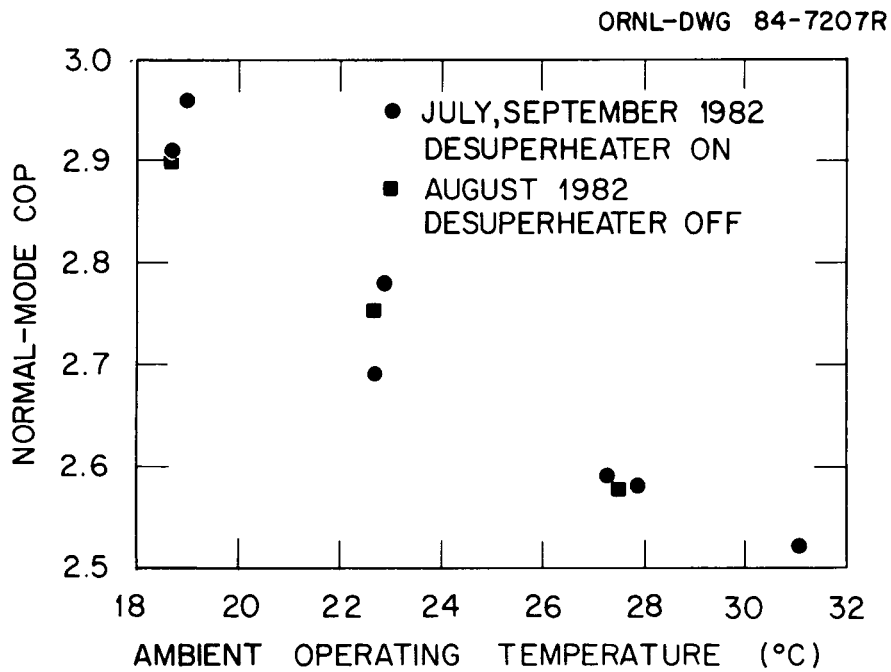

Fig. 4.21. Normal-mode COP vs ambient operating temperature with and without desuperheater active.

that the cycling rate was lower in August, leading to greater off-times and therefore to greater start-up energy use penalty. Higher latent-to-total cooling ratio and lower average operating temperature in September as opposed to August can explain the higher COP in September.

5. ANNUAL PERFORMANCE SUMMARY

An annual performance summary for the 1982–83 heating season and the 1983 cooling season is given in Table 5.1. The data in column 1 are taken from Table 3.2 and Table 4.6. As noted earlier, the data from those tables represent only a portion of the year because of DAS outages and data irregularities that made analysis of the dynamic losses impossible. Overall energy consumption and loads were measured for the full year, and column 2 contains estimated totals for the various energy use penalties based on the total measured

Table 5.1. Annual performance summary: 1982–1983

	(1)[a] (kWh)	(2)[b] (kWh)
Heating season		
Steady-state energy use required to meet the load	2581.4	3615.3[c]
Supplemental heat required	7.6	7.6
Supplemental heat use due to frosting	4.4	4.4
Heat pump energy use due to frosting	136.1	184.2[c]
Heat pump energy use due to defrosting	348.2	471.8[c]
Heat pump energy use due to start-up transients	276.9	445.5[c]
Off-cycle parasitic energy use	166.0	311.5
Total heating season energy use	3520.6	5040.3
Cooling season		
Steady-state energy use required to meet the load	1437.3	2518.4[c]
Heat pump energy use due to start-up transients	210.9	350.0[c]
Off-cycle parasitic energy use	81.6	182.9
Total cooling season energy use	1729.8	3051.3
Total annual energy use	5250.4	8091.6

[a]Extracted from Tables 3.2 and 4.6 (represents an incomplete year).

[b]Synthesized totals for September 28, 1982, through September 30, 1983.

[c]Estimated.

energy use. Table 5.2 gives the percentage of total annual energy consumption due to the various dynamic losses and the steady-state energy use needed to meet the loads.

Table 5.3 gives the total measured heating and cooling loads and seasonal performance factors (SPFs) for 1982–83 along with rated SPFs from the ARI directory.[9] The ARI ratings are not for the same heat pump model as tested since the manufacturer has discontinued that line and the rating guide in effect at the time the test unit was purchased did not include seasonal ratings.[10] Rather, they are for models from the same manufacturer that have steady-state COP and capacity ratings similar to those of the test unit. The rated heating SPF is nearly identical to that measured for the test unit, while the rated cooling SPF is about 34% higher than measured. It is likely that the apparent degradation in steady-state performance discussed in Sect. 4 had much to do with this difference. If the unit had performed up to the manufacturer's steady-state ratings (Eqs. 4.1 and 4.2), energy consumption for June–August 1983, as listed in Table 4.6, would have been lower by about 125 kWh. The cooling SPF for those months would then have been about 2.44 or about 18% lower than the rated value.

Table 5.2. Annual energy consumption fractions

Energy use due to	Percent of total annual consumption	
	(1)[a]	(2)[b]
Steady-state	76.6	75.8
Frosting[c]	2.7	2.3
Defrosting	6.6	5.8
Start-up transients	9.3	9.8
Off-cycle parasitics	4.7	6.1
Supplemental heat	0.1	0.1

[a]From column 1, Table 5.1 (represents an incomplete year).
[b]From column 2, Table 5.1 (represents a synthesized complete year).
[c]Includes supplemental heat use due to frosting.

Table 5.3. Rated vs measured seasonal performance factors

Season	Load (GJ)	Seasonal performance factor	
		Measured	Rated[a]
Heating	35.53	1.96	1.99
Cooling	24.26	2.21	2.96

[a]For models with steady-state ratings similar to those of the test heat pump.

6. CONCLUSIONS AND RECOMMENDATIONS

This section contains a summary of the major conclusions drawn from the tests and analyses discussed in this report. Several recommendations regarding future research efforts are also included.

6.1 HEATING SEASON CONCLUSIONS

Over the eight winter months covered during the tests

1. defrosting was responsible for 10.1% of the heating season energy consumption,
2. frosting for 3.7%,
3. start-up transients for 8.4%, and
4. off-cycle parasitics for 4.3%.

Overall heating SPF degradation due to these causes was 26.5%. Approximately 52% of this degradation was due to frosting and defrosting with the remainder due to cycling losses.

Reducing the maximum cycling rate from 6 cph (1981-82) to 5 cph (1982-83) resulted in reduced start-up transient energy use penalties, though per-cycle losses changed little. Frosting energy use penalties tended to increase, possibly because of increased on-time per cycle. Neglecting supplemental heat and adjusting for differences in off-cycle parasitic energy use and defrost energy use penalties, the heating SPFs for 1981-82 and 1982-83 were 1.96 and 1.99, respectively. It therefore appears that the slight reduction in cycling rate had no significant impact on heating performance.

A transient time of 4 min rather than 2 min seems to more clearly approximate the time required for the unit to reach steady-state operation, especially at higher temperatures. Based on 4-min transient time data, the field-measured heating C_d (neglecting the effects of off-cycle energy use) is approximately 0.24.

Heating output loss per cycle and input energy increase per cycle are directly related to off-time per cycle. For off-times up to about 20 min, both output loss and increase in energy input depend strongly on off-time. For longer off-times, the dependence is very weak.

Defrost time varies directly with frosting potential and with ambient temperature for high frosting potentials. At low values of frosting potential, the effect of ambient temperature on defrost time is not clearly understood.

Use of a desuperheater water heater reduced the space heating capacity of the unit but had no measurable effect on dynamic loss levels.

6.2 COOLING SEASON CONCLUSIONS

The steady-state cooling capacity and COP of the unit were degraded from the manufacturer's ratings and the 1980 performance levels, especially at high ambient

temperatures. Because of this degradation, analysis of cooling mode cycling losses for this experiment is speculative at best. However, based on best estimates of the actual steady-state performance, the cooling C_d appears to be between 0.20 and 0.25. The percentage of the cooling season energy consumption (neglecting off-cycle energy use) due to start-up transients tends to increase with increasing off-time per cycle.

From the data for these tests, it appears that the reduced cycling rates in June 1982 and summer 1983 led to increased start-up transient energy use penalties. However, cycling rates during these tests were extremely low. It is not clear what the effect of much higher cycling rates would be.

6.3 ANNUAL PERFORMANCE

Based on annual performance estimates for September 28, 1982, through September 30, 1983,

1. defrosting losses accounted for 5.8% of the total energy use,
2. frosting losses for 2.3%,
3. start-up transient losses for 9.8%, and
4. off-cycle parasitic losses for 6.1%.

ARI-rated heating SPFs for units with steady-state performance ratings similar to those of the field test unit closely match the measured value. Rated cooling performance is much higher than the measured SPF; however, the performance degradation makes it difficult to assess by how much the measured and rated SPFs differ.

The results from this study can be particularly useful for validating annual performance factor (APF) estimation computer codes. Once validated, a code could then be used to predict the APFs of similar air-source heat pumps in different locations with a higher degree of confidence.

6.4 RECOMMENDATIONS

Four major recommendations for further research emerge from these tests.

1. Analyze existing data from other investigations and perform further laboratory investigations to study the effect of off-time per cycle on cyclic capacity reduction and increased energy input.
2. Perform further laboratory and field investigations of the effect of defrost degradation on different heat pump systems and the extent to which the degradation is reduced by demand-type defrost controls.
3. Investigate the basic mechanisms involved in frost formation on finned tubes (both spine- and plate-type) as a means to minimize the impact on energy use of frosting and defrosting.
4. Conduct further study (field and laboratory tests and analyses) of the effect of cycling on cooling performance of heat pumps.

REFERENCES

1. A. S. Holman and L. A. Abbatiello, *Annual Cycle Energy System (ACES) Performance Report November 1977 through September 1978*, ORNL/CON-42, Oak Ridge National Laboratory, May 1980.

2. V. D. Baxter, *ACES: Final Performance Report December 1, 1978 through September 15, 1980*, ORNL/CON-64, Oak Ridge National Laboratory, April 1981.

3. V. D. Baxter, "Comparison of Field Performance of a High-Efficiency Heat Pump With and Without a Desuperheater Water Heater," *ASHRAE Trans.* **90** (Pt. 1), 180-90 (1984).

4. J. L. Bledsoe and D. R. Miller, *Data Collection and Processing for the ACES*, ORNL/CON-59, Oak Ridge National Laboratory, November 1981.

5. B. A. McGraw and D. R. Miller, "Successful Instrumentation Techniques Developed for the TECH Facility," pp. 244-249 in *Solar Engineering—1983: Proceedings of the Fifth Annual Technical Conference of the ASME Solar Energy Division, Orlando, Florida, April 18-21, 1983*, American Society of Mechanical Engineers, New York, 1983.

6. W. A. Miller, *Laboratory Evaluation of the Heating Capacity and Efficiency of a High-Efficiency, Air-to-Air Heat Pump with Emphasis on Frosting/Defrosting Operation*, ORNL/CON-69, Oak Ridge National Laboratory, December 1982.

7. W. H. Parken, G. E. Kelly, and D. A. Didion, *Method of Testing, Rating and Estimating the Heating Seasonal Performance of Heat Pumps*, NBSIR 80-2002, U.S. Department of Commerce, Washington, D.C., April 1980.

8. H. S. Kirschbaum, and S. E. Veyo, *An Investigation of Methods to Improve Heat Pump Performance and Reliability in a Northern Climate*, vol. III: Appendixes B, C, and D, EPRI EM-319, Westinghouse Electric Corporation Research Laboratories, Pittsburgh, Pa., January 1977.

9. *Directory of Certified Unitary Air Conditioners, Unitary Air Source Heat Pumps, Sound-Rated Outdoor Unitary Equipment, Solar Collectors, July 1-December 31, 1983*, Air-Conditioning and Refrigeration Institute, Arlington, Va., 1983.

10. *Directory of Certified Unitary Air Conditioners, Air-Source Unitary Heat Pumps, Sound-Rated Outdoor Unitary Equipment, Central System Humidifiers, July 1-December 31, 1979*, Air-Conditioning and Refrigeration Institute, Arlington, Va., 1979.

Appendix A

TEST DATA AND SAMPLE CALCULATIONS

A.1 TABLES A.1–A.4

Data from the heating season hourly data sets, condensed into 5°C temperature bins, are listed in Table A.1. Included are heating delivered, energy consumed, COPs, and operating times for transient, normal, and defrost modes; average operating temperatures; bin temperatures; and total bin hours. Similar data for the cooling season are given in Table A.3.

Tables A.2 and A.4 give selected results based on the bin data for heating and cooling modes, respectively.

A.2 SAMPLE CALCULATIONS

A.2.1 Procedure Used to Calculate Steady-State Energy Input and Energy Use Penalties

For each hour in a given bin, the following calculations are performed.

1. Steady-state COP and capacity:

$$\mathrm{CAP}_{ss} = 7346 + 217 \times T, \quad \mathrm{W} ,$$

$$\mathrm{COP}_{ss} = 2.53 + 0.0465 \times T ,$$

where T = ambient temperature;

2. Heat delivered if heat pump operated at steady-state capacity (QH_{ss}):

$$Tim_{ss} = \frac{QH_T}{\mathrm{CAP}_{ss}} ,$$

QH_T = total actual heat required,

Tim_{ss} = run time necessary to deliver QH_T while operating at steady-state capacity,

$$QH_{ss} = \begin{Bmatrix} QH_T & \text{if } Tim_{ss} \leq 1.0 \\ \mathrm{CAP}_{ss} & \text{if } Tim_{ss} > 1.0 \end{Bmatrix} ;$$

3. Steady-state energy input (EC_{ss}):

$$EC_{ss} = QH_{ss}/\mathrm{COP}_{ss} ;$$

Table A.1. Heating season condensed data

Bin temp range (°C)	Av bin temp (°C)	Av oper. temp (°C)	Bin R.H. (%)	Bin hours	Operating time (h)			Cycles		Input energy[d] (kWh)					Output energy[d] (kWh)				Suppl. heat (I^2R) (kWh)	D (I^2R) (kWh)	COP[d]				Capacity (kW)	
					T[a]	N[b]	D[c]	Thermostat	D	T	N	D[e]	Off-cycle	Total	T	N[f]	D	Total			T	N	D	Total[g]	T	N
December 1981																										
<−10	−12.2	−12.3	76	13	0.18	11.12	1.16	14	9	0.52	28.07	12.07	0.03	40.69	0.87	53.97	4.30	59.14	12.34	9.01	1.67	1.92	0.36	1.45	4.83	4.85
−10:−5	−7.4	−7.5	61	38	1.89	31.11	1.95	46	23	5.54	82.38	17.82	0.16	105.90	10.88	172.89	7.83	191.60	15.28	12.70	1.96	2.10	0.44	1.81	5.76	5.56
−5:0	−2.0	−2.1	67	100	22.77	37.90	5.36	394.5	44	69.44	106.63	47.10	1.82	224.99	146.21	238.24	15.39	399.84	7.60	33.89	2.11	2.23	0.33	1.78	6.42	6.29
0:5	2.7	2.5	70	152	45.41	21.46	4.41	710	35	146.84	64.90	42.99	4.32	259.05	327.22	160.80	12.18	500.20	0	31.46	2.23	2.48	0.28	1.93	7.21	7.49
5:10	6.7	6.7	69	47	12.70	2.68	0	195	0	42.30	8.46	0	1.69	52.45	92.71	23.83	0	116.54	0	0	2.19	2.82		2.22	7.30	8.89
>10	12.9	13.3	69	10	2.71	0.55	0	43.5	0	9.78	1.85	0	0.36	11.99	24.04	5.79	0	29.83	0	0	2.46	3.13		2.49	8.87	10.53
February 1982																										
<−5	−6.9	−7.0	66	26	2.34	17.22	1.86	71.5	14	6.73	46.87	19.43	0.25	73.28	14.17	100.70	6.38	121.25	7.65	14.47	2.11	2.15	0.33	1.65	6.06	5.85
−5:0	−1.6	−1.7	61	108	15.45	42.84	4.45	486.5	45	48.76	126.38	44.08	2.42	221.64	98.62	288.29	13.43	400.34	1.34	29.82	2.02	2.28	0.30	1.81	6.38	6.73
0:5	2.7	2.6	61	208	30.10	62.38	4.29	949	46	98.08	195.27	40.74	5.95	340.04	199.85	471.96	13.46	685.27	0	29.51	2.04	2.42	0.33	2.16	6.64	7.57
5:10	7.4	7.2	65	174	22.40	33.20	0.53	706.5	8	74.35	110.71	4.89	6.31	196.26	151.60	283.86	2.04	437.50	0	3.36	2.04	2.56	0.42	2.23	6.77	8.55
10:15	12.0	11.6	57	111	9.00	9.21	0.09	285.5	0	30.29	32.39	0.77	4.96	68.41	63.82	86.93	0.32	151.07	0	0.54	2.11	2.68	0.42	2.21	7.09	9.44
>15	18.5	17.4	39	42	1.65	1.57	0	53.5	0	5.71	5.55	0	2.07	13.33	11.84	15.24	0	27.08	0	0	2.07	2.75		2.03	7.18	9.71
April 1982																										
<0	−1.7	−1.9	63	17	2.47	5.43	0.43	79.5	6	7.95	16.49	3.41	0.46	28.31	15.43	37.22	1.59	54.24	0	2.32	1.94	2.26	0.47	1.92	6.25	6.85
0:5	2.9	2.7	57	69	8.58	12.74	0.36	273.5	7	28.20	41.18	2.89	2.53	74.80	51.17	97.62	1.54	150.33	0	1.91	1.81	2.37	0.53	2.01	5.96	7.66
5:10	7.5	7.0	53	143	11.69	15.00	0.23	375.5	5	39.24	50.48	1.92	6.21	97.85	74.60	126.36	1.08	202.04	0	1.27	1.90	2.50	0.56	2.06	6.38	8.42
10:15	12.7	12.6	53	238	8.09	7.42	0.11	261.5	1	27.41	26.28	1.10	11.90	66.69	52.25	68.60	0.32	121.17	0	0.80	1.91	2.61	0.29	1.82	6.46	9.25
15:20	17.2	16.9	39	181	3.08	2.60	0	101.5	0	10.75	9.50	0	9.38	29.63	21.17	25.87	0	47.04	0	0	1.97	2.72		1.59	6.87	9.95
>20	22.3	21.6	35	98	0.87	0.63	0	28	0	3.14	2.39	0	5.16	10.69	6.47	6.80	0	13.27	0	0	2.06	2.85		1.24	7.44	10.79
December 1982																										
<−5	−6.5	−6.6	94	10	0.21	8.48	0.95	6	6	0.58	24.82	9.67	0.03	35.10	1.29	47.04	3.00	51.33	3.25	7.33	2.22	1.90	0.31	1.46	6.14	5.55
−5:0	−2.0	−2.3	84	82	8.27	40.31	5.11	239	38	24.26	113.34	47.78	2.26	187.64	51.00	251.01	15.66	317.67	0	34.72	2.10	2.21	0.33	1.69	6.17	6.23
0:5	2.4	2.3	77	185	23.83	60.41	5.05	687	43	72.79	179.89	47.20	7.66	307.54	155.42	428.51	15.55	599.48	0	34.29	2.14	2.38	0.33	1.95	6.52	7.09
5:10	7.3	7.2	72	161	19.70	30.24	0.65	567	8	62.04	95.95	6.32	8.83	173.14	135.62	247.27	2.35	385.24	0	4.69	2.19	2.58	0.37	2.22	6.88	8.18
10:15	12.6	11.9	70	98	3.66	3.20	0.14	107	1	11.90	10.88	1.06	7.28	31.12	23.88	28.70	0.42	53.00	0	0.74	2.01	2.64	0.40	1.70	6.52	8.97
15:20	17.0	17.3	63	78	0.56	0.38	0	17	0	1.92	1.36	0	6.16	9.44	3.85	3.71	0	7.56	0	0	2.01	2.73		0.80	6.88	9.76
>20	22.0	20.9	51	33	0.13	0.06	0	4	0	0.44	0.24	0	2.62	3.30	0.88	0.68	0	1.56	0	0	2.00	2.83		0.47	6.77	11.33
January 1983																										
<−5	−6.9	−7.0	54	24	0.56	20.95	1.17	16	15	1.63	64.35	8.16	0.11	74.25	3.50	120.43	4.96	128.89	7.72	5.23	2.15	1.87	0.61	1.74	6.25	5.75
−5:0	−2.3	−2.5	65	170	17.59	92.71	8.07	505	80	52.79	266.80	73.83	4.13	397.55	111.05	589.84	27.99	728.88	1.03	51.13	2.10	2.21	0.38	1.83	6.31	6.36
0:5	2.4	2.3	68	224	29.14	77.57	6.25	850	61	90.99	234.82	60.20	8.88	394.89	194.28	560.67	22.45	777.40	0	42.19	2.14	2.39	0.37	1.97	6.67	7.23
5:10	6.8	6.6	70	161	20.81	30.74	0.73	599	8	66.76	99.64	7.18	8.70	182.28	141.87	252.44	2.63	396.94	0	5.03	2.13	2.53	0.37	2.18	6.82	8.21
>10	11.9	11.9	58	43	4.18	3.70	0	121	1	13.67	12.56	1.06	2.81	30.10	28.05	33.36	0.42	61.83	0	0.74	2.05	2.66	0.40	2.05	6.71	9.02

Table A.1 (continued)

Bin temp range (°C)	Av bin temp (°C)	Av oper. temp (°C)	Bin R.H. (%)	Bin hours	Operating time (h)			Cycles		Input energy[d] (kWh)					Output energy[d] (kWh)				Suppl. heat (I^2R) (kWh)	D (I^2R) (kWh)	COP[d]				Capacity (kW)	
					T[a]	N[b]	D[c]	Thermostat	D	T	N	D[e]	Off-cycle	Total	T	N[f]	D	Total			T	N	D	Total[g]	T	N
													February 1983													
<−5	−5.6	−5.6	75	5	0.24	3.86	0.39	7	3	0.70	10.66	3.66	0.04	15.06	1.52	22.90	1.34	25.76	0	2.58	2.17	2.15	0.37	1.71	6.33	5.93
−5:0	−1.6	−1.7	68	97	10.77	50.94	3.73	310	41	32.22	145.79	36.05	2.52	216.58	67.16	331.92	13.80	412.88	0	25.44	2.08	2.28	0.38	1.91	6.24	6.52
0:5	2.2	2.0	68	164	21.61	54.41	4.19	623	44	66.56	163.33	43.90	6.70	280.49	139.37	388.78	15.05	543.20	0	31.54	2.09	2.38	0.34	1.94	6.45	7.15
5:10	7.4	7.3	63	101	10.91	14.53	0.42	308	5	34.74	46.84	4.43	6.01	92.02	71.17	119.94	1.50	192.61	0	3.28	2.05	2.56	0.34	2.09	6.52	8.25
10:15	12.2	12.1	59	86	8.06	7.77	0	238	1	26.48	26.69	1.06	5.61	59.84	55.65	72.80	0.42	128.87	0	0.74	2.11	2.73	0.40	2.15	6.90	9.37
>15	16.9	16.9	41	35	1.84	1.60	0	53	0	6.18	5.53	0	2.52	14.23	13.21	15.37	0	28.58	0	0	2.14	2.78		2.01	7.18	9.61
													March 1983													
<0	−1.8	−1.9	70	35	3.90	16.92	1.03	111	12	11.87	49.57	9.99	1.05	72.48	24.19	112.25	3.92	140.36	0	6.41	2.04	2.26	0.39	1.94	6.20	6.63
0:5	2.6	2.4	63	122	14.70	36.87	2.10	422	26	45.87	113.47	20.30	5.47	185.11	93.43	269.67	7.64	370.74	0	14.14	2.04	2.38	0.38	2.00	6.36	7.31
5:10	7.4	7.1	61	162	16.10	23.95	0.15	463	3	52.11	78.32	1.92	9.74	142.09	107.24	198.38	0.76	306.38	0	1.43	2.06	2.53	0.40	2.16	6.66	8.28
10:15	12.1	11.9	55	141	7.55	6.70	0	217	0	24.84	23.12	0	10.14	58.10	49.11	61.50	0	110.61	0	0	1.98	2.66		1.90	6.50	9.18
15:20	17.2	16.9	43	77	2.64	2.07	0	74	0	8.89	7.33	0	5.78	22.00	18.25	20.27	0	38.52	0	0	2.05	2.77		1.75	6.91	9.79
>20	22.5	21.5	37	60	0.56	0.42	0	19	0	1.85	1.54	0	4.72	8.11	3.77	4.33	0	8.10	0	0	2.04	2.81		1.00	6.73	10.31
													April 1983													
<0	−1.8	−2.0	76	37	4.49	15.94	1.08	128	14	13.62	46.38	10.58	1.24	71.82	27.14	103.81	4.24	135.18	0	7.46	1.99	2.20	0.41	1.88	6.05	6.51
0:5	2.9	2.8	74	95	11.91	23.94	1.13	346	14	37.56	74.78	11.73	4.64	128.71	74.53	179.07	4.37	257.96	0	8.49	1.98	2.33	0.37	2.00	6.26	7.48
5:10	7.7	7.3	69	185	18.83	28.62	0.34	541	3	61.42	94.60	3.12	10.98	170.11	126.54	243.07	1.03	370.64	0	2.27	2.06	2.48	0.33	2.18	6.72	8.49
10:15	12.4	12.0	64	187	12.82	13.91	0	377	0	42.90	47.83	0	12.82	103.55	88.00	127.08	0	215.08	0	0	2.05	2.52		2.08	6.86	9.14
15:20	17.4	16.7	59	148	3.64	3.10	0	104	0	12.39	10.94	0	11.30	34.63	25.47	29.92	0	55.40	0	0	2.06	2.56		1.60	7.00	9.65
>20	22.6	21.3	39	67	0.36	0.24	0	11	0	1.24	0.88	0	5.31	7.43	2.50	2.52	0	5.02	0	0	2.01	2.61		0.68	6.94	10.50

[a]T denotes transient mode.
[b]N denotes normal mode.
[c]D denotes defrost mode.
[d]Exclusive of supplemental I^2R.
[e]Includes I^2R during defrost.
[f]Includes heat delivered during fan slowdown.
[g]Includes off-cycle energy input.

Table A.2. Dynamic loss characterization of heating operation

Bin temp range (°C)	Cycle parameters				Total input energy[a] (kWh)	Steady-state dry-coil			CAPRAT	COPRAT	Heating load factor	Energy use penalties					Output loss per cycle[e] (kJ)	Input increase per cycle[e] (kJ)
	On (min)	Off (min)	Period (min)	% on		Capacity (kW)	COP	Input[b] (kWh)				Frosting I^2R[c] (kWh)	Frosting[d] (kWh)	Defrost (kWh)	Startup transient (kWh)	Off-cycle (kWh)		
December 1981																		
<−10	48.4	2.3	50.7	95.4	53.03	4.68	1.96	30.18	1.04	0.98	0.99	0	0.55	9.85	0.08	0.03	0	17.4
−10:−5	43.0	4.0	47.0	91.5	121.18	5.73	2.18	88.99	0.97	0.96	0.89	2.66	1.97	14.20	0.62	0.16	−29.5	27.8
−5:0	9.2	5.2	14.4	64.1	232.59	6.88	2.43	167.41	0.92	0.90	0.59	6.47	5.53	40.71	9.63	1.82	−28.1	36.5
0:5	5.7	6.8	12.5	45.3	259.05	7.90	2.65	188.92	0.92	0.87	0.42	0	3.83	38.30	23.68	4.32	66.1	74.9
5:10	4.7	9.7	14.4	32.7	52.45	8.79	2.84	41.03	0.86	0.81	0.28	0	0.06	0	9.67	1.69	373.2	173.3
>10	4.5	9.3	13.8	32.6	11.99	10.23	3.15	9.47	0.89	0.81	0.29	0	0.04	0	2.12	0.36	371.5	173.7
February 1982																		
<−5	16.4	3.8	20.2	81.0	80.93	5.82	2.20	54.89	1.01	0.97	0.82	3.32	1.09	16.67	0.38	0.25	−24.5	6.8
−5:0	7.2	5.6	12.8	56.3	222.98	6.98	2.45	165.59	0.95	0.90	0.54	1.34	8.78	36.23	8.62	2.42	39.8	40.9
0:5	5.8	7.0	12.8	45.4	340.04	7.92	2.65	258.58	0.92	0.86	0.42	0	17.19	35.60	22.72	5.95	105.8	58.4
5:10	4.7	10.0	14.7	32.0	196.26	8.90	2.86	152.85	0.88	0.82	0.28	0	0	4.17	32.93	6.31	203.4	77.6
10:15	3.8	19.5	23.3	16.4	68.41	9.86	3.07	49.24	0.84	0.78	0.14	0	0	0.66	13.55	4.96	266.4	82.1
>15	3.6	43.5	47.1	7.7	13.33	11.12	3.34	8.10	0.76	0.72	0.06	0	0	0	3.16	2.07	281.0	94.1
April 1982																		
<0	6.0	6.5	12.5	47.7	28.31	6.93	2.44	22.21	0.96	0.88	0.46	0	1.23	2.76	1.65	0.46	68.0	50.4
0:5	4.7	10.4	15.1	31.1	74.80	7.94	2.66	56.63	0.88	0.81	0.27	0	4.40	2.30	8.94	2.53	191.8	87.1
5:10	4.3	18.5	22.8	18.7	97.85	8.87	2.86	70.71	0.85	0.78	0.16	0	0	1.54	19.39	6.21	228.9	90.5
10:15	3.6	51.0	54.6	6.5	66.69	10.09	3.12	39.12	0.77	0.72	0.05	0	0	0.99	14.68	11.90	310.4	101.8
15:20	3.4	103.6	107.0	3.1	29.63	11.01	3.32	14.19	0.75	0.70	0.02	0	0	0	6.06	9.38	336.1	105.6
>20	3.2	206.8	210.0	1.5	10.69	12.03	3.53	3.75	0.74	0.68	0.02	0	0	0	1.78	5.16	375.5	111.3
December 1982																		
<−5	86.9	3.6	90.5	96.0	38.35	5.92	2.22	23.07	0.94	0.86	0.90	2.59	3.68	8.31	0.01	0.03	−75.1	−60.4
−5:0	12.2	7.1	19.3	63.2	187.64	6.85	2.42	131.02	0.91	0.91	0.57	0	9.67	41.29	3.40	2.26	7.5	18.6
0:5	7.4	8.4	15.8	46.8	307.54	7.84	2.63	227.54	0.88	0.88	0.41	0	17.15	41.25	13.94	7.66	71.3	39.5
5:10	5.3	11.7	17.0	31.1	173.14	8.90	2.86	134.55	0.86	0.85	0.27	0	0	5.49	24.27	8.83	161.7	59.8
10:15	3.8	51.0	54.8	7.0	31.12	9.93	3.08	17.20	0.77	0.75	0.05	0	0	0.92	5.72	7.28	301.0	95.8
15:20	3.3	272.0	275.3	1.2	9.44	11.09	3.33	2.26	0.73	0.69	0.01	0	0	0	1.02	6.16	342.5	107.7
>20	2.9	492.2	495.1	0.5	3.30	11.89	3.50	0.44	0.69	0.65	0.004	0	0	0	0.24	2.62	531.0	116.5
January 1983																		
<−5	80.7	5.0	85.7	94.2	81.97	5.83	2.21	58.38	0.99	0.85	0.93	0.80	9.76	5.91	0.09	0.11	−63.2	−54
−5:0	13.1	6.1	19.2	68.1	397.55	6.80	2.41	301.80	0.93	0.91	0.64	1.03	22.22	62.23	7.17	4.13	6.1	18.2
0:5	7.5	7.8	15.3	49.0	394.89	7.84	2.63	294.86	0.90	0.88	0.44	0	22.00	51.66	17.49	8.88	69.2	40.8
5:10	5.2	10.9	16.1	32.2	182.28	8.79	2.84	139.95	0.87	0.83	0.28	0	0	6.24	27.39	8.70	174.4	64.7
>10	3.9	17.4	21.3	18.3	30.10	9.92	3.08	21.01	0.79	0.76	0.14	0	0	0	6.28	2.81	286.7	92.5

Table A.2 (continued)

Bin temp range (°C)	Cycle parameters				Total input energy[a] (kWh)	Steady-state dry-coil			CAPRAT	COPRAT	Heating load factor	Energy use penalties					Output loss per cycle[e] (kJ)	Input increase per cycle[e] (kJ)
	On (min)	Off (min)	Period (min)	% on		Capacity (kW)	COP	Input[b] (kWh)				Frosting I^2R[c] (kWh)	Frosting[d] (kWh)	Defrost (kWh)	Startup transient (kWh)	Off-cycle (kWh)		
February 1983																		
<−5	35.1	4.4	39.5	88.9	15.06	6.13	2.27	11.36	0.97	0.95	0.86	0	0.56	3.07	0.03	0.04	−49.5	−3.9
−5:0	11.9	6.1	18.0	66.2	216.58	6.97	2.45	168.45	0.93	0.92	0.61	0	10.26	30.41	4.94	2.52	35.0	31.6
0:5	7.3	8.1	15.4	47.6	280.49	7.78	2.62	207.16	0.89	0.88	0.42	0	14.92	38.14	13.57	6.70	86.9	46.3
5:10	5.0	14.6	19.6	25.3	92.02	8.94	2.87	67.08	0.84	0.82	0.21	0	0	3.91	15.02	6.01	220.8	81.2
10:15	4.0	17.7	21.7	18.4	59.84	9.98	3.09	41.64	0.81	0.78	0.15	0	0	0.92	11.67	5.61	300.5	91.9
>15	3.9	35.7	39.6	9.8	14.23	11.01	3.32	8.62	0.75	0.74	0.07	0	0	0	3.09	2.52	303.3	96.9
March 1983																		
<0	11.3	7.1	18.4	61.3	72.48	6.92	2.44	58.14	0.95	0.91	0.58	0	3.54	7.76	1.99	1.05	54.6	38.5
0:5	7.3	9.7	17.0	43.0	185.11	7.86	2.64	140.43	0.90	0.86	0.39	0	11.21	17.37	10.63	5.47	120.2	55.9
5:10	5.2	15.8	21.0	24.7	142.09	8.89	2.86	107.10	0.86	0.82	0.21	0	0	1.66	23.59	9.74	203.1	76.0
10:15	3.9	35.0	38.9	10.1	58.10	9.93	3.08	35.87	0.78	0.75	0.08	0	0	0	12.09	10.14	335.0	105.8
15:20	3.8	58.6	62.4	6.1	22.00	11.02	3.32	11.61	0.74	0.72	0.05	0	0	0	4.61	5.78	369.8	111.4
>20	3.1	186.4	189.5	1.6	8.11	12.02	3.53	2.29	0.69	0.68	0.01	0	0	0	1.10	4.72	379.6	96.5
April 1983																		
<0	10.1	7.2	17.3	58.1	71.82	6.95	2.44	55.44	0.92	0.89	0.53	0	3.78	8.83	2.53	1.24	57.9	42.0
0:5	6.4	10.1	16.5	38.9	128.71	7.98	2.67	97.06	0.88	0.84	0.34	0	7.37	10.08	9.56	4.64	151.6	67.0
5:10	5.3	15.2	20.5	25.8	170.11	9.01	2.89	129.18	0.85	0.80	0.22	0	0	2.76	27.19	10.98	221.2	81.0
10:15	8.6	21.2	29.8	14.3	103.55	10.04	3.11	69.70	0.80	0.75	0.12	0	0	0	21.03	12.82	279.1	93.4
15:20	3.9	81.5	85.4	4.6	34.63	11.12	3.34	16.75	0.75	0.71	0.03	0	0	0	6.58	11.30	333.7	106.5
>20	3.3	362.2	365.5	0.9	7.43	12.26	3.58	1.42	0.70	0.66	0.01	0	0	0	0.70	5.31	418.9	120.1

[a]Includes supplemental I^2R.
[b]Input to meet heating requirement at SSDC COP (calculated and summed from hourly data within bin).
[c]I^2R required due to frosting capacity loss.
[d]Heat pump input required due to frosting capacity and COP loss.
[e]Based on normal capacity.

Table A.3 Cooling season condensed data

Bin temp range (°C)	Av bin temp (°C)	Av oper. temp (°C)	Bin R.H. (%)	Bin hours	Operating time (h)		No. of Thermostat cycles	Input energy (kWh)				Output energy (kWh)				Latent-to-total cooling ratio	COP[a]		
					Trans.	Norm.		Trans.	Norm.	Off-cycle	Total	Trans.[b]	Norm.[b,c]	Latent	Total		Trans.[d]	Norm.[d]	Total
June 1982																			
<20	17.6	18.6	64	235	0.52	9.76	14.5	1.66	29.85	12.02	43.54	2.24	67.53	17.45	87.43	0.200	1.69	2.83	2.77
20:25	22.3	22.8	57	270	2.93	66.60	64.5	9.70	215.38	10.73	235.80	13.04	456.17	110.16	580.18	0.190	1.66	2.62	2.58
25:30	26.9	26.9	48	195	3.19	91.96	57	11.12	309.71	5.34	326.17	14.43	620.34	139.66	775.03	0.180	1.58	2.44	2.42
>30	30.7	30.7	46	14	0.19	8.22	5	0.69	28.29	0.30	29.28	0.78	55.57	12.04	68.44	0.176	1.38	2.38	2.36
July 1982																			
<20	18.7	19.0	78	20	0.29	2.49	4.5	0.90	7.53	0.92	9.35	1.53	17.78	4.90	24.05	0.204	2.14	2.96	2.88
20:25	22.4	22.9	76	190	4.32	39.91	66	14.22	126.84	7.80	148.85	22.80	278.94	79.57	378.18	0.210	2.03	2.78	2.71
25:30	27.7	27.9	62	120	3.01	65.44	44.5	10.53	221.56	2.76	234.85	16.33	456.85	117.94	585.69	0.201	1.94	2.58	2.55
>30	31.1	31.1	56	53	1.55	32.24	22.5	5.57	110.35	1.03	116.95	8.46	223.63	56.47	285.88	0.198	1.89	2.52	2.49
August 1982																			
<20	17.7	18.7	88	83	0.54	4.41	8	1.92	13.37	4.18	19.47	2.70	30.12	9.50	42.42	0.224	1.81	2.90	2.77
20:25	22.1	22.7	87	179	2.38	28.69	39.5	8.94	92.18	7.91	109.04	11.80	195.54	61.09	268.98	0.227	1.71	2.75	2.66
>25	27.5	27.5	68	119	3.39	50.25	48.5	13.25	169.63	3.50	186.38	16.79	343.41	97.66	458.44	0.213	1.61	2.57	2.51
September 1982																			
<20	16.1	18.7	83	525	0.98	10.59	18	3.35	31.54	27.47	62.35	4.41	69.45	23.87	98.00	0.244	1.74	2.91	2.81
20:25	22.1	22.7	79	315	3.66	45.71	55.5	13.51	143.13	14.21	170.85	16.81	296.06	94.05	407.60	0.231	1.62	2.69	2.60
>25	27.1	27.3	60	151	3.15	52.57	44	12.02	171.75	5.10	188.86	14.91	349.32	100.12	468.87	0.214	1.58	2.59	2.53
June 1983																			
<20	17.8	19.0	74	201	0.21	6.17	9	0.67	19.34	15.57	35.58	0.79	41.10	11.85	53.84	0.220	1.51	2.73	2.69
20:25	22.2	22.8	69	205	1.17	39.62	39	3.90	129.09	13.14	146.12	4.07	267.24	72.21	344.01	0.210	1.32	2.62	2.59
25:30	27.7	27.8	52	186	2.02	95.49	48	6.95	326.12	7.08	340.15	6.76	627.68	147.38	782.43	0.188	1.20	2.37	2.35
>30	31.2	31.1	49	49	0.46	27.57	13	1.63	96.48	1.68	99.79	1.57	184.34	45.66	231.73	0.197	1.20	2.38	2.36
July 1983																			
<20	18.9	19.6	78	43	0.09	1.48	2	0.28	4.65	3.31	8.25	0.47	10.30	2.79	13.59	0.205	2.07	2.79	2.75
20:25	22.2	22.8	73	165	2.64	30.83	34	8.83	100.54	10.52	119.89	13.95	209.72	55.94	280.04	0.200	1.97	2.61	2.56
25:30	27.7	28.1	57	70	1.59	36.90	22	5.61	126.82	2.52	134.95	8.52	245.09	56.19	310.08	0.181	1.86	2.36	2.34
>30	31.7	31.8	47	83	2.32	47.95	22	8.42	169.44	2.62	180.48	12.53	317.91	72.68	403.41	0.180	1.82	2.29	2.27
August 1983																			
<20	18.2	19.2	77	49	0.09	1.82	3	0.28	5.71	3.77	9.76	0.47	12.62	3.59	16.72	0.215	2.14	2.82	2.79
20:25	22.4	22.9	77	215	2.95	38.32	39	9.80	124.17	13.90	147.88	15.45	258.07	68.05	342.06	0.199	1.97	2.60	2.55
25:30	27.4	27.7	61	129	3.42	60.54	40	11.93	206.10	5.20	223.24	18.11	401.53	97.83	517.95	0.189	1.87	2.40	2.38
30:35	32.1	32.2	53	90	1.83	61.49	15	6.61	217.73	2.13	226.47	9.61	400.92	95.63	506.35	0.189	1.79	2.27	2.26
>35	36.3	36.3	44	19	0.35	15.62	2	1.27	57.21	0.24	58.73	1.84	100.19	23.06	125.12	0.184	1.78	2.15	2.14

[a]Does not include off-cycle energy use.
[b]Sensible cooling only.
[c]Includes cooling delivered during fan slowdown.
[d]Assumes the same latent-to-total cooling ratio for both transient and normal modes.

Table A.4 Cooling mode cycling parameters and losses

Bin temp range (°C)	Cycle parameters				Total input energy (kWh)	Steady-state (1)[a]			Steady-state (2)[b]			Energy use penalties	
	On (min)	Off (min)	Period (min)	% on		Capacity (kW)	COP	Input[c] (kWh)	Capacity (kW)	COP	Input[c] (kWh)	Startup transient[d] (kWh)	Off-cycle (kWh)
						June 1982							
<20	42.5	929.9	972.4	4.4	43.54	10.66	3.38	25.92	10.91	3.49	25.11	5.60	12.02
20:25	64.7	186.5	251.2	25.8	235.80	10.08	3.10	189.22	10.54	3.27	179.21	37.83	10.73
25:30	100.2	105.1	205.3	48.8	326.17	9.51	2.82	275.42	10.18	3.05	254.18	45.41	5.34
>30	101.2	66.8	168.0	60.2	29.28	8.98	2.56	26.71	9.84	2.85	23.99	2.26	0.30
						July 1982							
<20	37.1	229.6	266.7	13.9	9.35	10.60	3.35	7.25	10.88	3.47	7.01	1.17	0.92
20:25	40.2	132.5	172.7	23.3	148.85	10.06	3.09	123.78	10.53	3.26	117.16	17.27	7.80
25:30	92.3	69.5	161.8	57.0	234.85	9.37	2.75	215.30	10.09	3.00	197.36	16.78	2.76
>30	90.1	51.2	141.3	63.8	116.95	8.93	2.54	113.70	9.80	2.83	101.85	2.22	1.03
						August 1982							
<20	37.1	585.4	622.5	6.0	19.47	10.65	3.37	12.58	10.90	3.48	12.18	2.71	4.18
20:25	47.2	224.7	271.9	17.4	109.04	10.09	3.10	86.76	10.55	3.27	82.21	14.34	7.91
>25	66.4	88.8	147.2	45.1	186.38	9.43	2.78	164.99	10.12	3.02	151.72	17.88	3.50
						September 1982							
<20	38.6	1711.4	1750.0	2.2	62.35	10.65	3.37	29.06	10.90	3.48	28.13	5.82	27.47
20:25	53.4	287.2	340.6	15.7	170.85	10.09	3.10	131.56	10.55	3.27	124.64	25.07	14.21
>25	75.9	130.0	205.9	36.9	188.86	9.45	2.79	166.71	10.14	3.03	153.45	17.04	5.10
						June 1983							
<20	42.5	1297.5	1340.0	3.2	35.58	10.60	3.35	16.08	10.88	3.47	15.54	3.92	15.57
20:25	62.8	252.6	315.4	19.9	146.12	10.08	3.10	111.21	10.54	3.27	105.31	21.78	13.14
25:30	121.9	110.6	232.5	52.4	340.15	9.39	2.76	282.54	10.10	3.01	259.22	48.99	7.08
>30	129.4	96.8	226.2	57.2	99.79	8.91	2.53	91.44	9.79	2.83	81.85	6.67	1.68
						July 1983							
<20	47.1	1242.9	1290.0	3.7	8.25	10.52	3.31	4.10	10.82	3.44	3.95	0.83	3.31
20:25	59.1	232.1	291.2	20.3	119.89	10.08	3.10	90.44	10.54	3.27	85.67	18.93	10.52
25:30	105.0	85.9	190.9	55.0	134.95	9.34	2.74	113.29	10.07	2.99	103.73	19.14	2.52
>30	137.1	89.3	226.4	60.6	180.48	8.83	2.49	162.13	9.74	2.80	144.30	15.72	2.62
						August 1983							
<20	38.2	941.8	980.0	3.9	9.76	10.58	3.34	5.01	10.86	3.46	4.84	0.98	3.77
20:25	63.5	267.3	330.8	19.2	147.88	10.06	3.09	110.83	10.53	3.26	104.89	23.15	13.90
25:30	95.9	97.6	193.5	49.6	223.24	9.40	2.77	187.33	10.10	3.01	172.02	30.71	5.20
30:35	253.3	106.7	360.0	70.4	226.47	8.78	2.46	205.64	9.70	2.78	182.42	18.69	2.13
>35	479.1	90.9	570.0	84.1	58.73	8.21	2.19	57.16	9.34	2.56	48.83	1.32	0.24

[a]Based on derived steady-state performance: Eqs. 4.6 and 4.7.

[b]Based on manufacturer's ratings: Eqs. 4.1 and 4.2.

[c]Input energy required to meet cooling load at steady-state COP (calculated and summed from hourly data within bin).

[d]Based on steady-state COP (1) (calculated and summed from hourly data within bin).

4. Defrost energy penalty (PEC_d):

$$PEC_d = EC_d - \frac{QH_d}{\mathrm{COP}_{ss}} ,$$

where

EC_d = measured defrost energy use,
QH_d = measured net heat input to space in defrost mode;

5. Supplemental heat use caused by capacity loss due to frosting (I^2R_f):

$$I^2R_f = I^2R_m - I^2R_{sh} ,$$

where

I^2R_m = measured supplemental heat use,

I^2R_{sh} = required supplemental heat,

$I^2R_{sh} = QH_T - QH_{ss}$;

6. Frosting energy use penalty (PEC_f):

$$PEC_F = \left\{ \begin{array}{ll} EC_n - \dfrac{QH_n}{\mathrm{COP}_{ss}} & \text{if } T \leqslant 5.0°\mathrm{C} \\ 0 & \text{if } T > 5.0°\mathrm{C} \end{array} \right\} ,$$

where

EC_N = measured normal-mode energy use,

QH_n = measured heat delivery in normal mode;

7. Start-up transient energy use penalty (PEC_t):

$$PEC_t = \left\{ \begin{array}{ll} EC_t - \dfrac{QH_t}{\mathrm{COP}_{ss}} & \text{if } T \leqslant 5.0°\mathrm{C} \\ (EC_t + EC_N) - \dfrac{(QH_t + QH_n)}{\mathrm{COP}_{ss}} & \text{if } T > 5.0°\mathrm{C} \end{array} \right\} ,$$

where

EC_T = measured transient-mode energy use,

QH_T = measured heat delivery in transient mode.

A.2.2 Average Defrost Cycle Energy Consumption Rates, Cooling Capacity, and Time for December 1981 (Table 3.7)

1. Defrost time per cycle t_d:

$$DT = H_d \frac{1.25 \times D_{cyc}}{60} ,$$

where

DT = hours spent defrosting,

H_d = hours spent in defrost mode including recovery period,

D_{cyc} = number of defrost cycles.

$$DT = 12.89 - \frac{1.25 \times 111}{60} = 10.58 \text{ h} .$$

$$t_d = \frac{DT}{111} \times 60 = \frac{10.58}{111} \times 60 = 5.72 \text{ min} .$$

2. Average heat pump power draw during defrost mode (P_{HP}):

$$P_{HP} = \frac{IDF_d + COM_d}{H_d} = \frac{5.28 + 27.03}{12.89} = 2.51 \text{ kW} ,$$

where

IDF_d = defrost mode indoor fan energy use,

COM_d = defrost mode compressor energy use,

H_d = defrost mode hours.

3. Average resistance heater energy consumption during defrost (P_{rh}):

$$P_{rh} = \frac{I^2R_d}{DT} = \frac{87.06}{10.58} = 8.23 \text{ kW} .$$

4. Average defrost mode cooling capacity ($\dot{Q}C_d$):

$$QH_d = (1 - FQ_r) \times HFLD ,$$

where

QH_d = net heat to house during defrost cycles,

$HFLD$ = net heat to house in defrost mode,

FQ_r = fraction of heat delivered in recovery period = $0.38 - 0.029 \times t_d$.

$$QH_d = (1 - 0.214) \times 39.70 = 31.22 \text{ kWh} .$$

$$QC_d = I^2R_d - QH_d ,$$

where

QC_d = net cooling of indoor air stream,

$QC_d = 87.06 - 31.22 = 55.84$ kWh;

$$\dot{Q}C_d = \frac{QC_d}{DT} = \frac{55.84}{10.58} = 5.28 \text{ kW.}$$

A.2.3 CAPRAT, COPRAT, and heating load factor (Γ_h) for February 1982, $-5 < T \leqslant 0°C$

$$\text{CAPRAT} = \frac{\text{CAP}_{cyc}}{\text{CAP}_{ss}} :$$

$$\text{CAP}_{cyc} = \frac{\text{heating delivered (transient + normal)}}{\text{operating hours (transient + normal)}}$$

$$= \frac{98.62 + 288.29}{15.45 + 42.84}$$

$$= 6.64 \text{ kW} ;$$

$$\text{CAP}_{ss} = 6.98 \text{ kW} ;$$

$$\text{CAPRAT} = \frac{6.64}{6.98} = 0.95 .$$

$$\text{COPRAT} = \frac{\text{COP}_{cyc}}{\text{COP}_{ss}} ;$$

$$\text{COP}_{cyc} = \frac{\text{heating delivered (transient + normal)}}{\text{energy used (transient + normal)}}$$

$$= \frac{98.62 + 288.29}{48.76 + 126.38}$$

$$= 2.21 ;$$

$$\text{COP}_{ss} = 2.45 ;$$

$$\text{COPRAT} = \frac{2.21}{2.45} = 0.90 \ .$$

$$\Gamma_h = \frac{\text{heating delivered (transient + normal)}}{(\text{bin hours} - \text{defrost hours}) \times \text{CAP}_{ss}}$$

$$= \frac{98.62 + 288.29}{(108 - 4.45) \times 6.98}$$

$$= 0.54 \ .$$

A.2.4 Output Loss per Cycle (OLPC) and Input Increase per Cycle (IIPC) for February 1982, $-5 < T < 0°C$

$$OLPC = (\dot{Q}_n \times T_{op} - Q) \times 3600/N \ :$$

$$\dot{Q}_n = \frac{\text{normal-mode output energy}}{\text{normal-mode operating time}}$$

$$= \frac{288.29}{42.84} = 6.73 \text{ kW} \ .$$

$$T_{op} = T_{tran} + T_{norm} = 15.45 + 42.84 = 58.29 \text{ h} \ ;$$

$$Q = \text{transient output} + \text{normal output}$$

$$= 98.62 + 288.29 = 386.91 \text{ kWh} \ ;$$

$$N = \text{number of thermostat cycles in bin-month} = 486.5 \ ;$$

$$OLPC = (6.73 \times 58.29 - 386.91) \times 3600/486.5$$

$$= 39.8 \text{ kJ/cycle} \ .$$

$$IIPC = (E - Q/\text{COP}_n) \times 3600/N \ :$$

$$E = \text{transient input} + \text{normal input}$$

$$= 48.76 + 126.38 = 175.14 \text{ kWh} \ ;$$

$$Q = 386.91 \text{ kWh} \ ;$$

Appendix B

AIR-SIDE HEAT FLOW INSTRUMENTATION

This appendix gives a brief description of the system used to measure the heat pump heating and sensible cooling output in TECH House III.

The system basically consists of two 3-m-long averaging RTDs (Fig. B.1), a vane anemometer (Fig. B.2), and associated electronics for conditioning the signal to be compatible with the DAS. One RTD is located in the return air duct and the other in the supply air duct to measure the air temperature difference across the heat pump indoor unit. The anemometer, located in the return air duct, measures the air speed. Figure B.3 shows the relative locations of the RTDs and anemometer. Signals from the anemometer and RTDs are integrated electronically to produce a stream of discrete pulses, proportional to the heat flow, which are stored in a counter by the DAS.

ORNL-PHOTO 0762-84

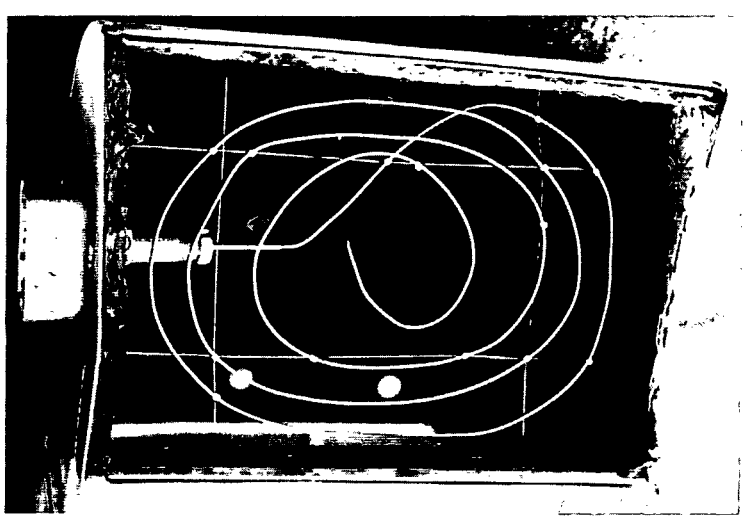

Fig. B.1. Averaging RTD used in air-side heat flow measurement.

The DAS counter is interrogated once each hour, and the heat flow for the hour is calculated by

$$Q = K \times N_c ,$$

ORNL-PHOTO 3166-81

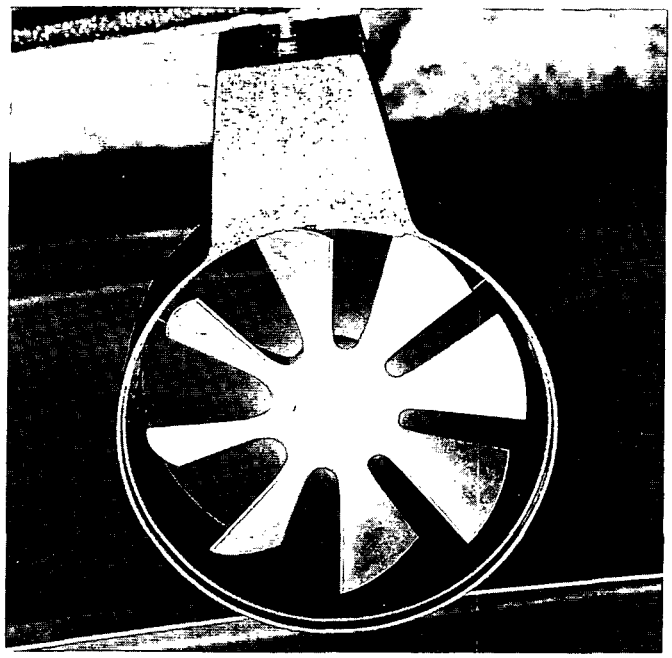

Fig. B.2. Vane anemometer used in air-side heat flow measurement.

ORNL-DWG 84-7232

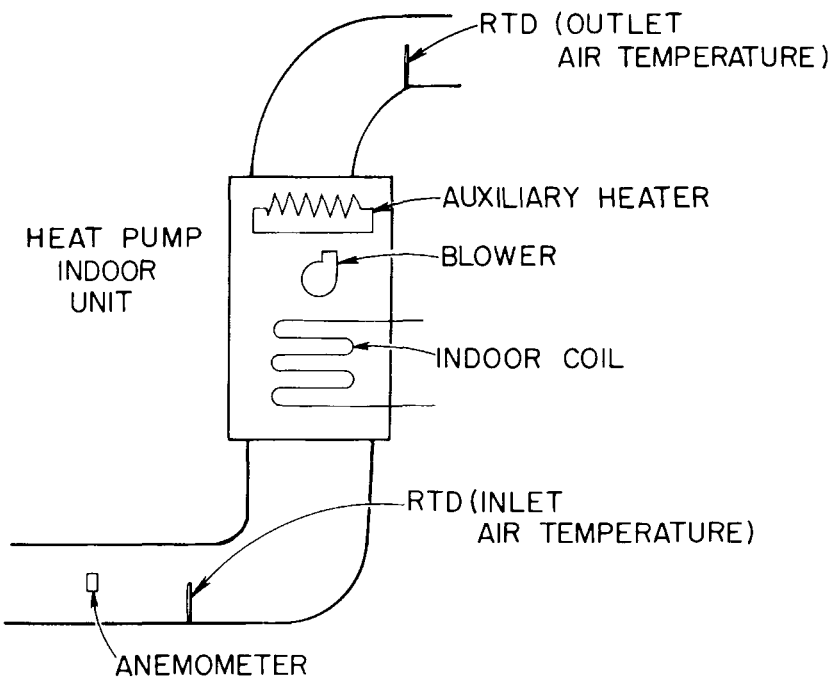

Fig. B.3. Schematic of heat pump indoor unit showing location of air-side heat flow instrumentation.

where

K = a calibration constant,

N_c = number of counts per hour; obtained by electronically multiplying the frequency signal from the anemometer and the temperature difference from the RTDs (converted to a frequency).

Calibration of the heat flowmeter is done by imposing a known heat flow on the airstream. The calibration constant K is evaluated by

$$K = Q'/N_c$$

where Q' = known heat flow. Complete details of air-side heat flow measurement techniques used at the TECH complex are available in ref. 5.

INTERNAL DISTRIBUTION

1. S. J. Ball
2. V. D. Baxter
3. J. L. Bledsoe
4. D. W. Burton
5. R. S. Carlsmith
6. J. A. Carpenter, Jr.
7. J. E. Christian
8. L. G. Christophorou
9. F. A. Creswick
10. N. Domingo
11. P. D. Fairchild
12. S. K. Fischer
13. W. Fulkerson
14. L. D. Gilliam
15. M. Guthrie
16. V. O. Haynes
17. W. L. Jackson
18. J. E. Jones, Jr.
19. L. Jung
20. R. J. Kedl
21. M. Kuliasha
22. J. F. Martin
23. L. McCold
24. H. A. McLain
25. V. C. Mei
26. J. W. Michel
27. D. R. Miller
28. R. E. Minturn
29. W. R. Mixon
30. J. C. Moyers
31. E. A. Nephew
32. M. Olszewski
33. H. Perez-Blanco
34. C. K. Rice
35. A. C. Schaffhauser
36. F. Southworth
37. C. A. Srite
38. R. A. Stevens
39. M. P. Stulberg
40. M. P. Ternes
41. E. A. Vineyard
42. T. A. Vineyard
43. K. H. Zimmerman
44. Biology Division Library

45–46. Central Research Library

47. Document Reference Section
48. Laboratory Records (RC)

49–50. Laboratory Records Department

51. ORNL Patent Section

EXTERNAL DISTRIBUTION

52. Roy Abbott, Advance Technology Operations, General Electric Company, AP6, Appliance Park, Louisville, KY 40225
53. John Adams, Whirlpool Corporation, Research and Engineering Center, Monte Road, Benton Harbor, MI 49022
54. Richard Alben, General Electric Company, Corporate R&D Center, Bldg. K-1, Room 5B37, P.O. Box 8, Schenectady, NY 12301
55. C. A. Allen, Energy Information Administration, EI-60, Federal Building, 1200 Pennsylvania Avenue, NW, Washington, DC 20461
56. Lawrence Ambs, Department of Mechanical Engineering, University of Massachusetts, Amherst, MA 01003
57. Kent Anderson, The Trane Company, 2020 14th Street, Arlington, VA 22101
58. John Andrews, Solar Technology Group, Building 701, Brookhaven National Laboratory, Upton, NY 11973

59. B. Backstrom, Chalmers University of Technology, S-41296, Goteborg, Sweden
60. James Bard, Executive Vice-President, Bard Manufacturing Co., Inc., P.O. Box 607, Bryan, OH 43506
61. E. K. Bastress, Energy Conversion and Utilization Technology Division, CS-142, Forrestal Building, Department of Energy, Washington, DC 20585
62. William Beale, Sunpower, Inc., 6 Byard Road, Athens, OH 45701
63. Warren Beeton, Vice-President-Engineering, Bristol Corporation, 649 Industrial Park, Bristol, VA 24201
64. J. Berghmans, Universitiet Leuven, Instituut Mechanica, Celestynen Laan 300A, B3030 Heverlee, Belgium
65. Morton Blatt, 1200 Prospect Street, P.O. Box 2351, LaJolla, CA 92038
66. Peter Bodett, Duo-Therm Division, Motor Wheel Corporation, LaGrange, IN 46761
67. Ulrich Bonne, Honeywell Incorporated, 10701 Lyndale Avenue South, Corporate-Technology Center, Materials and Processes Department, Bloomington, MN 55420
68. J. E. Bose, Director, School of Technology, Oklahoma State University, Stillwater, OK 74078
69. T. Bostrom, Swedish Council for Building Research, St. Goransgatan 66, S-11233 Stockholm, Sweden
70. Joseph Braymer, Mechanical and Aerospace Engineering Department, Case Western Reserve, University Circle, Cleveland, OH 44106
71. James Brisee, North Carolina Energy Institute, Department of Commerce, P.O. Box 12235, Research Triangle Park, NC 27709
72. Jim Calm, Energy Management and Utilization Division, Electric Power Research Institute, Heat Pump Development, P.O. Box 10412, Palo Alto, CA 94303
73. Joe Canal, General Electric Company, Troup Highway, Tyler, TX 75711
74. C. Gerald Carrington, Birmingham, England
75. Roger Chesebro, Westinghouse Electric Corporation, Research & Development Center, 1310 Beulah Road, Pittsburg, PA 15235
76. Raymond Cohen, Ray W. Herrich Laboratories, Purdue University, West Lafayette, IN 47907
77. W. R. Coleman, Residential and Commercial Services, American Electric Power Services, 100 East Broad, Columbus, OH 43201
78. V. I. Conley, Virginia Polytechnic Institute and State University, Department of Mechanical Engineering, Blacksburg, VA 24061
79. Ken Cooper, York Division, Borg-Warner Corporation, P.O. Box 1592, York, PA 17405
80. Gerard Coyne, General Electric Company, Central Air Conditioning Department, Troup Highway, Tyler, TX 75711
81. James Crawford, Manager, Advanced Systems, General Electric Company, 6200 Troup Highway, Tyler, TX 75711
82. Kenneth Cuccinelli, Division of Marketing Services, American Gas Association, 1515 Wilson Boulevard, Arlington, VA 22209
83. J. J. Cuttica, Manager, Fuel Cell Energy Systems, Gas Research Institute, 8600 West Bryn Mawr Avenue, Chicago, IL 60631
84. Nicholas D'Aleandro, Vice-President, A/C Engineering, Fedders Corporation, Woodbridge Avenue, Edison, NJ 08817

85. Ali Dabiri, Science Applications, Inc., 1200 Prospect Street, P.O. Box 2351, LaJolla, CA 92038
86. Jerry Dapper, BDP Company, Division of Carrier Corporation, 7310 West Morris Street, Indianapolis, IN 46231
87. Douglas DeWerth, Project Manager, Utilization Technology, Research & Development, 8501 East Pleasant Valley Road, Cleveland, OH 44131
88. Thomas Dean, University of Kansas, Lawrence, KS 66045
89. R. J. Denny, Air-Conditioning & Refrigeration Institute, 1815 North Fort Meyer Drive, Arlington, VA 22209
90. Irvin Derks, Manager Engineering Development, Bard Manufacturing Company, Bryan, OH 43506
91. David Didion, Mechanical Systems Section, Building Environment Division, National Bureau of Standards, Building 226, Room B126, Washington DC 20234
92. Albert Domingorena, Carrier Corporation, Building TR-4, Carrier Parkway, P.O. Box 4808, Syracuse, NY 13221
93. Richard Dougall, University of Pittsburg, Department of Mechanical Engineering, Pittsburg, PA 15261
94. Alan Drucker, Consumer Products Division, Carrier Corporation, Syracuse, NY 13221
95. G. D. Duffy, Air Conditioning News, P.O. Box 2600, Troy, MI 48084
96. Amir Ecker, Northrup, Inc., 302 Nichols Drive, Hutchins, TX 75141
97. Thomas Edwards, The Rovac Corporation, 100 Rovac Parkway, Rockledge, FL 32955
98. A. H. Elmahdy, Energy and Services Section, National Research Council, Division of Building Research, Ottawa, Canada
99. Richard English, Energy Systems Division, Carrier Corporation, Carrier Parkway, P.O. Box 4895, Syracuse, NY 13221
100. Richard Erth, York Division, Borg-Warner, P.O. Box 1592, York, PA 17405
101. V. A. Eustace, IRD Company, Ltd., Fossway, Newcastle upon Tyne, Great Britain
102. J. N. Eustis, Department of Energy, Office of Industrial Programs, CE-121.1, 1000 Independence Avenue, SW, Washington, DC 20585
103. Scott Farley, The Coleman Company, Inc., Special Products Group, 250 North Saint Francis, Wichita, KS 67201
104. Arthur Fellerman, McQuay Group, 13600 Industrial Park Boulevard, Minneapolis, MN 55440
105. Robert Fischer, Battelle-Columbus Laboratory, 505 King Avenue, Columbus, OH 43201
106. R. J. Fiskum, Energy Conversion Equipment Branch, CE-113.2, Department of Energy, 1000 Independence Avenue, SW, Washington, DC 20585
107. G. W. Gatecliff, Research Laboratory, Tecumseh Products Company, Ann Arbor, MI 48105
108. J. H. Gibbons, Office of Technology Assessment, U.S. Congress, 600 Pennsylvania Avenue, SE, Washington, DC 20510
109. P. V. Gilli, Graz University of Technology, Kopernikusgasse 24, A-8010, Graz, Austria

110. S. Malcolm Gillis, Professor, Economics and Public Policy, Department of Economics, Duke University, Durham, NC 27706
111. A. C. Giurlando, P.E., Fedders Corporation, Edison, NJ 08817
112. Paul Glamm, The Trane Company, 3600 Dammel Creek Road, LaCrosse, WI 54601
113. L. R. Glicksman, Massachusetts Institute of Technology, 77 Massachusetts Avenue, Building 3-137, Cambridge, MA 02139
114. Alan Glover, School of Engineering, Mechanical Engineering Department, University of Auckland, Auckland, New Zealand
115. Victor Goldschmidt, Purdue University, Ray W. Herrick Laboratories, West Lafayette, IN 47907
116. Sheldon Goldstein, Carteret, NJ 07008
117. R. Eugene Goodson, Hoover Universal, Inc., P.O. Box 1003, 825 Victors Way, Ann Arbor, MI 48106
118. Peter Gorike, Abt. Anwendungstechnik, Rheinish-Westfakuscges, Krupstrasse 5, 4300 Essen 1, Federal Republic of Germany
119. D. E. Grether, International Environmental Corporation, 5000 7th Street, SW, Oklahoma City, OK 73125
120. Russ Griffith, Copeland Corporation, Campbell Road, Sidney, OH 45365
121. G. C. Groff, Research Division, Carrier Corporation, Syracuse, NY 13201
122. Marvin Gunn, Energy Conversion and Utilization Technology Division, CS-142, Forrestal Building, Department of Energy, Washington, DC 20585
123. John Hackstedde, Tecumseh Products Company, Tecumseh, MI 49236
124. R. Hanski, Studsvik Energiteknik AB, S-611 82 Nykoping, Sweden
125. James Harnish, Chief Engineer, Advanced Products, Unitary Products Engineering, York Division, Borg-Warner Corporation, York, PA 17405
126. D. J. Harrje, Princeton University, Energy and Environment, Von Neuman Building, Princetón, NJ 08544
127. Gordon Hart, Owens-Corning Fiberglass Technical Center, Granville, OH 43023
128. Floyd Hayes, Thermal Systems, The Trane Company, 3600 Pammell Creek Road, LaCrosse, WI 54601
129. Wayne Helmer, Southern Illinois University at Carbondale, School of Engineering and Technology, Department of Thermal and Environmental Engineering, Carbondale, IL 62901
130. R. J. Hemphill, Gas Research Institute, 8600 Bryn Mawr Avenue, Residential and Commercial Utilization, Chicago, IL 60631
131. Robert Hemphill, Deputy Manager of Power, 546 Chestnut Street Tower II, Tennessee Valley Authority, Chattanooga, TN 37401
132. Arlo Hendrickson, General Electric Company, Troup Highway, Tyler, TX 75711
133. Richard Higginbotham, Higginbotham Heating and Air Conditioning Service, 1700 Branner Street, Knoxville, TN 37917
134. James Hill, Thermal Solar Program, National Bureau of Standards, Washington DC 20234
135. C. C. Hiller, Sandia Laboratories, Livermore, CA 94550
136. Ralph Hise, Consolidated Natural Gas Service Company, 11001 Cedar Avenue, Cleveland, OH 44106

137. Larry Hobart, American Public Power Association, 2000 Virginia Avenue, NW, Washington, DC 20037
138. Tina Hobson, Building Equipment Division, CE-113.2, Department of Energy, 1000 Independence Avenue, SW, Washington, DC 20585
139. Allen Holman, Mechanical Data, 215 Center Park Drive, Suite 100, Knoxville, TN 37922
140. Robert Holtz, Program Manager, Closed Cycle Systems, Argonne National Laboratory, 9700 South Cass Avenue, Argonne, IL 60439
141. Fred Honnold, Consumer Products Division, Carrier Corporation, Syracuse, NY 13201
142. John Hughes, Commonwealth Edison Company, P.O. Box 767, Chicago, IL 60690
143. Michael Hughes, Friedrich Air Conditioning & Refrigeration, 2000 West Commercial Boulevard, Fort Lauderdale, FL 22209
144. Bao Hwang, David Taylor Naval Ship R&D Center, Mail Code 2722, U.S. Naval Academy, Annapolis, MD 21402
145. Howard Izawa, InterNorth, Inc., Northern Gas Company, 4840 F Street, Omaha, NE 68117
146. S. R. Jackbsen, Danish Ministry of Energy, Energy R&D Secretariat, Strandgage 29 DK 1401, Copenhagen, Denmark
147. Richard Jacobson, Honeywell, Inc., 10701 Lyndale Avenue South, Bloomington, MN 55420
148. T. Jacoby, Tecumseh Products Company, Tecumseh, MI 49286
149. H. Jaster, General Electric Corporate Research & Development, General Electric Company, P.O. Box 43, Schenectady, NY 13201
150. P. L. Johnson, Oak Ridge Associated Universities, Executive Office, Administration Building, Oak Ridge, TN 37830
151. Fritz R. Kalhammer, Vice President, Electric Power Research Institute, P.O. Box 10412, Palo Alto, CA 94303
152. F. Kalivoda, Copeland Corporation, Sydney, OH 45365
153. Mark Kalman, E-Tech Incorporated, 3570 American Drive, Atlanta, GA 30341
154. Herbert Kaufman, Empire State Electric Energy Research Corporation, 1271 Avenue of the Americas, New York, NY 10002
155. George Kelly, Building Environment Division, IAT, National Bureau of Standards, Building 226, Washington, DC 20234
156. Rube Kelto, Tecumseh Products Company, Tecumseh, MI 49286
157. R. W. King, Manager, Advanced Engineering, Copeland Corporation, Sydney, OH 45365
158. Sanford Klein, University of Wisconsin, Mechanical Engineering, Madison, WI 53706
159. Milton Kosfeld, Vice-President, Engineering Compressors, Fedders Corporation, Woodbridge Avenue, Edison, NJ 08817
160. H. Kruse, University Hannover, Welfengarten 1 A Hannover, West Germany
161. P. Kuppers, Kernforschungsanlage/Ple, Postfache 1913, D-5170, Julich 1, Germany
162. Todd R. LaPorte, Professor, Political Science, Institute of Government Studies, University of California, 109 Moses Hall, Berkeley, CA 94720

163. Gary Laden, Deputy Assistant Director, Division of Energy and Product Information, Bureau of Consumer Protection, Federal Trade Commission, Washington, DC 20580
164. M. Yves Langhame, Quebec, Canada
165. J. Langmead, Director of Technical Services, Gas Appliance Manufacturers' Association, 1901 North Fort Meyer Drive, P.O. Box 9245, Arlington, VA 22209
166. Arvo Lannus, Residential and Commercial Applications, Electric Power Research Institute, 3412 Hillview Avenue, P.O. Box 10412, Palo Alto, CA 94303
167. Martin Lessen, Consulting Engineer, 12 Country Club Drive, Rochester, NY 14618
168. Dr. Y. N. Lee, Roy C. Ingersoll Research Center, Wolf and Algonquin Roads, Borg-Warner Corporation, Des Plaines, IL 60018
169. W. David Lee, Arthur D. Little, Inc., Acorn Park, Cambridge, MA 02140
170. A. W. Liles, EXXON Enterprises, Inc., P.O. Box 192, Florham Park, NJ 07932
171. D. C. Lim, Energy Conversion Equipment Branch, CE-113.2, Department of Energy, 1000 Independence Avenue, SW, Washington, DC 20585
172. Nance Lovvorn, Alabama Power Company, 15 South 20th Street, P.O. Box 2641, Birmingham, AL 35291
173. R. A. Lucheta, Westinghouse Electric Corporation, Research & Development Center, 1310 Beulah Road, Pittsburg, PA 15235
174. H. P. Luckett, Editor in Chief, *Popular Science*, 380 Madison Avenue, New York, NY 10017
175. Ward MacArthur, Honeywell, Inc., 2600 Ridgeway Parkway, Minneapolis, MN 55413
176. J. F. T. MacLaren, University of Strathclyde, Glasgow, Scotland
177. J. C. Major, Swiss Federal Institut for Reactor Research, CH-5303 Wurenlingen, Switzerland
178. Robert Mauro, Energy Management and Utilization Division, Electric Power Research Institute, 3412 Hillview Avenue, P.O. Box 10412, Palo Alto, CA 94304
179. Jim McCallum, Executive Editor, Air Cond. & Refrig. Bus., 614 Superior Avenue, West, Cleveland, OH 44113
180. E. A. McPherson, SED Systems, Ltd., P.O. Box 1464, Saskatoon, Saskatchewan, Canada S7K3P7
181. F. C. McQuiston, Oklahoma State University, 301 Engineering North, Stillwater, OK 74074
182. Richard H. Merrick, Arkla Industries Inc., P.O. Box 534, Evansville, IN 47704
183. Philip Metz, Brookhaven National Laboratory, Upton, NY 11973
184. Alessio Mezzina, Solar Technology Group, Brookhaven National Laboratory, Building 701, Upton, NY 11973
185. Mark Middleton, Columbus Products Company, 300 Phillipi Road, Columbus, OH 43228
186. R. Scott Miller, General Electric Company, CRD-River Road, Building #37-615, Schenectady, NY 12345
187. J. P. Millhone, Office of Buildings Energy Research and Development, CE-11, Department of Energy, 1000 Independence Avenue, SW, Washington, DC 20585

188. F. H. Morse, Office of Solar Heat Technologies, CE-31, Department of Energy, 1000 Independence Avenue, SW, Washington, DC 20585
189. Robert Morse, Tecumseh Products Company, Tecumseh, MI 49286
190. Larry Moss, P.O. Box 1496, Estes Park, CO 80517
191. T. Mukai, Permanent Delegation-Japan, 7, Avenue Hoche, 75008, Paris, France
192. W. E. Murphy, Department of Mechanical Engineering, Texas Engineering Experiment Station, Texas A&M University, College Station, TX 77843
193. Neno Nenov, Linde Division, Union Carbide Corporation, Tonawanda, NY 14150
194. R. W. Newell, Vice President, Research & Development, City Investing Company, 5600 Old Greenwood Road, Fort Smith, AR 72903
195. Van-Thanh Nguyen, Mitre Corporation, Metreck Division, 1820 Dolley Madison Boulevard, McLean, VA 22102
196. Dennis O'Neal, 400 North River Road, Apartment 603, West Lafayette, IN 47906
197. Jerald Parker, School of Mechanical and Aerospace Engineering, Oklahoma State University, 218 Engineer North, Stillwater, OK 74074
198. A. Patani, Honeywell, Inc., 10701 Lyndale Avenue South, Bloomington, MN 55420
199. Michael Perlsweig, Division of Conservation Research and Technology, Department of Energy, 20 Massachusetts Avenue, NW, Washington DC 20545
200. Lawrence Peterson, 1671 Southwest Fairhill, Roseburg, OR 97470
201. Joe Pietsch, Northrup, Inc., 302 Nichols Drive, Hutchins, TX 75141
202. B. J. Pleiss, A. O. Smith Corporation, 531 North 4th Street, Tipp City, OH 45371
203. Lee Preston, A. O. Smith Corporation, 531 North 4th Street, Tipp City, OH 45371
204. T. Ratchford, Committee on Science and Technology, Subcommittee on Energy R&D, House of Representatives, Washington, DC 20515
205. V. Recchi, National Research Council, c/o O. T. B. Zona Industriale, Contrada del Parco, Bari, Italy
206. Robert Reid, Energy, Environment, and Resources Center, University of Tennessee, 329 South Stadium Hall, Knoxville, TN 37996-0710
207. Gordon Reistad, Oregon State University, Department of Mechanical Engineering, Corvallis, OR 97331
208. Patrick Reynolds, Mechanical Technology, Inc., 968 Albany-Shaker Road, Latham, NY 12110
209. Hal Rhea, Director of Engineering, Lennox Industries, Inc., P.O. Box 877, 1600 Metro Drive, Carrollton, TX 75006
210. Steve Riedel, General Electric Company, Fort Wayne, IN
211. Bill Riley, Advance Development, Heil Quaker Corporation, 647 Thompson Lane, P.O. Box 40566, Nashville, TN 37204
212. J. Rizzuto, New York State Energy Research and Development Authority, Agency Building No. 2, Empire State Plaza, Albany, NY 12223
213. Arthur Rosenfeld, Lawrence Berkeley Laboratory, Building 90, Room 3058, 1 Cyclotron Road, University of California, Berkeley, CA 94720
214. J. H. Rothenburg, Utilities Systems, Department of Housing and Urban Development, 451 Seventh Street, SW, Washington, DC 20410
215. William Rudoy, University of Pittsburg, Department of Mechanical Engineering, Pittsburg, PA 15261

216. J. D. Ryan, Energy Conversion Equipment Branch, CE-113.2, Department of Energy, 1000 Independence Avenue, SW, Washington, DC 20585
217. L. A. Sarkes, American Gas Association, 1515 Wilson Boulevard, Arlington, VA 22209
218. M. L. Savitz, Deputy Assistant Secretary for Conservation, CE-10, Department of Energy, 1000 Independence Avenue, SW, Washington, DC 20585
219. D. E. Scherpereel, Director, Mechanical Systems Research, Elisha Gray II—Research and Engineering Center, Monte Road, Benton Harbor, MI 49022
220. Carl Schmittle, York Division, Borg-Warner, York, PA 17405
221. Robert Schoenhals, Department of Mechanical Engineering, Purdue University, West Lafayette, IN 47907
222. Mark Schuetz, AMTI, 141 California Street, Newton, MA 02158
223. James Schultze, Technology Program Manager, General Electric Company, Appliance Park, Building 6, Room 208, Louisville, KY 40225
224. J. L. Schulze, General Electric Company, Appliance Park, Louisville, KY 40225
225. T. C. Scott, Department of Mechanical and Aerospace Engineering, University of Virginia, Charlottesville, VA 22901
226. Musoke Sendanla, Tennessee Valley Authority, Electrical Systems, 1150 Chestnut Street Tower II, Chattanooga, TN 37401
227. Takao Senshu, Mechanical Engineering Research Laboratory, Hitachi, Ltd., 390 Muramatsu, Shimizu-shi, Shizuoka-ken, Japan
228. Charles Sepsy, Ohio State University, Department of Mechanical Engineering, Room 2075—Robinson Laboratory, 206 West 18th Avenue, Columbus, OH 43210
229. Michael Sexton, Department of Mechanical and Aerospace Engineering, University of Virginia, Charlottesville, VA 22901
230. Ramesh Shah, Harrison Radiator Division, General Motors Corporation, Lockport, NY 14094
231. James Shaw, Public Service Company of Oklahoma, P.O. Box 201, Tulsa, OK 74102
232. Duncan Sheldon, Lincoln Laboratory, P.O. Box 73, Lexington, MA 02173
233. Samuel Shelton, School of Mechanical Engineering, Georgia Instute of Technology, Atlanta, GA 30332
234. Neil Sher, Technology Strategy Center, Honeywell Control Systems, 1700 West Highway 36, St. Paul, MN 55113
235. D. E. Sherpereel, Research and Engineering Center, Whirlpool Corporation, Benton Harbor, MI 49022
236. Tony Sigmon, Research Triangle Institute, Energy and Environmental Research, P.O. Box 12194, Research Triangle, NC 27709
237. J. A. Smith, Test and Evaluation Branch, CE-113.2, Department of Energy, 1000 Independence Avenue, SW, Washington, DC 20585
238. Mason Somerville, Department of Mechanical Engineering, University of Arkansas, Fayetteville, AR 72701
239. Dr. Yates Sorrell, N. C. Alternative Energy Corporation, P.O. Box 12699, Research Triangle Park, NC 27709
240. E. W. Spannhake, White Consolidated Industries, Inc., 11770 Berea Road, Cleveland, OH 44111

241. Ing. F. Steimle, Angewandte Thermodynamik & Kimatechnik, Fachbereich 13, Universitatsstr. 15, 4300 Essen 1, West Germany
242. Don Stephenson, National Research Council, Division of Buildings Research, Montreal Road, Ottawa, Canada KIA 0R6
243. John Stephenson, University of Auckland, Auckland, New Zealand
244. W. F. Stoecker, University of Illinois Urbana-Champaign, Department of Mechanical and Industrial Engineering, 144 Mechanical Engineering Building, Urbana, IL 61801
245. Robert Stricker, The Rovac Corporation, 100 Rovac Parkway, Rockledge, FL 32955
246. Shiv Sud, Strategic Planning and Analysis Group, Ministry of Energy, 56 Wellesley Street West, Queen's Park, Toronto, Canada
247. P. F. Swenson, Consolidated Natural Gas Service Company, 11001 Cedar Avenue, Cleveland, OH 44106
248. C. J. Swet, 7040 Woodville Road, Mt. Airy, MD 21771
249. W. D. Syniuta, Advanced Mechanical Technology, Inc., 141 California Street, Newton, MA 02158
250. C. C. Thiel, Jr., Division of Advanced Technology Applications, National Science Foundation, 1800 G Street, NW, Washington, DC 20550
251. W. H. Thielbahr, Energy Conservation Branch, Department of Energy, Idaho Operations Office, 550 Second Street, Idaho Falls, ID 83401
252. W. C. Thomas, Virginia Polytechnic Institute and State University, Blacksburg, VA 24061
253. Tommy Thompson, Vice-President, Engineering, BDP Company, Division of Carrier Corporation, 7310 West Morris Street, Indianapolis, IN 46231
254. William Toscano, Foster-Miller Associates, 135 Second Avenue, Waltham, MA 02154
255. E. L. Tramel, Residential Technical Applications, Conservation and Energy Management, Chattanooga Power Service Center, Chattanooga, TN 37401
256. D. Tree, Ray Herrick Laboratory, Purdue University, West Lafayette, IN 47907
257. Dutch Uselton, Northrup Incorporation, 302 Nichols Drive, Hutchins, TX 75141
258. Himanshu Vakil, General Electric Corporate R&D, P.O. Box 8, Schenectady, NY 12301
259. Hendrik Van Der Ree, TNO, Heat Pump Section, Laan Van Westenenk 501, Apeldoorn, The Netherlands
260. S. E. Veyo, Westinghouse Electric Corporation, Research & Development Center, 1310 Beulah Road, Pittsburg, PA 15235
261. Michael Wahlig, Lawrence Berkeley Laboratory, Building 90, Room 2024, 1 Cyclotron Road, University of California, Berkeley, CA 94720
262. D. J. Walukas, Foster-Miller Associates, Inc., 795 Oak Ridge Turnpike, Oak Ridge, TN 37830
263. Andy Wan, Room EM204, U.S. Department of Commerce, National Bureau of Standards, Washington DC 20234
264. Bernie Warning, Friedrich Air Conditioning & Refrigeration, 4200 North Pan Am Expressway, P.O. Box 1540, San Antonio, TX 78295
265. Ralph Webb, Department of Mechanical Engineering, Pennsylvania State University, 208 Mechanical Engineering Building, University Park, PA 16802

266. David Wensky, Copeland Corporation, 250 East Wilson Bridge Road, Suite 255, Worthington, OH 43085
267. Eugene West, Sr. Vice President, Engineering, Amana Refrigeration, Inc., Amana, IA 52204
268. G. W. Wiener, Manager, Materials Science Division, Westinghouse R&D Center, 1310 Beulah Road, Pittsburg, PA 15235
269. M. Wilden, University of New Mexico, Albuquerque, NM 87115
270. William H. Williams, Division Manager, AT&T Information Systems, Building 83, Room 1B23, 100 Southgate Parkway, Morristown, NJ 07960
271. J. C. Wilson, Carlyle Compressor Company, 4803, Syracuse, NY 13221
272. Lawrence Woodworth, Brookhaven National Laboratory, Building 120, Upton, NY 11973
273. Les Wright, Project Manager, Residential Space Conditioning Systems, 8600 West Bryn Mawr Avenue, 10 West 35th Street, Chicago, IL 60631
274. Hiromu Yasuda, Mechanical Engineering Research Laboratory, Hitachi, Ltd., 390 Muramatsu, Shimizu-shi, Shizuoka-ken, Japan
275. T. Yoshii, Mitsubishi Heavy Industries America, Inc., Suite 2101, John Hancock Center, 875 North Michigan Avenue, Chicago, IL 60611
276. David Young, Ontario Hydro, Research Division, 800 Kipling Avenue, Toronto, Canada M8Z 5S4
277. P. Zegers, Commission of the European Communities, 200 Rue de la Loi, Brussels 1049, Belgium
278. Ronald Zerkle, University of Cincinnati, Cincinnati, OH
279. R. V. Zigler, General Electric Company, 570 East 16th, Holland, MI 49423
280. Alan Zimmerman, Special Products Group, The Coleman Company, Wichita, KS 67201
281. Congressional Information Service, Research Building 83, Kodak Park, Rochester, NY 14050
282. Edison Electric Institute, 8th Floor, 1111 19th Street, NW, Washington DC 20036
283. Office of the Assistant Manager for Energy R&D, U.S. Department of Energy, Oak Ridge Operations, Oak Ridge, TN 37831
284. National Energy Information Center, Library, Room 1404, 12th and Pennsylvania Avenues, NW, Washington, DC 20461

285–311. Technical Information Center, Department of Energy, P.O. Box 62, Oak Ridge, TN 37831

312–361. External Energy Conservation Distribution, Oak Ridge National Laboratory, Building 9102-2, Room 112, Oak Ridge, TN 37831

☆U.S. GOVERNMENT PRINTING OFFICE: 1984-544-045/4210